Working Report 2011-08

Cyprus Natural Analogue Project (CNAP)

Phase II Final Report

Editors:

W.R.Alexander

A.E.Milodowski

February 2011

POSIVA OY
Olkiluoto
FI-27160 EURAJOKI, FINLAND
Tel +358-2-8372 31
Fax +358-2-8372 3709

Working Report 2011-08

Cyprus Natural Analogue Project (CNAP)

Phase II Final Report

Editors:

W.R.Alexander

Bedrock Geosciences, Auenstein, Switzerland

A.E.Milodowski

British Geological Survey, Keyworth, UK

February 2011

Cyprus Natural Analogue Project (CNAP), Phase II Final Report

ABSTRACT

Due to the extremely slow kinetics of bentonite reaction in low alkali cement leachates, natural analogues would appear to be the only viable method of studying bentonite reaction. As a result of a review of the available literature, several sites in Cyprus were selected as particularly promising for this purpose. This report presents the results of two short field campaigns in Cyprus in November/December, 2008 and February, 2009. The main aim of these campaigns was to establish if appropriate sites existed for a natural analogue study of bentonite-low alkali cement leachate reaction. Focus is on mineralogical changes and not changes in physical properties (such as porosity and permeability) of bentonite as the industrially-processed bentonite used in a repository will be completely different in terms of its engineering and hydrogeological properties to the unprocessed natural bentonite or analogue smectite-rich materials.

The first campaign was in the form of a reconnaissance study to identify sites of likely interest and the second, follow-up, campaign focussed on obtaining preliminary groundwater and solid phase (bentonites/clay-rich sediments/altered igneous rocks/soils) samples which would allow a more detailed assessment of several of the potential sites.

A large amount of information was collected during these short field campaigns and subsequent laboratory analysis of the collected samples so, to keep the main report down to a digestible size, much of the supporting information has been collated in seven appendices. These include full details of all 30 sites visited during both campaigns along with sample details, information on the analytical techniques, the analytical raw data and numerous photographs of the sites. The intention is that this report will provide full supporting information for a potential Phase III and a detailed database for our colleagues at the Geological Survey Department (GSD) in Cyprus. Consequently, all the information acquired during this study has been captured so that it might provide a useful resource for any future studies.

As with all such initial investigations, several surprises were unearthed, including the overwhelming degree of serpentinisation at some sites. More importantly, however, is that the main aims have been met insofar that:

- the groundwater chemistries have been shown to be similar to, and therefore fully relevant to, low alkali cement leachates;
- that indications of clay reaction have been identified;
- perhaps most importantly, confidence in the site conceptual model has been increased.

This has also led to the identification of general areas of Cyprus where bentonite (and analogous clay-rich sediments)/hyperalkaline fluid reaction could probably be studied, and of several specific sites where any future sampling and analysis is likely to be successful.

Keywords: Natural Analogue, Cyprus, bentonite, alkali, cement leachates.

Kyproksen Luonnonanalogia Projekti (CNAP), Vaihe II Loppuraportti

TIIVISTELMÄ

Emäksisissä sementin uutosvesissä tapahtuvien bentoniitin reaktioiden erittäin hitaasta reaktiokinetiikasta johtuen luonnonanalogiat näyttäisivät olevan ainoa toimiva menetelmä näiden tutkimiseen. Kirjallisuusselvityksen perusteella tähän tarkoitukseen valittiin Kyprokselta useita, erittäin lupaavia kohteita. Tässä raportissa esitetään kahden Kyprokselle marras-, joulukuussa 2008 ja helmikuussa 2009, tehdyn lyhyen paikkatutkimuksen tulokset. Näiden tutkimusten päätavoite oli paikallistaa ja varmistaa sopivien tutkimuspaikkojen esiintyminen. Pääpaino on mineralogisissa muutoksissa, ei bentoniitin fysikaalisten ominaisuuksien (kuten huokoisuus ja vedenläpäisevyys) muutoksissa, koska loppusijoitustilassa käytettäväksi suunnitellun teollisesti jalostetun bentoniitin tekniset ja hydrogeologiset ominaisuudet ovat hyvin erilaiset kuin jalostamattoman luonnon bentoniitin tai vastaavan smektiittirikkaan materiaalin. Ensimmäisessä paikkatutkimuksessa suoritettiin mahdollisesti mielenkiintoisten kohteiden alustava tutkimus ja toisella matkalla keskityttiin saamaan tarvittavat pohjavesi ja kiintoaines (bentoniitti / savirikas sedimentti/muuttunut syväkivi/maaperä) näytteet kohteiden tarkempaa arviointia varten. Näiden kahden lyhyen matkan aikana ja analysoimalla kerätyt näytteet saatiin suuri määrä tietoa, josta osa on esitetty seitsemässä liitteessä, jotta itse raportti olisi helpommin luettavissa ja ymmärrettävissä. Liitteissä kuvataan yksityiskohtaisesti kaikki 30 kohdetta joissa kahden matkan aikana käytiin, kuten myös näistä otettujen näytteiden tiedot. Samoin liitteissä on esitetty näytteiden tutkimisessa käytetyt analyyttiset menetelmät, raakatulokset sekä lukuisia kuvia kohteista. Raportin tarkoitus on antaa kattava tietopaketti mahdolliselle III vaiheelle ja yksityiskohtainen tietokanta kollegoillemme Kyproksen geologisella tutkimusosastolla (Geological Survey Department, GSD). Kaikki tutkimuksen aikana hankittu tieto on tallennettu siten, että siitä muodostuisi hyödyllinen resurssi minkä tahansa tutkimuksen käyttöön tulevaisuudessa.

Kuten kaikissa alustavissa tutkimuksissa, useita yllätyksiä tuli vastaan, mukaan lukien joidenkin kohteiden valtava serpentisoitumisaste. Mikä tärkeintä, tutkimuksilla saavutettiin projektin päätavoitteet:

- pohjavesien kemiallisen koostumuksen osoitettiin vastaavan matalan pH:n sementtien uutosvesiä ja olevan siten relevantti analogiatutkimukseen
- savissa havaittiin reaktioita
- ja ehkä tärkeimpänä, luottamus konseptuaaliseen malliin on kasvanut

Tutkimuksilla on myös pystytty tunnistamaan mahdollisia alueita Kyprokselta joissa bentoniitin (ja vastaavan savirikkaan sedimentin) ja hyperalkalisen nesteen vuorovaikutusta voitaisiin mahdollisesti tutkia, ja useita tarkkoja kohteita joissa tuleva näytteenotto ja analyysit todennäköisesti onnistuvat.

Avainsanat: Luonnonanalogia, Kypros, bentoniitti, alkali, sementin uuttoliuos.

TABLE OF CONTENTS

Contributors

Bedrock Geosciences, Auenstein, Switzerland

W.R.Alexander

British Geological Survey, Keyworth, UK

S.J. Carter
W.G. Darling
N.D. Eatherington
C.J.B. Gowing
L.D. Grimsley
H. Harrison
M.N. Ingham
S.J. Kemp
A.E.Milodowski
I. Mountenay
J. Rushton
R.A. Shaw
H. Taylor
D. Wagner
C.L. Williams

Geological Survey Department, Lefkosia, Cyprus

M.Rigas

1 INTRODUCTION

1.1 Background

Bentonite makes and important contribution to the performance of the engineered barrier system for the disposal concepts developed for many types of radioactive waste. The choice of bentonite results from its favourable properties – such as plasticity, swelling capacity, colloid filtration, low hydraulic conductivity, high retardation of key radionuclides – and its stability in relevant geological environments. However, bentonite – especially the swelling clay component (smectite) that contributes to its essential barrier functions – is unstable under higher pH conditions. This led to some repository designs (especially for disposal of high-level vitrified waste, HLW or spent fuel, SF) that exclude use of concrete from any sensitive areas containing bentonite, so avoiding any potential bentonite degradation in the cementitious leachates (which have an initial pH of up to about 13: see, for example, Atkinson et al. 1985; Haworth et al. 1987).

The option of avoiding the problem of incompatibility with conventional cement and concrete by constraining the design was considered acceptable during early, generic studies. However, as projects move closer to implementation, it is increasingly recognised that constructing extensive facilities underground without using concrete – a staple of the engineering community – would be difficult, expensive and potentially dangerous for workers (see analysis in Alexander and Neall, 2007, for example). This last point is especially important given the extreme sensitivity of most stakeholders towards even 'conventional' accidents at nuclear sites (see discussion in Alexander et al. 2007). This is especially the case in countries like Japan and the UK, where a volunteering approach to siting a repository means that repository construction could be in a technically challenging host rock.

The topic is also relevant for transuranic wastes (TRU, or other high toxicity/long half-life intermediate-level waste, ILW), particularly if this is co-disposed with HLW/SF. TRU waste contains large inventories of cementitious materials and hence, in principle, could pose a risk to the engineered barrier system (EBS) of HLW/SF, even if concrete was excluded from the HLW part of the repository (e.g. scenarios discussed in Nagra's Projekt Entsorgungsnachweis; Nagra 2002). Indeed, some designs of the EBS for various kinds of low- and intermediate level waste (L/ILW) include a bentonite layer, which is planned to act as an external barrier around concrete structures To date, there has been no comprehensive demonstration that the performance of such a barrier can be assured for relevant periods of time (see comments in Umeki, 2009).

The MX-80 bentonite, for example, has been shown to have a porewater pH of 8 in ambient groundwaters (Bradbury and Baeyens 2002), significantly less than that of low-alkali cement pH of 11 or less. The three pH units difference is the equivalent of three orders of magnitude in the OH^- activity, meaning there will still be potential for significant reaction with bentonite, it will simply be less than at pH 13. Karnland et al. (2005) and Ahokas et al. (2006) both noted that "According to Sellin et al. (2003) the dissolution rate for a number of silicates and aluminium silicates, e.g. quartz, kaolinite,

increases by a factor of 10 if pH is increased from 11 to 13 and laboratory experiments referred to implied that bentonite is much more stable at pH 11 as compared to pH 13."

Recently, therefore, there have been extensive efforts to better understand the interactions of hyperalkaline fluids with bentonite, coupled with studies aimed at reducing the risk by development of low alkali cement formulations. The greatest challenge is bringing the information produced by laboratory (conventional and underground rock laboratories, URL) and modelling studies together to form a robust safety case. This is complicated by the inherently slow kinetics of such reactions and the commonly observed persistence of metastable phases for geological time periods (for a good overview of the issues involved, see Metcalfe and Walker, 2004). Clearly, this is an area where analogues could play a valuable role – bridging the disparity in realism and timescales between laboratory studies and the systems represented in repository performance assessment (see also discussion in Alexander et al. 1998; Miller et al. 2000). Indeed, in this particular case, natural analogues would appear to be the only viable method of studying bentonite reaction.

Before looking any further at possible bentonite reaction, it is important to clarify the terminology surrounding the material and also the use of the term in this report. The term bentonite was first proposed in the 19th century by Knight (1898) and the name is from the Benton Shale in which the clay was thought at that time to occur. Once the origins of bentonite were understood, several updated definitions followed, but all have limitations. The strict geological definition of "bentonite" is a soft, plastic, porous light-coloured rock composed essentially of clay minerals from the smectite group plus colloidal silica, and produced by chemical alteration of volcanic ash (cf. Hallsworth and Knox 1999). The name implies a definite genetic origin from alteration of volcanic ash, either in situ or transported material. The non-genetic term "smectite-claystone" is now recommended where the origin of the smectite-rich clay sediment is uncertain (Hallsworth and Knox 1999).

Industrial bentonite, such as the "bentonite" that will be used in the engineered barrier of a radioactive waste repository, is derived from natural bentonite rock but may be processed to improve the smectite content (i.e. beneficiated) of the material and/or chemically treated to enhance its cation exchange, swelling or other physico-chemical properties (e.g. conversion or "activation" of natural calcium montmorillonite to sodium montmorillonite by treatment with sodium carbonate). As such, the physical and chemical properties of industrial bentonite may differ significantly from that of the natural rock.

In order to avoid confusion in this report, the term "*bentonite analogue*" is used to refer to the natural smectite-rich rocks, soils and sediments that are being studied as natural analogues for the interaction between cement-derived high pH porefluids and the "*industrial bentonite*" that will be used as buffer material in the repository. The focus of this natural analogue study is on geochemical and mineralogical alteration of smectite clay minerals as an analogue of the long-term geochemical and mineralogical alteration that might be expected during the geochemical evolution of the repository engineered barrier system, over timescales exceeding those that can be studied in laboratory experimental systems. The term "bentonite analogue" as used in this report does not

necessarily refer to a true bentonite in the "geological sense" nor does it imply that the material has similar physical or hydrogeological properties to the "bentonite buffer" of the repository engineered barrier.

1.2 The natural analogue concept

Argumentation by use of analogy is well established in many fields including philosophy, biology, linguistics and law (e.g. Petit, 1992). For the specific case of radioactive waste management, the term "natural analogue" (NA) has developed a particular meaning associated with supporting arguments for the long-term safety of repositories (see Chapman et al. 1984; Miller et al. 2000 and www.natural-analogues.com for discussion). Key factors here are the heterogeneity and complexity of natural systems and, in particular, the very long timescales over which safety must be assured. The potential evolution of repositories, designed for specific types of waste and disposal site, can be simulated by the use of mathematical models, but the extent to which such models can be validated by conventional approaches is inherently limited. Here natural analogues – systems which have similar properties to components of repositories – have a unique role to play. The extent to which NA system evolution in the past can be understood and modelled with existing tools and data, gives an indication of the ability to determine future development of the repository.

The initial use of NAs focussed on improving understanding of key processes and model/database testing (e.g. McKinley, 1989) and, indeed, this is still a major justification for some analogue projects. More recently, however, additional roles in public communication (e.g. West et al. 2002) and staff training (e.g. Alexander et al. 2008a) have received greater emphasis. In particular, using natural analogues to provide general support for the safety case (by studying the evolution relevant systems over geological timescales) and to increase confidence in extrapolating results from laboratory and field experiments to the repository have been a recent focus. This study most certainly belongs in this more recent domain.

Improving system understanding can range from examining global concepts (e.g. fundamental feasibility of preserving geochemical anomalies for millions of years – see discussions on Oklo and Cigar Lake in Miller et al. 2000) to direct quantification of specific processes (e.g. matrix diffusion depths – see Smellie et al. 1985). Similarly, model testing can range from rather weak qualitative comparison of expectations with observations (e.g. relative retention of elements within Oklo reactor cores) to quantitative assessment of the relevance of laboratory databases (e.g. for material corrosion) to more formal assessment of the predictive capability of specific model and databases (e.g. blind predictive modelling of solubility limits).

As such, for this project, an initial literature study with search parameters that included both aspects of the target geology and also themes of relevance to radioactive waste management programmes was carried out. Factors considered included:

- Details of ophiolite terrains available
- Existence of relevant hyperalkaline groundwaters

- Availability of bentonites/ clay-rich (and particularly smectite-rich) bentonite analogues
- H_2 or CH_4 gas in groundwaters
- tuffaceous deposits
- coastal sites
- logistics (e.g. potential support from local mining operations, ease of transport etc)

This initial literature search indicated that no useful information on this topic could be "mined" from past studies such as the previous work carried out in Oman (e.g. Bath et al. 1988) or Jordan (e.g. Pitty 2009) and hence the option of a new project was examined. The basic idea was to use a "top-down" approach to identify sites where bentonite and bentonite analogue deposits have been exposed to relevant hyperalkaline water for very long periods.

Especially given the current interest in low alkali cements, the focus was on sites that have natural waters with pH in the appropriate range (around 10-11). As indicated in Figure 1.1, the cement leachate is simulated by natural hyperalkaline water, which, if the timescale of interaction can be determined, allows the models that are being developed to quantify the specific processes shown in the figure to be tested.

As noted in Metcalfe and Walker (2004), the cement leachate is simulated by natural hyperalkaline water, which, if the timescale of interaction can be determined, allows the models that are being developed to quantify the specific processes shown in the figure to be tested.

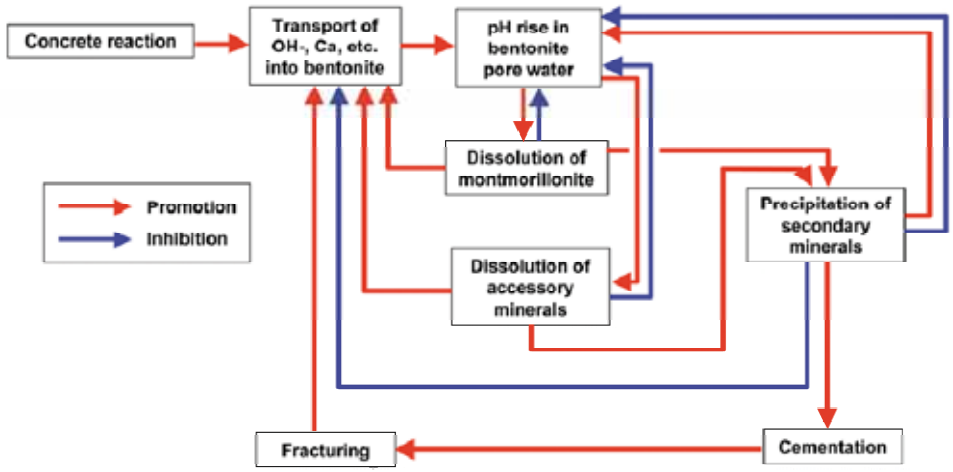

Figure 1.1. *Some of the important processes involved in bentonite alteration (from Metcalfe and Walker 2004); at the natural analogue sites in Cyprus, natural hyperalkaline groundwaters simulate the concrete leachate.*

The challenge is to maximise the value of this test, by assuring that materials and boundary conditions are as similar as possible to those in a repository. Nevertheless, it

must be emphasised that such sites are no more than an analogy of a repository, not a copy, and hence certain differences are inevitable (discussed below). Currently, the technical focus is on:

- long-term bentonite stability in analogue low alkali cement leachates
- if possible, same system as above interacting with seawater/brines for a coastal repository
- if possible, same system as above interacting with a range of leachate chemistries as the precise situation in a repository will depend both on the site conditions and the composition of the cementitious materials – neither of which have been fixed as yet
- low alkali cement leachate/host rock interaction – is there any?

In principle, there are a number of locations worldwide where such a NA might be found, including New Caledonia, Bosnia, California, China, Japan, Korea and the Philippines. Based on a multi-attribute analysis, considering factors such as probability of finding suitable locations, relevance to European programmes, low risk of disrupting calls for volunteers, political stability and cost-effectiveness, Cyprus was selected by the Technical Steering Committee (TSC, consisting of the NDA, Posiva and SKB) as the preferred option and has since been the focus of more detailed literature studies and a limited number of field investigations to confirm fundamental feasibility.

1.3 Background to the Cyprus Natural Analogue Project (CNAP)

1.3.1 Introduction

As noted above, the island of Cyprus was proposed as the focus for the project due to the known wide occurrence of both hyperalkaline springs (resulting from serpentinisation of ophiolites) and extensive bentonite and bentonite analogue deposits (e.g. Bear 1960). Other attributes of relevance include:

- Coastal locations where the influence of saline waters can possibly be studied
- Presence of gas (hydrogen and/or methane) in many relevant waters
- Good support infrastructure available at reasonable cost
- Ease of access from Europe (compared to the other potential NA sites noted above)
- Existence of a national Geological Survey (the GSD) for local support
- Lack of political sensitivity to field work

To most efficiently utilise resources, it was proposed that the project be split into three phases with go/no go decision points at the end of Phases I and II.

Phase I – data mining

The actual sites to be investigated in Phase II were determined on the basis of a data-mining project, which was based on the significant volume of literature on the island geology. Although much of the existing literature is focussed on the ophiolites (which are the source of the hyperalkaline leachates), enough information was found on the bentonites/bentonite analogues (e.g. Pantazis 1967) and hyperalkaline groundwaters (e.g. Neal and Shand 2002) to indicate that it was worthwhile moving on to Phase II.

Phase II – site reconnaissance and preliminary mineralogical and geochemical study

Following identification of likely sites, a short reconnaissance field trip took place from 26th November to 3rd December to confirm their appropriateness to the project aims. In addition to a preliminary assessment of sites identified in Phase I, meetings were held with the GSD to assess their potential interest in the project.

Following an assessment of the outcome of the first trip, the go ahead was given for a second field trip (9th to 14th February, 2009). In addition to confirming groundwater pH and the presence of appropriate bentonite sources, samples were taken at several sites for full groundwater chemical characterisation (i.e. major and trace elements, stable isotopes) and for mineralogical, petrographical and chemical (major and trace elements) characterisation of the host rock and bentonite/bentonite analogues to assess evidence of interaction with hyperalkaline groundwaters. The most promising sites were assessed for future detailed study (as part of any potential future Phase III programme) and other sampling considerations, such as borehole drilling, will be examined.

Other tasks included continuing contact with the GSD to maintain links for Phase III (should it go ahead) and assessing potential coastal sites where leachate/bentonite and leachate/host rock interaction can be examined in a saline environment. Finally, on the basis of the findings from the Phase II study, a detailed programme for Phase III will be proposed.

Go/no go decision point for the TSC. Selection of site(s) for detailed field work using a formal MAA (multi-attribute analysis) methodology.

Phase III – main project

Following the reconnaissance mission making a successful report to the TSC and a positive decision to proceed, the main project phase should begin soon afterwards (so as to maintain project momentum). The minimum requirement would be one or more specific locations where hyperalkaline waters are in contact with relevant host rock and bentonite/bentonite analogue formations. Particular characteristics that would favour a site include:

- Indicators of the timescale of hyperalkaline leachate/bentonite and leachate/host rock interaction

- Ease of sampling profiles of bentonite/bentonite analogue and host rock (NB as the bentonite can be taken as representative of an unfractured diffusive system, the focus will be on an advective fractured system for the host rock)
- Options for water sampling with minimum contact with air
- Options for coastal location
- Ease of access/local infrastructure

In order to allow maximum flexibility for the TSC, most practical details of the Phase III have been left open for the moment.

1.3.2 The analogy with the repository process

The design of the repository EBS will vary depending on the waste type and geological conditions but, as was noted above, in many cases industrial bentonite and cementitious material will be present together (e.g. Figure 1.2). When the low alkali cement reacts with groundwater and produces leachates, these could react with the industrial bentonite, so changing its original physico-chemical conditions. In Cyprus, the presence of bentonite and analogue bentonite in close proximity to natural hyperalkaline groundwaters (Figure 1.3) permits the zones of potential bentonite/hyperalkaline water reaction to be studied as an analogy of the reaction zones in the repository.

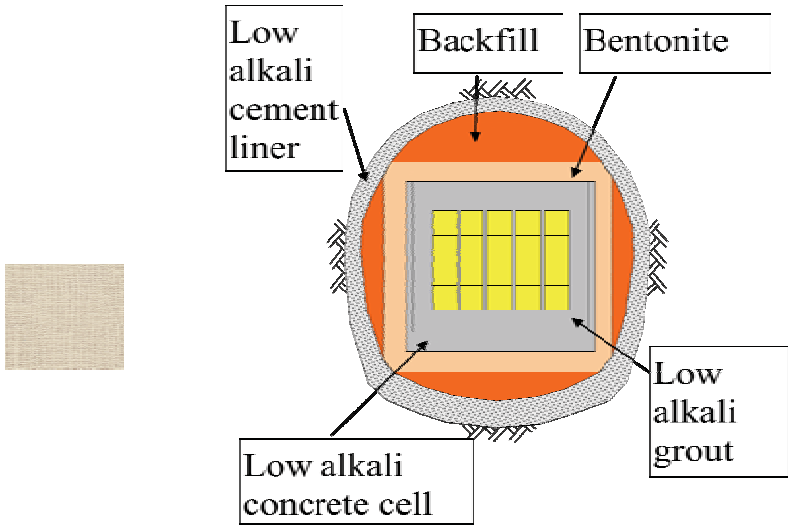

Figure 1.2. *An example of a repository design where OPC cement has largely been replaced with low alkali cement. Note the industrial bentonite barrier around the waste cell.*

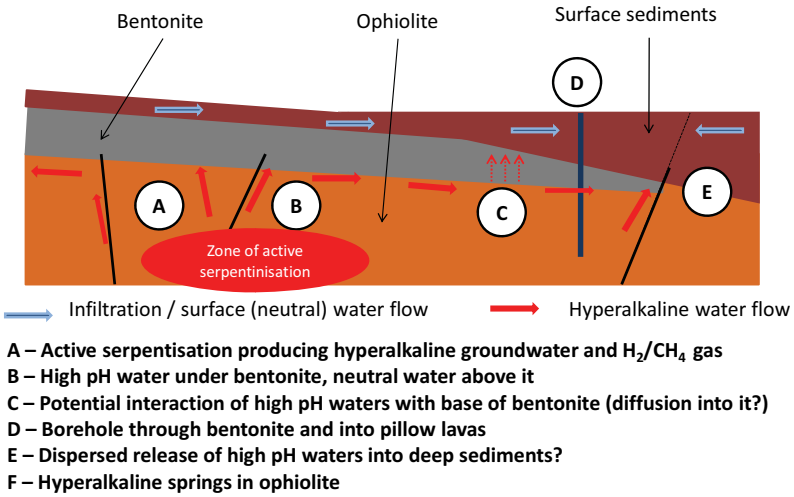

Figure 1.3. *The natural system in Cyprus. Hyperalkaline groundwaters could react with bentonite (and bentonite analogues) wherever they meet.*

1.4 Geological setting and lithological definitions

1.4.1 Ophiolite

All hyperalkaline groundwaters studied so far in Cyprus originate from the Troodos ophiolite or the Mamonia terrain (see Figure 1.4). The term ophiolite was originally used by Brongniart (1813) for an assemblage of green rocks (serpentine, diabase) in the French Alps. Ophiolites, as defined here, adapt the nomenclature of the Penrose Conference of 1972 (Geotimes, 1972) and, from top to bottom, consists of (see also Figure 1.5):

deep (abyssal) marine sediments, including bentonites/bentonite analogues
pillow lavas (basalt)
sheeted dyke complex
high level/isotropic gabbro
layered mafic cumulates (gabbro)
layered ultramafic cumulates
transition zone dunites and residual peridotites

If any of the above lithologies is missing, it should be called an ophiolite *complex*, but this term is frequently misused in the literature. Most ophiolites can be divided into one of two groups: Tethyan and Cordilleran. Tethyan ophiolites are characteristic of those which consist of a relatively complete rock series corresponding to the classic ophiolite assemblage and which have been emplaced onto a passive continental margin more or less intact, e.g., Troodos in Cyprus and Semail in Oman. Cordilleran ophiolites are characteristic of those that occur in the western mountain belts of the Americas (the "Cordillera" or backbone of the continent). These ophiolites sit on subduction zone accretionary complexes (subduction complexes) and have no association with a passive continental margin. These include the Coast Range and Josephine ophiolites of

California and the Quebradagrande Complex of Western Colombia and the Larsen Harbour Complex on South Georgia. Ophiolites are additionally sub-classified as either supra-subduction zone (SSZ), which exhibit island-arc geochemical and petrological characteristics, or mid-ocean ridge (MOR) which possess deep ocean crust geochemical and petrological features.

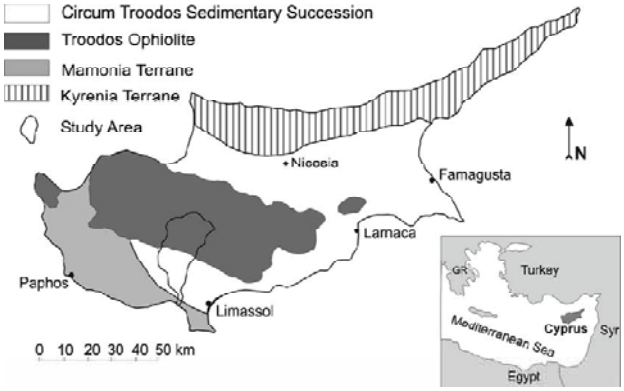

Figure 1.4. *Main geological terrains in Cyprus (from Boronina et al. 2005)*

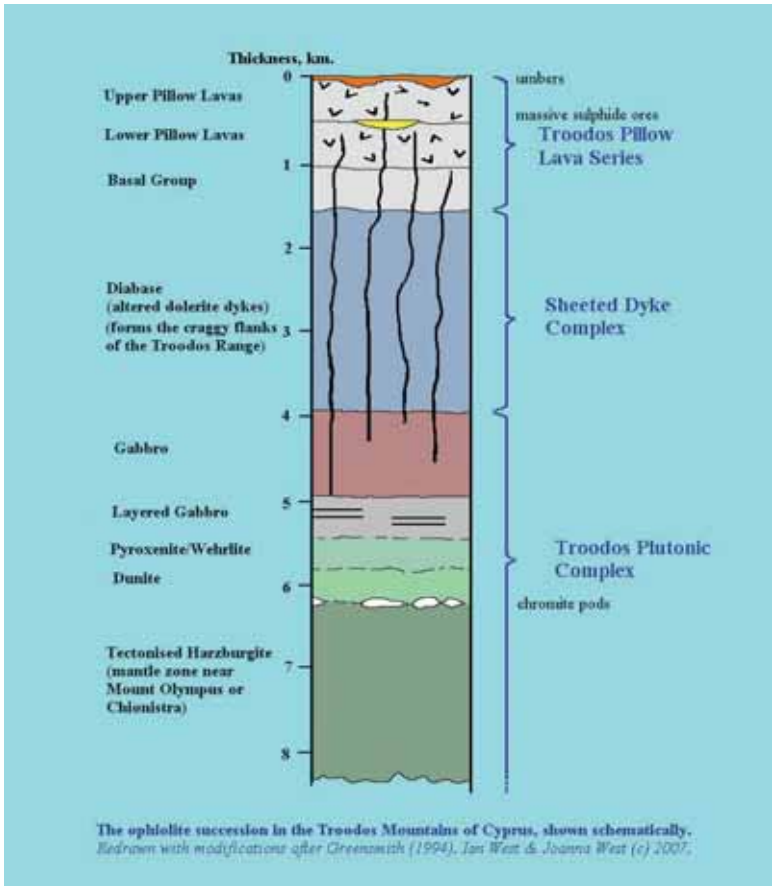

Figure 1.5. *Schematic lithographic section of the Troodos ophiolite (from West, 2007). The 'umbers' at the top of the sequence include bentonites.*

1.4.2 Sedimentary sequences

The sediments of the Troodos ophiolite are shown in Table 1.1.

Sediments between the Pillow Lavas

The sedimentary deposits which overlie the Lower Pillow Lava unit and are themselves overlain by the Upper Pillow Lavas unit (Figure 1.5) are represented by commonly metalliferous mudstones and siltstones with occasional horizons of volcaniclastic sandstones. The thickness of this sedimentary unit ranges from a few centimetres to 250 m (MacLeod 1990).

Volcanoclastic breccias

The volcaniclastic breccias and sandstones of the Troodos ophiolite directly overlie the eroded surface of the Upper Pillow Lavas or forms interbeds in the basalts. This unit has its widest distribution along the Arakapas (Transform) Fault (Simonian and Gass 1978), and can be subdivided in this region into two members: a lower, chaotic, and an upper, stratified part. This

Table 1.1. *Details of the Troodos ophiolite sedimentary carapace (from Robertson et al. 2003).*

<table>
<tr><th colspan="3">Age (Ma)</th><th>Formation</th><th>Lithology</th></tr>
<tr><td>2.0</td><td colspan="2">Pleistocene</td><td rowspan="2">'Fanglomerate'
Apalos
Kakkaristra
Athalassa</td><td rowspan="2">Conglomerates and Sandstones, Calcarenite, Sandstones, Conglomerates</td></tr>
<tr><td rowspan="2">5.2</td><td colspan="2" rowspan="2">Pliocene</td></tr>
<tr><td>Nicosia</td><td>Marls, Silts, Muds, Sandstones, Conglomerates</td></tr>
<tr><td rowspan="4">23.3</td><td rowspan="4">Miocene</td><td rowspan="2">Upper</td><td rowspan="3">Kalavasos</td><td rowspan="3">Evaporites</td></tr>
<tr><td rowspan="3">Pakhna</td></tr>
<tr><td>Middle</td><td rowspan="2">Pelagic Chalks, Marls, Calcarenites, Conglomerates</td></tr>
<tr><td>Lower</td><td>Reefal and Bioclastic Limestone</td></tr>
<tr><td>35.4</td><td colspan="2">Oligocene</td><td>Upper Lefkara[1]</td><td>Pelagic Chalk and Marls</td></tr>
<tr><td>56.5</td><td colspan="2">Eocene</td><td rowspan="2">Middle Lefkara</td><td>Massive Pelagic Chalks</td></tr>
<tr><td>65.0</td><td colspan="2">Palaeocene</td><td>Pelagic Chalks, Replacement Chert</td></tr>
<tr><td>74.0</td><td colspan="2">Maastrichtian</td><td>Lower Lefkara</td><td>Pelagic Chalks</td></tr>
<tr><td>83.0</td><td colspan="2">Campanian</td><td>Kannaviou</td><td>Volcaniclastic Sandstones, Bentonite</td></tr>
<tr><td>90.4</td><td colspan="2">Turonian</td><td>Perapedhi</td><td>Umbers[2], Radiolarites</td></tr>
<tr><td colspan="5">Ophiolitic Basement</td></tr>
</table>

unit has been interpreted as an ophiolitic olistostrome that was deposited along the depression of the transform fault. The clastics of the lower member were formed by submarine erosion and collapse of the steep slopes of the fault sidewalls. The upper member was formed by high-density debris flows and turbidites. Volcanic activity continued during deposition of the breccia unit. The lower member is well exposed near Perapedhi village (032520, 034520) and it is represented by dark-gray, brownish-gray and black chaotic breccia without any stratification, with rectangular, non-rounded

[1] Formerly the Lapithos Group

[2] This is often no more than a field classification, however, and can also include bentonites (see comments in Wilson and Ingham, 1959; Christidis, 2006).

fragments of gabbro-diabases and pillow lavas ranging in size from 1-50 cm. Importantly, the breccia has a clayey or tuffaceous matrix which may be worth examining as a bentonite analogue.

The Perapedhi Formation

The Perapedhi Formation (Turonian-Lower Campanian, Table 1.1) consists mainly of umbers that are distributed over the palaeo-depressions in the Upper Pillow Lavas as lenses of various thickness. Deposition of the Perapedhi sediments is believed to have taken place directly after the formation of the Troodos ophiolites, and before their collision with the allochthonous Mamonia Complex (Robertson and Woodcock 1979). The Perapedhi Formation type section is located near Perapedhi village and can be examined in a road cut near Saittas village (150 m from the Perapedhi-Saittas-Kouka road connection; around 032530, 034520). The sequence is represented by (Bragina and Bragin 1996):

- volcaniclastic breccias with a tuffaceous matrix and fragments of basalt and diabase. The observed thickness in this outcrop is 1 m.
- red and yellow to rust-colored clays which fill the depressions on the eroded surface of the breccias. The thickness varies from 0 to 1 m.
- black and dark-brown loose manganese-bearing mudstones with weakly rounded fragments (up to 2 cm) of yellowish-gray phosphatic clayey limestones (8-10 cm). Thickness is 0.1-0.2 m.
- umbers that are dark brown and yellow, platy, sometimes massive, with brownish-black intercalations of massive Fe/Mn bearing cherts

According to Bragin et al. (2005), much of these umbers are composed of "...uncrystallised substance and mixed-layered mineral like smectite-illite with minor goethite. Nearly 25 % of the total volume of these rocks is represented by an argillirated volcanoclastic [*sic*] substance (secondary clayey material)." In the central part of the Akamas Peninsula (around 032230, 035001), the umbers of the Perapedhi Formation (0.5 m) lie upon the Upper Pillow Lavas and is itself directly overlain in this section by the bentonitic clays of the Kannaviou Formation.

Finally, it is of note that umbers in the area of the Mamonia Allochthonous Complex include hyaloclastite intercalations composed of vitroclasts and fragments of basaltoids (up to 7-10 cm in size) are completely replaced by dioctahedrical smectite-like montmorillonite.

The Kannaviou Formation

The Kannaviou Formation (Campanian-Lower Maastrichtian, Table 1.1) is represented by bentonites that lie on the Perapedhi Formation and directly on the Upper Pillow Lavas. The Kannaviou Formation is widely distributed along the southern flank of the Troodos Massif and in the area of the Mamonia Terrain (see Figures 1.4). The Formation thickness varies between several 10s of m up to 100m at the type locality (near Kannaviou village; 032350, 034550). The lower part is exposed along the Kannaviou-Pano Panagia (032380, 034550) road. Green non-layered bentonites with

intercalation of clayey siltstones lie directly on the Upper Pillow Lavas and are overlain by greenish-gray bentonites, tuffaceous sandstones, and thin-layered light gray cherty mudstones. A final exposure is at the Mavrokolymos River (032240, 034530) where the bentonites lie on umbers and Upper Pillow Lavas. The total thickness of the basal unit is ~25m.

The upper part of the Kannaviou Formation has been studied (Bragina and Bragin, 1995) along the Kritou Marattou-Agios Dimitrianos road (032330,034555 to 032325,034540) and it consists of greenish-gray bentonites and massive, interlayers of light-gray cherty claystone and greenish-gray tuffaceous siltstones. A 2m thick horizon in the lower part of the outcrop consists of white and light-gray massive lithoclastic tuffs and the total thickness of the upper unit is ~30m.

Finally, there are currently several working bentonite quarries on Cyprus (Table 1.2) and these may allow access to the base of the bentonite.

Table 1.2. *Operating bentonite mines on Cyprus.*

Mine	**Location**	**Operator**
Pentakomo	033135, 034440	Peletico Penta Ltd
Troulloi	033380, 035030	Peletico Penta Ltd
Drapia	033175, 034480	Drapia Mining Co.
Monagroulli	033125, 034445	Drapia Mining Co.
Parsata	033160, 034497	Drapia Mining Co.
Kato Moni	033055, 035045	Oryktako Ltd

1.4.3 Production of the hyperalkaline groundwaters

The hyperalkaline pH values (generally between pH 10 and 11) observed in the groundwaters are a product of the serpentinisation of the ophiolites, a reaction which has several possible pathways with the exact reaction pathway depending on Mg content of the precursor olivine/pyroxene or serpentine product, CO_2 fugacity, water-rock ratio, Ca^{2+} content of groundwater, etc.

When considering the origin of the hyperalkaline groundwaters at most ophiolites, two processes generally need to be considered:

- high to medium temperature alteration
- low temperature precipitation

The former often shows itself in the form of pervasive serpentinisation of the entire mantle sequence and is presumed to be pre- or syn-tectonic. This hydrothermal alteration may be characterised by the reaction:

$6Mg_2SiO_4 + Mg_3Si_4O_{10}(OH)_2 + 9H_2O \rightarrow 5Mg_3Si_2O_5(OH)_4$ equation 1
forsterite talc serpentine

which fixes the upper temperature of serpentine formation at 500°C (Moody, 1976). In addition, serpentinisation may occur at slightly lower temperatures (down to 180°C at atmospheric pressure), but as these are all associated with the original alteration on the seabed, they are considered no further here. Of more relevance to the conditions of meteoric groundwater circulation of interest here is low temperature serpentinisation (e.g. Barnes and O'Neil 1969; Barnes et al. 1972). In this case, $Mg(HCO_3)_2$-type meteoric groundwaters react with the ultramafic rocks of the ophiolite in an essentially open system and produce $Ca(OH)_2$-type (spring) waters. The partial reactions may be expressed as (but see also alternatives in Moody 1976):

olivine dissolution

$3H_2O + 2\,Mg_2SiO_4 \rightarrow 5Mg_3Si_2O_5(OH)_4 + Mg^{2+} + 2OH^-$ equation 2
forsterite serpentine

$2H_2O + Fe_2SiO_4 \rightarrow 2Fe(OH)_2 + SiO_2$ equation 3
fayalite

pyroxene dissolution

$2H_2O + 3MgSiO_3 \rightarrow Mg_3Si_2O_5(OH)_4 + SiO_2$ equation 4

$H_2O + FeSiO_3 \rightarrow Fe(OH)_2 + SiO_2$ equation 5

$H_2O + CaSiO_3 \rightarrow Ca^{2+} + 2OH^- + SiO_2$ equation 6

precipitation

$3(Mg^{2+} + 2OH^-) + 2SiO_2 \rightarrow Mg_3Si_2O_5(OH)_4 + H_2O$ equation 7

along with the groundwater components:

$Mg^{2+} + HCO_3^- + OH^- \rightarrow MgCO_3 + H_2O$ equation 8

$Ca^{2+} + HCO_3^- + OH^- \rightarrow CaCO_3 + H_2O$ equation 9

Of course, without full petrological details and kinetic information, the total reaction equation is always indeterminate. Nevertheless, from the viewpoint of the cement leachate analogy, it is worth noting that:

- the fluid output (Table 1.3) contains low Mg and SiO_2, regardless of the input water chemistry, so they are conserved within the system
- equation 7 involves a balance between Mg (from equation 2) and the input groundwater, with SiO_2 derived from equations 3 to 6 – so serpentine precipitation is buffered by differential olivine-pyroxene dissolution
- hydroxide is produced in equations 2, 3, 5 and 6, but the $(Mg^{2+} + 2OH^-)$ of equation 2 is consumed in equation 7, leaving only Ca and Fe sources, with Ca likely to dominate based on the source mineralogy

- any HCO_3^- in the input groundwater is generally consumed in equations 8 and 9, giving rise to aragonitic, magnesitic to dolomitic secondary carbonates and output groundwaters dominated by Ca-OH-Na-Cl compositions

The serpentinite mineral assemblages are very strongly reducing and the hyperalkaline waters are often effervescent with H_2 and/or CH_4 gas. Some of the reaction pathways are also strongly exothermic, frequently producing hydrothermal groundwaters: although only one thermal spring has been reported in Cyprus (Neal and Shand, 2002), they are commonplace in the ophiolites of the Philippines, for example (Alexander et al. 2008a).

Table 1.3. *Hydrochemistry of hyperalkaline groundwaters: examples from around the world for comparison with the Cyprus groundwater data and low pH cement leachates. All data in ppm.*

Location	**pH**	**Na**	**K**	**Ca**	**Mg**	**Cl**
Cyprus[1]						
Cyprus 3a	11.5	385	15.1	1.0	0.3	420.0
Cyprus 3b	11.2	163.0	1.2	93.0	0.5	190.0
Worldwide[2]						
Greece	11.3	24.0	1.0	34.0	0.3	15.0
Bosnia	11.7	35.0	1.5	29.0	7.0	20.0
Oman	11.5	132	4.8	34.0	1.3	127.5
PNG	10.8	15.0	3.0	14.0	2.3	22.0
Western USA	11.5	19.0	1.0	40.0	0.3	63.0
Philippines[3]						
Manleluag 1	11.1	28.0	0.5	18.6	0.2	17.4
Manleluag 2	10.4	20.6	0.4	18.1	---	15.8
Poon Bato	10.9	18.4	0.9	33.1	0.05	20.9
Narra 1	10.8	158	0.9	3.1	0.0	95.0
Narra 3	10.3	157	0.9	2.4	0.1	80.0
Cement leachate[4]						
ALL-MR f63	11.0	42	7.3	20	<0.5	52
OL-SR f63	10.0	4400	150	4300	0.56	13000

1: Neal and Shand (2002) 2: Neal and Stanger (1983) 3: Alexander et al. (2008a) 4: Vuorinen et al. 2005

2 SITE DESCRIPTION

2.1 Preliminary site investigation

All sites visited in the preliminary site investigation in November/December, 2008 are listed for completeness in appendix 1 and plotted in Figure 2.1. Short descriptions of each site are provided and include GPS co-ordinates (all of which are set to UTM zone 36 S) and photographs where appropriate. Note that spelling is generally phonetic and varies from road sign to road sign and map to map – a common example is Ayos and Agas, which are completely interchangeable.

Figure 2.1. *Location of preliminary sampling sites across south-west Cyprus (with thanks to Garmin GPS).*

2.2 Detailed site investigation

The second field campaign, in February, 2009, focussed on those sites which appeared most likely to offer the best chance of observing hyperalkaline leachate/bentonite/ bentonite analogue reaction in some form or another. Unfortunately, the field time available was not enough to allow detailed examination and sampling at all sites identified in the reconnaissance study and this is discussed further in the concluding chapters.

Brief descriptions of the sampling sites are presented in the following sections and full details (and additional photographs) of the sampling sites for groundwaters and solid phase samples are summarised in appendices 2 and 3 respectively.

2.3 Allas Springs

2.3.1 Introduction

The Allas Springs (Figure 2.2) are located ~5 km ENE of Mount Olympus, the highest point of Cyprus (1952 m). They are a sequence of surface seeps in the steep, north-facing Argaki tou Karvouna valley at an elevation of ~1200-1300 m, some distance above the local Cyprus Forestry Department office and picnic site (at Platania). Most of the springs have been contained in concrete cisterns by the Forestry Dept. for use in irrigation and fire fighting and, as such, it has not yet proven possible to directly access the seeps. It is of note, however, that all the cisterns include gas vents and most of the seeps appeared to be emitting gas.

Figure 2.2. *Satellite image of the Allas Springs area, northern Troodos.*

2.3.2 Sites A1-1, A1-2, A1-3 and A1-4

These four high pH groundwater sampling sites, within the Allas Springs area, represent a sequence along a line of flow from: (i) an up-slope discharge point (A1-1) on the

eastern hillside of the main Allas Springs valley, through (ii); an intermediate point (A1-3) about 6-10 m down-gradient of A1-1; to a lower discharge point (A1-2) in the eastern bank of the main Allas Springs stream, about 30 m down stream of A1-1; to the lower discharge point (A1-4), approximately 3-4 m downstream of A1-2.

Site A1-1

At Site A1-1 groundwater discharges with artesian flow through a steeply inclined N-S oriented fracture within a block of relatively fresh harzbergite forming a prominent outcrop up to 4 m high, located within a small gully on the eastern wall of the main Allas Springs valley and about 30 m above where the unmade forest road crosses the main Argaki tou Karvouna valley streambed (Figure 2.3). This fracture strike corresponds to the regional orientation of youngest fractures in the Troodos (Gass et al. 1994).

Figure 2.3*. Site A1-1. Hyperalkaline groundwater discharging with artesian flow through a steeply inclined fracture in harzbergite. Travertine (tufa) is deposited over the harzbergite surface as the discharging Ca-rich hyperalkaline groundwater reacts with atmospheric CO2. The brown straining is caused by biofilms or bacterial mats coating the surface of the travertine deposit. Allas Springs, Troodos.*

The margins of the conductive fracture, at the sides of the outcrop through which groundwater originally flowed, have become sealed by calcareous precipitates (travertine) and the groundwater currently flows up the fracture plane to spill over the lip of the fracture and down over the surface of the rock beneath (Figure 2.3). The

harzbergite outcrop is fresh and hard, with little visual evidence of weathering alteration. Boulders at the foot of the outcrop are extensively coated with travertine (e.g. Figure 2.4). The travertine itself is competent and hard, forming a "ribbed" flowstone over the sub-vertical surface of the outcrop beneath the discharge point, where the Ca-rich high-pH groundwater has interacted with CO_2 from the air. The surface of the travertine deposit is streaked by a brown-to-orange gelatinous coating or film of odourless organic matter that probably represents biofilm or bacterial mat.

Figure 2.4. *Site A1-1. High pH groundwater was sampled by collecting water dripping from a broken stalactite/flowstone "rib" on the underside of the travertine-coated harzbergite block. Orange-brown biofilm or bacterial mat stains and coats the outer surface of the travertine. Allas Springs, Troodos.*

Groundwater was collected directly into a glass bottle, from drips discharging from a broken stalactitic projection on the surface of the ribbed flowstone (Figure 2.4). Approximately 2 litres of groundwater water were collected this way within 60 minutes. Temperature, dissolved O_2, pH and conductivity were measured directly in the water on-site at the time of collection. Samples of travertine and harzbergite associated with the discharging groundwater were also collected.

Site A1-3

The groundwater discharging from fractures in the harzbergite at site A1-1 flows through the poor forest soil developed on scree. The surface of the soil is coated in a thick deposit of litter (> 0.5 m) comprising pine needles, woody branch fragments and twigs, leaves and reed-like grasses. Reed-like grass grows on the surface of the litter. The litter is impregnated and cement by tufa to a depth of at least 0.5 m (Figure 2.5).

A shallow pit (30 cm deep) was dug into the litter and rapidly filled with hyperalkaline groundwater. Samples of groundwater were collected by dipping bottles into the water collecting in the pit. Temperature, dissolved O_2, pH and conductivity were measured directly in the water on-site at the time of collection. Samples of travertine/carbonate-cemented forest litter were collected.

Figure 2.5. *Site A1-3. High pH groundwater seeps through the soil and along the top surface of the soil, coating and cementing the organic forest litter of wood fragments, twigs, pine needles, leaves and grass, within in hard pale brown deposit of calcareous travertine/tufa. Allas Springs, Troodos.*

Site A1-2

Site A1-2 lies approximately 30 m downslope of Site A1-1. It is located in the eastern bank of the main Allas Springs stream draining the valley from Troodos Mountain ridge to the south, just above the point where the unmade forestry road crosses the Allas Springs stream. Here, the groundwater is collected in large concrete cisterns (Figure

2.6) for local irrigation further down the valley. The cisterns were vented (via open steel pipes) for gas to prevent any possible build up of H_2/CH_4. The high-pH groundwater seeps through a poorly-sorted deposit of soil, scree or colluvium, at the interface with serpentinite bedrock (Figure 2.7). The sepentinite bedrock is highly fractured with fine scale (1- 10 mm) fracture spacings, and very altered to a soft to clay-like consistency. Groundwater seeps through the fine fractures in the serpentinite as well as along the colluvium (scree)-serpentinite interface and through the colluvium (scree) itself.

Water was collected directly into Nalgene® plastic bottles at small flowing seeps along the colluvium-serpentinite interface, in the bank immediately behind the concrete cisterns (Figure 2.6). Temperature, dissolved O_2, pH and conductivity were measured directly in the water on-site at the time of collection. Samples of travertine/carbonate-cemented colluvium and altered serpentinite were collected.

Figure 2.6. *Sampling site A1-2. Concrete cisterns collecting high-pH groundwater for local irrigation supply. The hyperalkaline groundwater was sampled at small seeps through altered serpentinite and harzbergite scree (colluvium) within the stream bank behind the concrete cisterns. Open steel pipes vent gas (?H2/CH4) exsolved from the groundwater. Allas Springs, Troodos*

Site A1-4 is situated very close to, and about 3 m north of, A1-2. Like A1-2, this also corresponds to a small spring discharge in the eastern bank of scree/colluvium located close to forestry road, at confluence of small valley draining from A1-1 and the main mountain stream draining northwards from high Troodos ridge. However, the water appears to be derived from flow that may be draining the hillside slightly further north

of the flow along the gully from A1-1, through A1-3 to A1-2.

The spring discharge is collected in a concrete cistern for local irrigation purposes. Water was collected for analysis from the discharge at interface between colluvium/scree/soil and highly fractured bedrock surface

Figure 2.6. *Sampling site A1-2. Small spring seepages of high-pH groundwater discharge through altered serpentinite and harzbergite scree (colluvium) within the stream bank and are associated with pale brown deposits of travertine/tufa, which coat and cement the scree. Allas Springs, Troodos.*

2.3.3 Site A6

Site A6 is located about 50 m further down the valley below Site A1-2. It is located in the steep stream gully below and to the north of the forest road. Here the high pH groundwater discharges through highly fractured serpentinite, which varies in alteration from hard competent serpentinite with calcium carbonate coatings resting on earlier haematitised and hydrothermally mineralised fracture surfaces (often with fibrous serpentine minerals), to highly altered and “argillised”, soft, plastic serpentinite.

Water was collected from strong flows discharging directly from fractures in the serpentinite. Temperature, dissolved O_2, pH and conductivity were measured directly in the water on-site at the time of collection.

2.3.4 Site A2

Site A2 is located about 16 m upstream of A1-2. High pH groundwater discharges through stoney soil and scree at the base of old tree roots, exposed in the eastern bank of the main Allas Springs stream (Figure 2.7). A concrete cistern embedded into the base of the stream bank below the seepage collects the groundwater seeping through fractures in the underlying serpentinite (Figure 2.7). Unlike the cisterns at A1-2, this cistern was not gas-vented. The surfaces of some serpentinite clasts within the soil around the seeps are coated with a thin calcium carbonate film, and the soil itself is very weakly impregnated with patches of the same cement.

Groundwater seeping through the soil just above the soil-bedrock interface was collected in a glass bottle pushed gently into the stoney gravel at the base of the soil. Temperature, dissolved O_2, pH and conductivity were measured directly in the water on-site at the time of collection

2.3.5 Site A3

Site A3 is located 10-15 m upstream of Site A2. The site is very similar to Site A2, with high-pH groundwater discharging through fractured harzburgite and along interface between soil/scree and underlying bedrock, exposed in the eastern bank of the main Allas Springs stream. Groundwater was sampled for analysis in the same way as at A2. Temperature, dissolved O_2, pH and conductivity were measured directly in the water on-site at the time of collection

2.3.6 Site A5

Sampling site A5 is very similar to A1.2, A1.4, A2 and A3 and is located within the eastern bank of the main Allas Spring stream, approximately 10 m upstream of A3. Here high pH groundwater discharges along the interface between colluvium/soil/scree and the underlying altered serpentinite bedrock, and through the highly altered and highly fractured serpentinite itself. The water is also collected in a large concrete cistern for local irrigation purposes. Water and altered serpentinite bedrock were collected for analysis from the discharge through highly fractured bedrock just below the interface between colluvium/scree/soil and the serpentinite (Figure 2.7).

Figure 2.7. *Sampling site A2. Hyperalkaline groundwater seeps through stoney soil beneath vegetation in the top of the bank. A concrete cistern is embedded into fractured serpentinised harzbergite to collect the groundwater for local irrigation. Allas Springs, Troodos.*

Figure 2.8. *Sampling site A5. high-pH groundwater seeps through highly fractured and altered ("argillised") serpentinite bedrock (pale green) just below the interface with overlying colluvium, in the bank of the stream. Allas Springs, Troodos.*

2.3.7 Site A4

This site is the highest of the Allas Springs, at over 1300m, and it issues from a horizontal, tufa-filled fracture or joint at the top of the harzburgite/base of altered gabbro (Figure 2.9). The tufa-filled horizon is broken by vertical N-S faults separated every 5-10m or so.

Figure 2.9a and b. *Left – view from NE, thick (15-25cm) tufa deposits mark the A4 site at Allas Springs. The tree in the background is ~4m tall. Right – view from NW, thick, almost colloform tufa very clear.*

Additional springs occur to the west of A4, clearly marked by thick tufa deposits. Although flow is currently restricted to 3 or 4 points across a distance of 2-300m, there is evidence of widespread alteration across the site.

Figure 2.9c. *Heavily altered harzburgite near A4 spring, immediately west of the stream (clay/soil sample A4-1-1 collected ~30cm to right of pen).*

Groundwater sample was collected at approximately 7m vertically below the seep (climbing equipment will be required to get any closer) and solid phase samples were collected immediately adjacent to the stream. It was not possible to observe any gas release at the spring itself (observation point is too low down).

2.4 Valley E1

This sampling area is in an unnamed valley immediately southeast of the Argaki tou Karvouna valley which contains the Allas Springs and is accessed by a strenuous walk over the intervening ridge (Figure 2.10). The valley is characterised by steep scree slopes and, although flowing water could be heard below the scree, no samples could be collected until reaching the valley bottom at ~1250m, by which time atmospheric reaction had buffered the waters to below pH10. Several solid phase samples displaying reaction were collected and one groundwater sample (E1-1) was collected near the valley bottom.

Figure 2.10. *Ridge (~1600m) between the Argaki tou Karvouna valley containing the Allas Springs and valley E1.*

2.5 Chrisovrysi Springs

2.5.1 Introduction

The Chrisovrysi Springs area (Figure 2.11) is situated about 2.5 km northwest of the village of Pano Amiandos, and 1 km northeast of the large disused open-cast Amiandos Asbestos Mine (seen in the south west corner of the satellite image in Figure 2.11). The springs are located on the south eastern flank of one of the main northeast-trending ridges of the Troodos and which separates this valley from the Allas Springs on the opposite flank of the same ridge ~2 km to the northwest. Three sites were sampled (see appendix 1 for details):

- sampling site C1 was a decorative limestone cistern by the roadside, located on the B9 road from Platania to Troodos Square

- C2 is located on the hillside about 50m above the B9 road and the C1 site. High pH spring water is piped from several seepages and collected in a series of large concrete cisterns. This water flows further down to C1
- C3 is located within a small stream gully draining the hillside about 20 m above the B9 road and about 20 m north of C1

Figure 2.11. *Satellite image of the Chrysovrysi Springs area, Troodos. The extensive area of terraced excavations representing the former Amiandos open-cast chrysotile asbestos mine can be seen in the bottom left corner of the image.*

2.6 Parsata Spring and road cutting

The original spring is to the west of Parsata village and below the main road (Figure 2.12). It is dry in all but the very wettest periods and the groundwater (pH11.4) is currently accessed by a farmer's borehole and pump (Figure 2.13). This borehole is sitting on top of the bentonite/bentonite analogue and penetrates ~30 m through the bentonite into the PLV below. Approximately 150 m immediately to the west of the borehole there is a narrow gully (Figure 2.14) which contained a small trickle of neutral water. The stream has eroded through the bentonite and down onto the weathered PLV below, so the bentonite has a maximum thickness of ~15-20 m at this point.

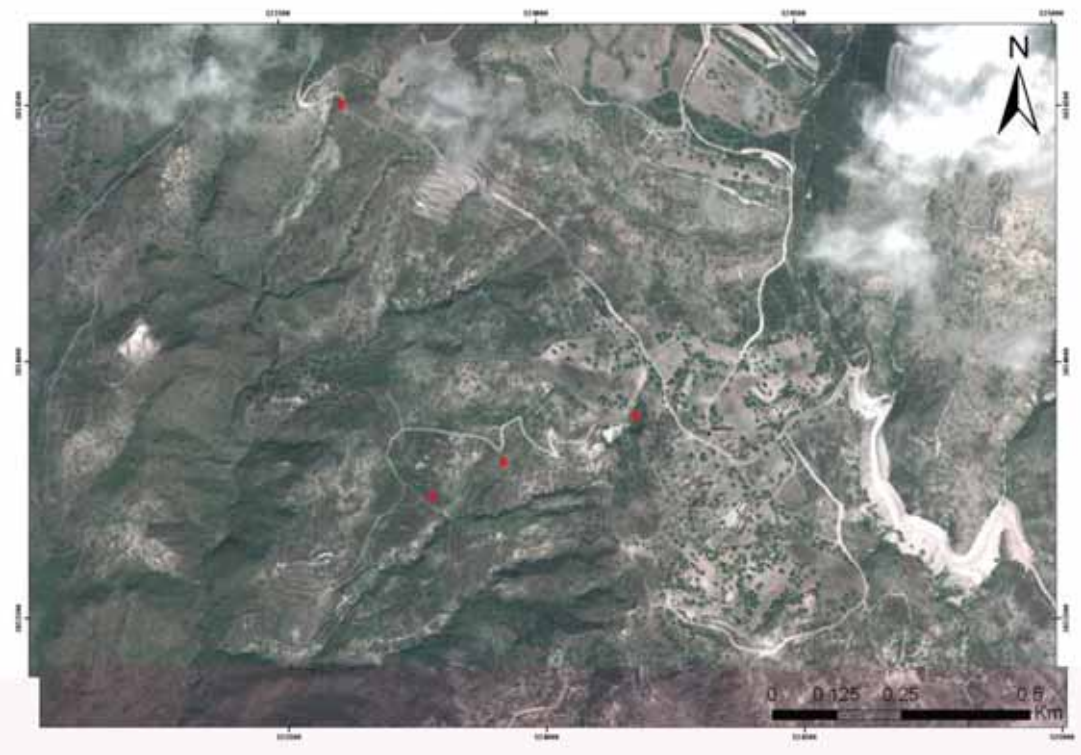

Figure 2.12. *Satellite view of the area around Parsata Spring (marked here by the red pin to the west of Parsata (Parsada) village, middle right of image).*

Figure 2.13. *Typical pumped well (grey cylinder in middle ground) on a farm near Parsata, southwest Cyprus (looking south). Note the solar panels which power the pump.*

Figure 2.14. *Gully in bentonite/bentonite analogue just below and to the west of the Parsata Spring farm borehole (see Figure 2.13).*

A sequence of samples was collected in a road cutting (most northerly red pin in Figure 2.12) across the contact between altered autobrecciated basalt pillow lava and interstitial sediment between the basalt pillows (Figure 2.15). The sequence is cut by tufa-lined fractures (details in appendices 2 and 3).

Figure 2.15. *A sequence of samples was collected across autobreccia and associated samples to the NW of Parsata village.*

2.7 Trimiklini

This site is a road cutting on the F812 between Trimiklini and Agios Mamas (see Figure 2.16). A vertical profile was sampled through an exposure of parallel-laminated marly clay and silt resting on altered PLV and autobrecciated PLV. The pillows are highly altered with steep irregular tufa or carbonate veins penetrating the overlying sediments.

Figure 2.16. *The Trimiklini site, a road cutting on the F812 between Trimiklini and Agios Mamas. Heavily altered PLV at the base is overlain by laminated marly clays and silts.*

Immediately to the west and north of the site, the sediments have been quarried leaving the surface of the PLV exposed. It is assumed that the material was removed due to the high smectite content of the sediments (see chapter 4), but it may also have been to access pockets of manganese lying on top of the PLV and below the sediments.

2.8 Waterfall site

The so-called 'Waterfall' site is accessed vie a builder's yard on the west side of the road from Ayos Mamas to Limassol (see appendix 1 for details). The site is spectacular (Figure 2.17), featuring a 'waterfall' of tufa some 30 m high. Just above the waterfall, the land opens into a verdant valley centred on the small stream which feeds the waterfall. The stream bed consists of tufa (mixed with vegetation) lying on top of heavily altered PLV (Figure 2.18). The pH of the stream decreased from 8.4 just above the waterfall to 7.2 at the spring source, some 300 m upstream. It appears likely that small seeps of hyperalkaline groundwater are slowly leaking out of the PLV into the stream, so increasing the pH and Ca concentration, leading to the extensive tufa precipitation. One groundwater sample (D2) was collected here.

Figure 2.17. *The waterfall site on the west side of the Ayos Mamas to Limassol road. Concrete parapet in the right foreground is ~1 m high.*

Figure 2.18. *Mixture of tufa, vegetation and altered PLV in the stream bed feeding the tufa waterfall.*

3 SAMPLING AND ANALYTICAL METHODS

3.1 Groundwater and solid phase sampling

Groundwater sampling was carried out using hand-held, mobile equipment. To maintain the same standards between different operators (and the same operator on different days – see discussion in Ota et al. 2009), a standardised routine was used:

- The sample bottles were labelled and the preservation procedures (Table 3.1.1) carried out beforehand to minimise contamination in the field
- Sufficient sample bottles (including spares), syringes and filters were made up into an individual pack for each site, again to minimise any possible contamination
- Groundwaters were drawn directly from the source in a 50 mL syringe (after a full volume had been used to rinse the syringe) and a disposable, sealed 0.45 μm nominal pore size filter was then placed over the end of the syringe. Approximately 5 mL of sample was then used to rinse the filter (filtrate discarded) before the sample bottles were then filled. A new filter was used for each sample split[3].
- Sample bottles were then placed in sealed plastic bags to minimise contamination and stored in a cool box until shipping for analysis (at BGS)

On-site measurement of pH, temperature, conductivity and dissolved oxygen were made (see Figure 3.1.1). pH, temperature and conductivity were determined by specific ion electrodes, using portable meters. pH (±0.01 pH unit) and temperature (±0.1°C) were determined using a Ross combination glass electrode. BGS had found that this type of electrode had previously proved very reliable for use in the study of high pH groundwaters at Maqarin and in experimental laboratory studies of high pH pore fluid-rock interaction (Linklater, 1998; Smellie, 1998). The pH electrode was calibrated with standard buffer solutions at pH 4, 7 and 10. The conductivity probe was calibrated using a KCl conductivity standard solution. The instruments were calibrated each time they were used to measure a sample collected.

Dissolved oxygen was determined using portable CHEMets® dissolved oxygen test kits. The kits utilised disposable, self-filling glass ampules for colorimetric analysis of water quality. The ampule contains a solution of colorimetric reagent sealed under vacuum. The unfiltered groundwater sample is placed in a specialised snap-cup' which facilitates breaking off the end of the ampule. The vacuum in the ampule pulls the sample up from the snap cup into the ampule when the tip is broken off. After tilting the ampule several times to mix the sample and reagent, and waiting for the colour to develop, the colour is visually compared to a standard reference set of sealed ampules containing pre-developed reagent corresponding to known dissolved oxygen concentrations. Two kits were used to cover the ranges 0.1-1 ppm and 1-10 ppm dissolved oxygen

[3] In this instance, there was no intention to collect colloid samples. Where this is the case, multiple filters would be utilised – see discussion in Alexander (2009).

Water samples were sub-sampled and preserved directly on-site as follows (summarised in Table 3.1.)

Major and Trace Cations
Two 30 mL samples were collected for the analysis of major cations (Ca, Mg, Na, and K), total S and Si. These were sampled by using a plastic syringe to minimise atmospheric contact, and filtered 'on-line' through 0.45 µm pore diameter Acrodisc® disposable nylon filter cartridges directly into Nalgene bottles. The samples were preserved by acidification to 1 % with respect to AristaR® nitric acid. The bottles were completely filled to allow no headspace. A blank reference sample was prepared on-site using double-distilled water (provided by the BGS) and processed using the same protocol. Separate 125 mL samples were collected and preserved in the same manner for determination of trace cations.

Major and Trace Anions, Total Organic Carbon and Total Inorganic Carbon
30 mL samples were collected for the analysis of major anions (Cl, SO4, NO3, NO2), Total Organic Carbon (TOC) and Total Inorganic Carbon (TIC). These were sampled by using a plastic syringe to minimise atmospheric contact, and filtered 'on-line' through 0.45 µm pore diameter Acrodisc® disposable nylon filter cartridges directly into Nalgene bottles. The samples were preserved unacidified and the bottles completely filled to allow no headspace. A blank reference sample was prepared on-site using double-distilled water (provided by the GSD) and processed using the same protocol.

Reduced Sulphur
30 mL samples for determination of reduced sulphur were taken by plastic syringe directly at the sampling points. The samples were not filtered but were preserved to 1 % with respect to sodium hydroxide, by the addition of a pellet of sodium hydroxide. The bottles completely filled to allow no headspace. A blank reference sample was prepared at the GSD using double-distilled water (provided by the GSD) and processed using the same protocol.

Ammonium
30 mL samples for the analysis of ammonium were sampled and filtered as for major and trace cations but were preserved by acidification to 1 % with respect to AristaR sulphuric acid. A blank reference sample was prepared at the GSD using double-distilled water (provided by the BGS) and processed using the same protocol.

Ferrous Iron
15 mL samples were collected and preserved for the determination of ferrous iron using a plastic syringe and filtered through a 0.45 µm pore diameter Acrodisc® disposable nylon filter cartridges directly into Sterylin® polycarbonate tubes, to which 1 mL of 1 % 2,2-dipyridyl solution (hydrochloric acid acidified) had previously been added. The volume was made up to 10 mL. The 2,2-dipyridyl forms a stable red complex with ferrous iron in solution. A blank reference sample was prepared at the GSD using double-distilled water (provided by the GSD) and processed using the same protocol.

Stable Isotopes
28 mL samples of water were collected for stable isotope ($\delta^{18}O$ and δD) analysis. The samples were unfiltered and stored in glass bottles, which were filled to leave no headspace.

Table 3.1.1. *Sample split preservation for selected inorganic determinands.*

Container	**Split label**	**Procedure***	**Technique/ Determinand(s)**
2 x 30 ml Nalgene	F/HNO_3	Completely fill both containers with filtered sample then carefully add two or three drops of concentrated nitric acid using a Pasteur pipette	ICP-AES cations
30 ml Nalgene	F/UA	Completely fill container(s) with filtered sample	IC anions, NPOC, pH and alkalinity
30 ml Nalgene	F/NH_4^+	Completely fill both containers with filtered sample then carefully add two or three drops of concentrated sulphuric acid using a Pasteur pipette	Ammonium
30 ml Nalgene	UF/NaOH	Using a spatula, add one pellet of sodium hydroxide to the empty container then carefully fill completely with **unfiltered** sample: N.B. this reaction is exothermic	Sulphide
15 ml Sterylin® polycarbonate	Fe^{2+}	Fill a tube, pre-loaded at the BGS and shipped, with 1 ml of 1 % 2,2-dipyridyl solution (hydrochloric acid acidified), to the 15 ml graduated mark with filtered sample	Reduced iron
28 ml glass	Stable O+H	Completely fill container with **unfiltered** sample.	Stable isotopes
500 ml glass	^3H	Fill bottle leaving a small headspace (c.25 ml)	Tritium

* Filtered through 0.45 μm nominal pore size, Acrodisc® sealed disposable nylon filter cartridges

Figure 3.1.1. *On site measurement of pH, temperature, conductivity and dissolved oxygen.*

3.2 X-ray diffraction analysis

38 samples were analysed using a variety of X-ray diffraction (XRD) techniques in the Mineralogy Laboratories at BGS. The samples were initially jaw-crushed and the subsamples were taken prepared as milled powders in an agate ball mill. Subsamples of both jaw-crushed and milled powders were taken for XRD analysis. Full sample details and the XRD technique(s) applied to each are summarised in appendix 4.

3.2.1 Whole rock XRD sample preparation

In order to achieve a fine and uniform particle-size for whole-rock XRD analysis, c.3 g of the milled powders were micronised under acetone for 10 minutes and then spray dried following the method and apparatus described by Hillier (1999) and then front-loaded into the stainless steel sample holders.

3.2.2 Clay fraction separation and preparation of oriented XRD mounts

Approximately 10 g jaw-crushed material was dispersed in deionised water using a reciprocal shaker combined with treatment with ultrasound. The resulting suspensions were then sieved on 63 μm and the <63 μm material placed in measuring cylinders and allowed to stand. In order to prevent flocculation of the clay crystals, 1 ml 0.1M 'Calgon' (sodium hexametaphosphate) was added to each suspension. After a period determined using Stokes' Law, a nominal <2 μm fraction was removed and dried at 55 °C.

Approximately 100 mg of the <2 μm material was then re-suspended in a minimum of deionised water and pipetted onto a ceramic tile in a vacuum apparatus to produce an

oriented mount. The mounts were Ca-saturated using 2 ml 0.1M $CaCl_2.6H_2O$ solution and washed twice to remove excess reagent and allowed to dry at room temperature.

3.2.3 Whole-rock XRD analysis

XRD analysis was carried out using a PANalytical X'Pert Pro series diffractometer equipped with a cobalt-target tube, X'Celerator detector and operated at 45kV and 40mA. The whole-rock samples were scanned from 4.5-85°2θ at 2.76°2θ/minute. The diffraction data were then initially analysed using PANalytical X'Pert Pro software (PANalytical, 2006a,b) coupled to the latest version (ICDD, 2008) of the International Centre for Diffraction Data (ICDD) database.

Following identification of the mineral species present in the samples, mineral quantification was achieved using the Rietveld refinement technique (e.g. Snyder & Bish, 1989) using Siroquant v2.5 software. This method avoids the need to produce synthetic mixtures and involves the least squares fitting of measured to calculated XRD profiles.

Errors for the quoted mineral concentrations are typically ±2.5 % for concentrations >60 wt%, ±5 % for concentrations between 60 and 30 wt%, ±10 % for concentrations between 30 and 10 wt%, ±20 % for concentrations between 10 and 3 wt% and ±40 % for concentrations <3 wt% (Hillier et al. 2001). Where a phase was detected but its concentration was indicated to be below 0.5 %, it is assigned a value of <0.5 %, since the error associated with quantification at such low levels becomes too large.

3.2.4 Specific phase analysis

Where the mineralogy of a specific phase(s) was required from particular samples (e.g. different precipitate layers within travertine (tufa) deposits, small samples were removed from the parent hand-specimen rock sample with a scalpel blade and were then hand-ground in an agate pestle and mortar. Approximately 10 mg of this powdered material was then deposited onto the surface of a 'zero-background' silicon crystal from suspension using a single drop of acetone. The silicon crystal mounts were scanned using the same analytical program as the whole-rock mounts.

3.2.5 Clay mineral analysis

Clay fraction (nominally <2 μm) oriented mounts were scanned from 2-40°2θ at 1.02°2θ/minute after air-drying, ethylene glycol solvation and heating at 550 °C for 2 hours. Clay mineral species were then identified from their characteristic peak positions and their reaction to the diagnostic testing program.

In order to gain further information about the nature of the clay minerals present in the samples, modelling of the <2 μm glycol-solvated XRD profiles was carried out using Newmod-for-Windows™ (Reynolds & Reynolds 1996) software.

Modelling was also used to assess the relative proportions of clay minerals present in the <2 μm fractions by comparison of sample XRD traces with Newmod-for-Windows™ modelled profiles. The modelling process requires the input of

diffractometer, scan parameters and a quartz intensity factor (instrumental conditions), and the selection of different sheet compositions and chemistries. In addition, an estimate of the crystallite size distribution of the species may be determined by comparing peak profiles of calculated diffraction profiles with experimental data. By modelling the individual clay mineral species in this way, *mineral reference intensities* were established and used for quantitative standardisation following the method outlined in Moore & Reynolds (1997).

3.3 Petrographical analysis

3.3.1 Optical petrography

The samples were prepared as polished thin sections following vacuum impregnation with epoxy-resin. A blue dye was added to the epoxy-resin in order to highlight the porosity during optical petrographical examination. The samples were then observed in transmitted light using a petrological microscope.

3.3.2 Scanning electron microscopy methods

After preliminary optical microscopic examination the polished sections were examined by backscattered scanning electron microscopy (BSEM). BSEM images provide high-resolution mineralogical and spatial information on mineral relationships and rock microfabric, based on differentiation of the average atomic number of the different phases (Goldstein et al. 1981). Microchemical information obtained by energy-dispersive X-ray microanalysis (EDXA) - recorded simultaneously during BSEM observations - was used to identify minerals on the basis of their chemistry.

BSEM-EDXA analyses were performed using a LEO 435VP, variable pressure digital scanning electron microscope, fitted with an Oxford Instruments ISIS 300 digital EDXA system and a KE-Developments four-element solid-state backscattered electron detector. BSEM-EDXA observations were typically made using a 10 to 20 kV electron beam accelerating potential and 100 to 800 pA beam currents. EDXA observations were largely semi-quantitative but occasionally more quantitative information was required for mineral identification and obtained by processing X-ray spectra using the Oxford ISIS 300 SEMQuant© software package.

Mineral and major elemental distributions were examined in selected polished thin sections by microchemical mapping with the EDXA system. Maps were acquired from selected areas of the sections for Si, Ti, Al, Fe, Mg, Ca, Na, K, S and P. Cl was also included in the mapping suite since it provides a proxy for porosity due to the presence of a small amount of Cl in the epoxy resin (i.e. indicates areas of sample porosity impregnated by epoxy-resin). Images of elemental concentrations are processed and displayed on a ‘rainbow colour scale’ where progressively increasing concentration is displayed in a sequence of colours from black (zero concentration), progressively through blue, green, yellow, orange, to red (high concentration).

The instrument was largely operated under conventional high-vacuum mode (i.e. $<10^{-4}$ torr). To facilitate this, the polished sections were coated under vacuum with a thin film of carbon approximately 25 nm thick (using an EMITECH 960L carbon evaporation-

coating unit), to provide them with an electrically conductive surface prior to examination in the scanning electron microscope.

3.4 Rock chemical analysis

3.4.1 Introduction

Whole-sample chemical composition of rocks and soil samples was determined by X-ray fluorescence spectrometry (XRFS) at the BGS Analytical Geochemistry Laboratories. Major and minor oxides were analysed as fused beads by Wavelength Dispersive X-ray Fluorescence Spectrometry (WD-XRFS). Trace elements were analysed as pressed powder pellets by WD-XRFS and Energy Dispersive Polarised X-ray Fluorescence Spectrometry (ED(P)-XRFS). In addition, samples were analysed for Loss on Ignition (LOI) gravimetrically. This work is covered under UKAS accreditation. The laboratory is a UKAS accredited testing laboratory, No. 1816.

3.4.2 Loss on Ignition (LOI)

The samples were dried overnight at 105°C before LOI and fusion. Loss on ignition was determined after 1 hour at 1050°C. Approximately 1 g of sample was weighed accurately into a porcelain crucible. The crucible was weighed before and after heating and the two weights compared. The resulting relative loss or gain in sample weight was reported as the LOI. Quality Control (QC) was monitored by the regular analysis of three materials covering the range of LOI values found in most geological and related materials.

3.4.3 Fused bead major and minor oxide WD-XRFS Analysis

Fused beads were prepared by fusing 0.9000 g sample plus 9.000 g flux (66/34 $Li_2B_4O_7$ and $LiBO_2$) at 1200°C. After fusion the melt was cast into a 40 mm glass bead which was then analysed by WD-XRFS.

The XRF spectrometer used was a Philips MagiX-PRO with a 60 kV generator and 4 kW rhodium (Super Sharp) end–window X-ray tube. The instrument is controlled via a PC running PANalytical SuperQ XRF application packages (PANalytical, 2008). The PANalytical calibration algorithm is used to fit calibration curves and inter-element effects are corrected by theoretical alpha coefficients, calculated by the PANalytical method. All spectral backgrounds and peaks are corrected for instrument drift using two external ratio monitors.

Routine calibrations cater for a wide variety of environmental and geological matrices; the application quantifies 19 elements on fused beads, calibrated as oxides with the reporting limits shown in Table 3.4.1. The lower limits of detection (LLD) were calculated from instrument sensitivity at calibration and lower limits of reporting (LLR) were calculated from the LLDs. The upper reporting limits (URL) were determined from the highest concentration standard used on the calibration.

Fused bead QC was monitored by the analysis of two bulk rock materials chosen for their variety of matrix type and analyte values. The results were entered into run charts for statistical analysis using a Statistical Process Control (SPC) package.

3.4.4 Sample preparation for pressed powder pellet analysis by XRFS

Pressed powder pellets are prepared by grinding 12.00 g of sample and 3.00 g of binder in an agate planetary ball mill for 30 minutes. The mixture is then pressed at 25 tons load into 40 mm diameter pellets. The binder used is a mixture of 9 parts EMU120FD, a styrene copolymer, and 1 part Ceridust 3620, a micronised polyethylene wax.

3.4.5 Pressed Powder Trace Element WD-XRFS Analysis (Sc-Mo and Nd-U)

The XRF spectrometer used was an Axios Advanced with a 60 kV generator and 4 kW rhodium (Super Sharp Max) end–window X-ray tube. The instrument is controlled via a PC running PANalytical SuperQ XRF Pro-Trace application packages.

For trace element analysis, a set of synthetic standards (Pro-Trace) is used to calibrate the instruments and to determine background and spectral interference correction factors. The PANalytical Pro-Trace calibration algorithm is used to fit calibration lines, applying matrix correction using mass attenuation coefficients and jump edge correction for the iron, manganese and titanium absorption edges. The Pro-Trace package also corrects for background, tube spectral lines and spectral line overlap interferences. The calibrations were validated by analysis of a wide range of Reference Materials.

Quality Control is maintained by regular analysis of two glass monitor samples containing 47 elements at nominally 30 ppm and 300 ppm and the results entered into run charts for statistical analysis using a SPC package. Lower limits of detection (LLD) are theoretical values for the concentration equivalent to three standard deviations (99.7 % confidence interval) above the background count rate for the analyte in an iron-rich alumino-silicate matrix. High instrumental stability results in the practical detection limits for most elements in silicates approaching the theoretical values. LLDs are calculated from a matrix blank and the synthetic Pro-Trace standards using Equation . The lower (LLR) and upper limits (URL) of reporting for the slow speed, low LLD WD-XRFS application used for the analysis are shown in Table 3.4.2.

Equation 10. The theoretical lower limit of detection

$$\text{L.L.D.} = \frac{3}{m}\sqrt{\frac{R_b}{T_b}}$$

Where:

m = sensitivity (counts per second per %)

R_b = the background count rate (counts per second)

T_b = the counting time on the background (s)

3.4.6 Pressed Powder Trace Element ED(P)-XRFS Analysis (Ag-Ce)

The ED(P)-XRFS Spectrometer used was an Epsilon 5 with 100 kV generator, 600W gadolinium side–window X-ray tube with liquid nitrogen cooled germanium detector. The polarising target used was an Al_2O_3 Barkla target and matrix correction was achieved by means of Compton scatter using a CsI target. The lower (LLR) and upper limits of reporting (URL) for the slow speed, low LLD ED(P)-XRF application used for the analysis are shown in Table 3.4.3

Table 3.4.1. *Fused Bead Major Element Lower Limits of Detection, Lower and Upper Reporting Limits.*

Oxide	LLD (%) 3σ	LLR (%)	URL (%)
Na_2O	0.009	0.05	50
MgO	0.006	0.05	100
Al_2O_3	0.002	0.01	100
SiO_2	0.002	0.01	100
P_2O_5	0.002	0.01	50
SO_3^*	0.004	0.1	75
K_2O	0.002	0.01	50
CaO	0.002	0.01	100
TiO_2	0.002	0.01	100
Cr_2O_3	0.003	0.01	25
Mn_3O_4	0.002	0.01	100
Fe_2O_3	0.003	0.01	100
NiO*	n.d.	0.01e	25
CuO*	n.d.	0.01e	25
ZnO*	n.d.	0.01e	25
SrO	0.003	0.01	1
ZrO_2	0.004	0.02	100
BaO	0.005	0.02	100
PbO*	n.d.	0.02e	10

Fe_2O_3t represents total iron expressed as Fe_2O_3.
SO_3 represents sulphur retained in the fused bead after fusion at 1200°C.
SO_3, NiO, CuO, ZnO, PbO are not included in the UKAS Accreditation Schedule
n.d. not determined
e estimated

Table 3.4.2. *WD-XRFS Pressed Powder Trace Element Lower and Upper Reporting Limits [Slow speed, low LLD application (PS-S-U)].*

Analyte	LLR ppm	URL ppm
Sc	1	2000
V	1	4500
Cr	1	25000
Co	1	3000
Ni	1	14000
Cu	1	12000
Zn	1	12000
Ga	1	2000
Ge	1	2000
As	1	4000
Se	1	2000
Br	1	2000
Rb	1	8500
Sr	1	4000
Y	1	2000
Zr	1	2000
Nb	1	2000
Mo	1	2000
Nd	3	2000
Sm	3	2000
Hf	1	2000
Ta	1	2000
W	1	2000
Tl	1	2000
Pb	1	10000
Bi	1	2000
Th	1	2000
U	1	2000

Table 3.4.3. *ED(P)-XRFS Pressed Powder Trace Element Lower and Upper Reporting Limits [Slow speed, low LLD application (PC-Ag-Ce)].*

Analyte	LLR ppm	URL ppm
Ag	0.5	2000
Cd	0.5	2000
In	0.5	2000
Sn	0.5	2000
Sb	0.5	2000
Te	0.5	2000
I	1.0	2000
Cs	1.0	3000
Ba	1.0	5000
La	1.0	2000
Ce	1.0	2000

3.5 Groundwater analysis

Most of the analysis of the groundwater samples was carried out in the Analytical Geochemistry Laboratories of the BGS which are accredited by the United Kingdom Accreditation Service (UKAS Testing Laboratory 1816). The groundwater samples were analysed by the following methods.

3.5.1 Cation analysis

Cations were determined using inductively coupled plasma-atomic emission spectrometry (ICP-AES). The nitric acid-preserved groundwater samples were aspirated into an argon plasma and undergo rapid desolvation, atomisation and ionisation with the resultant emission of characteristic radiation from the excited atoms and ions. ICP-AES analysis is carried out on a Varian/Vista AX CCD simultaneous instrument. The instrument views the plasma along its axis and is equipped with a high resolution echelle polychromator with a 70,000 pixel charge coupled device (CCD) detector with continuous wavelength coverage from 167-785 nm. The system is controlled by a dedicated PC, running software supplied by the instrument manufacturer.

3.5.2 Anion analysis

Anions were determined using ion chromatography (IC). A known volume of sample is injected into a mobile eluent phase which passes through a separating column containing a stationary phase which differentially retards the aqueous anions, according to charge and charge mass, relative to the mobile phase. The anions are detected by suppressed conductivity detection and UV/visible absorbance detection using a Dionex DX-600 Ion Chromatograph system. The whole system is controlled and data captured by a dedicated PC, installed with the Chromeleon Software.

3.5.3 Ammonium analysis

Ammonium was determined on the filtered and sulphuric acid preserved water samples by colourimetric analysis. Ammonium is strongly affected by the sampling method and the amount of free ammonia present varies with pH. Above pH12, the ammonium/ammonia equilibrium in solution is such that over 90% exists as free ammonia. However, the pH of all of the groundwaters sampled is <pH 12. Therefore, it seems unlikely that any significant ammonia will have been lost from these moderately high pH groundwaters during sample collection and filtering in the field. Nevertheless, for waters approaching pH12 the ammonium values should probably be regarded as minimum values and this should be taken into consideration when interpreting the data.

3.5.4 Reduced Iron (Fe^{2+})

Ferrous iron was determined by colourimetric analysis on filtered and acidified water samples preserved with the chromogenic reagent 2,2-dipyridyl which forms a stable ferrous iron complex in solution. The deterioration of this complex is considered to be negligible over the timescale between sample collection and analysis. The validity of the data can also be checked by comparing the results for the colorimetric determination

of ferrous iron with the determination of total iron by ICP-AES. The value for reduced iron should not exceed that of the total iron (within analytical error).

3.5.5 Oxidised Iron (Fe^{3+})

Ferric iron is assumed to be the difference between the measured total iron and the measured total ferrous iron. In the case of these Cyprus groundwater samples the determined ferrous iron contents were all below detection limit. Therefore, it may be assumed that, within analytical error, all of the iron present is in the ferric form.

3.5.6 pH and speciated alkalinity analysis

pH was measured potentiometrically by immersing a hydrogen ion selective electrode and a reference electrode into the solution to be analysed. Alkalinity was measured titrimetrically by monitoring the change in pH of the solution as a function of the volume of titrant added. The pH and total alkalinity measurements are made on a Radiometer TIM 865 TitraLab with accompanying PC software TitraMaster 85 Data Collector.

3.5.7 Total organic carbon

Total organic carbon (TOC) of water samples was determined as non-purgeable organic carbon (NPOC) content. This was carried out using a Shimadzu TOC-V CPH analyser with an associated ASI-V auto-sampler. The system is controlled and data captured by a PC, installed with TOC Control V Software. NPOC analysis involves the removal of inorganic carbon content by acidification and sparging prior to analysis. The oxidation of organic carbon to carbon dioxide is achieved by high temperature combustion; the evolved carbon dioxide is then measured using a non-dispersive infra-red (NDIR) detector.

3.5.8 Reduced sulphur

Reduced sulphur (sulphide) was determined using colorimetric analysis at an UKAS accredited external laboratory.

3.5.9 Stable isotope analysis

Stable isotopes were determined by isotope ratio mass spectrometry using a gas source mass spectrometer. These analyses fall outside the scope of UKAS accreditation.

3.5.10 Tritium analysis

Tritium analysis was determined by liquid scintillation counting using an accredited external laboratory.

4 ANALYTICAL RESULTS

4.1 Mineralogical analysis

4.1.1 Whole rock XRD analysis

The results of quantitative whole-rock XRD analyses are summarised in Tables 4.1.1 and 4.1.2. The samples from the Allas and Chrisovrysi Springs sites (samples series numbered A* and C*) are composed of more than 90 % of the serpentine-group mineral, lizardite (as both 1M and 1T forms). Traces of quartz, garnet (andradite pyroxene (diopside), calcite, aragonite, dolomite, and the complex Mg-Fe hydroxycarbonate pyroaurite ($Mg_6Fe_2(SO_4,CO_3)(OH)_{16}.4H_2O$), brucite, halite and magnetite were also sporadically identified in these samples.

The sample from the Waterfall site (sample D2) is composed of major amounts of quartz, anorthite and amphibole (tremolite) with subordinate pyroxene (diopside), K-feldspar, analcime, chlorite and smectite together with a trace of calcite.

Samples from the road cutting on the F812 between Trimiklini and Agios Mamas (sample series numbered T*) are predominantly composed of pyroxene (diopside) and smectite with subordinate anorthite, phillipsite and calcite and traces of quartz, amphibole (tremolite), analcime, 'mica' (undifferentiated mica species possibly including muscovite, biotite, illite and illite/smectite etc) and talc.

The samples from the Parsata area are predominantly composed of anorthite, calcite, smectite, pyroxene and K-feldspar with sporadic quartz, analcime, 'mica' and talc.

4.1.2 Specific phase analysis

The results of quantitative XRD analyses on white crusts removed from the surface of four of the samples (three from the Allas Springs and one from the Chrisovrysi Springs) are summarised in Table 4.1.3. All the crusts appear to be predominantly composed of calcite with subordinate aragonite present in samples A4 and C3 and subordinate lizardite in samples A4, A6 and C3. A trace of garnet was also identified in sample A1-1-2.

The results of quantitative <2 μm XRD analyses are summarised in Table 4.1.4.

During the <2 μm-size separation process, several of the samples from the Allas and Chrisovrysi Spring locations (A4-4-1, A5-2, C3-1, C3-2, C3-3 and C3-4) demonstrated a dramatic flocculation of clay minerals (Figure 4.1.1).

Table 4.1.1. *Summary of quantitative whole-rock X-ray diffraction analysis.*

Original sample name	MPL code	Silicates						Zeolites		Carbonates/hydrated carbonates			
		andradite	anorthite	diopside	K-feldspar	quartz	tremolite	analcime	phillipsite	aragonite	calcite	dolomite	pyroaurite
A1-2	MPLN807	2.5	nd	1.1	nd	1	nd	nd	nd	nd	0.7	nd	nd
A2-1	MPLN808	1.7	nd	1.2	nd	1.3	nd	nd	nd	nd	nd	nd	nd
A2-2	MPLN809	1.5	nd	1.2	nd	1.3	nd	nd	nd	nd	0.7	nd	nd
A3-1	MPLN810	0.6	nd	nd	nd	<0.5	nd	nd	nd	nd	<0.5	<0.5	5.1
A3-2	MPLN811	2.5	nd	nd	nd	<0.5	nd	nd	nd	nd	<0.5	1.1	0.6
A3-3	MPLN812	1.8	nd	2.1	nd	<0.5	nd	nd	nd	nd	<0.5	1.7	1.2
A4-1	MPLN813	2.9	nd	0.9	nd	0.6	nd	nd	nd	nd	0.6	<0.5	nd
A4-2-1	MPLN815	2.4	nd	1.2	nd	nd	nd	nd	nd	3	1.3	nd	1.1
A4-2-2	MPLN816	3.2	nd	nd	nd	0.5	nd	nd	nd	6.9	1.4	nd	0.9
A4-4-1	MPLN821	1	nd	nd	nd	<0.5	nd	nd	nd	nd	9.3	nd	nd
A4-4-2	MPLN822	1.2	nd	nd	nd	0.7	nd	nd	nd	3.8	6.7	nd	0.5
A5-1	MPLN824	1.3	nd	nd	nd	<0.5	nd	nd	nd	0.7	<0.5	nd	3.3
A5-2	MPLN825	1	nd	nd	nd	<0.5	nd	nd	nd	nd	nd	nd	2.2
C2-1	MPLN827	0.5	nd	nd	nd	0.5	nd	nd	nd	nd	<0.5	nd	nd
C2-2	MPLN828	1.1	nd	nd	nd	<0.5	nd	nd	nd	nd	nd	nd	nd
C3-1	MPLN829	5.6	nd	nd	nd	<0.5	nd	nd	nd	nd	nd	nd	nd
C3-2	MPLN830	1	nd	nd	nd	<0.5	nd	nd	nd	nd	0.7	nd	nd
C3-3	MPLN831	nd	nd	nd	nd	0.5	nd	nd	nd	0.8	0.6	nd	0.8
C3-4	MPLN832	1.4	nd	nd	nd	<0.5	nd	nd	nd	0.5	1.2	nd	0.9
D2	MPLN837	nd	36.2	4.5	3.6	26.5	17	2.8	nd	nd	0.8	nd	nd
T2	MPLN839	nd	2.5	45.6	nd	nd	1.3	nd	6.5	nd	5.1	nd	nd
T3	MPLN840	nd	4.3	36.6	nd	<0.5	0.7	1.8	6.1	nd	3.6	nd	nd
T4	MPLN841	nd	4.1	31.8	nd	<0.5	0.8	2.3	6.2	nd	6.1	nd	nd
T5	MPLN842	nd	3.8	31.6	nd	0.7	0.9	2.1	5.2	nd	10.3	nd	nd

Table 4.1.1. *cont. Summary of quantitative whole-rock X-ray diffraction analysis*

Original sample name	MPL code	Phyllosilicates/clay minerals							Others		
		chlorite	kaolinite	lizardite-1M	lizardite-1T	'mica'	smectite	talc	brucite	halite	magnetite
A1-2	MPLN807	nd	nd	59.6	35.1	nd	nd	nd	nd	nd	nd
A2-1	MPLN808	nd	nd	59.3	36.5	nd	nd	nd	nd	nd	nd
A2-2	MPLN809	nd	nd	60.3	35	nd	nd	nd	nd	nd	nd
A3-1	MPLN810	nd	nd	56.5	37.3	nd	nd	nd	nd	nd	nd
A3-2	MPLN811	nd	nd	62.2	32.8	nd	nd	nd	nd	nd	nd
A3-3	MPLN812	nd	nd	59.7	33.2	nd	nd	nd	nd	nd	nd
A4-1	MPLN813	nd	nd	63	31.8	nd	nd	nd	nd	nd	nd
A4-2-1	MPLN815	nd	nd	58.9	32.1	nd	nd	nd	nd	nd	nd
A4-2-2	MPLN816	nd	nd	57.3	29.8	nd	nd	nd	nd	nd	nd
A4-4-1	MPLN821	nd	nd	64.3	23.8	nd	nd	nd	1.3	<0.5	nd
A4-4-2	MPLN822	nd	nd	59	27.6	nd	nd	nd	0.5	nd	nd
A5-1	MPLN824	nd	nd	59	35.3	nd	nd	nd	nd	nd	nd
A5-2	MPLN825	nd	nd	73.1	23.4	nd	nd	nd	nd	nd	nd
C2-1	MPLN827	nd	nd	59.9	38.9	nd	nd	nd	nd	nd	nd
C2-2	MPLN828	nd	nd	63.3	35.3	nd	nd	nd	nd	nd	<0.5
C3-1	MPLN829	nd	nd	66.8	27.1	nd	nd	nd	nd	nd	nd
C3-2	MPLN830	nd	nd	74.5	23.4	nd	nd	nd	nd	nd	<0.5
C3-3	MPLN831	nd	nd	64.4	32.7	nd	nd	nd	nd	nd	<0.5
C3-4	MPLN832	nd	nd	66.1	29.6	nd	nd	nd	nd	nd	<0.5
D2	MPLN837	3.2	1.3	1.7	nd	nd	2.4	nd	nd	nd	nd
T2	MPLN839	nd	nd	nd	nd	<0.5	39	nd	nd	nd	nd
T3	MPLN840	nd	nd	nd	nd	nd	46	0.6	nd	nd	nd
T4	MPLN841	nd	nd	nd	nd	nd	47.9	<0.5	nd	nd	nd
T5	MPLN842	nd	nd	nd	nd	nd	45.4	nd	nd	nd	nd

Table 4.1.2. *Summary of quantitative whole-rock X-ray diffraction analysis*

Original sample name	MPL code	Silicates						Zeolites		Carbonates/hydrated carbonates				Phyllosilicates/clay minerals							Others		
		andradite	anorthite	diopside	K-feldspar	quartz	tremolite	analcime	phillipsite	aragonite	calcite	dolomite	pyroaurite	chlorite	kaolinite	lizardite-1M	lizardite-1T	'mica'	smectite	talc	brucite	halite	magnetite
T6	MPLN843	nd	3	22.9	nd	0.8	<0.5	1	2.8	nd	32.1	nd	nd	nd	nd	nd	nd	nd	36.9	nd	nd	nd	nd
T7	MPLN844	nd	3.4	20.2	nd	1.5	<0.5	1	2.7	nd	38.6	nd	nd	nd	nd	nd	nd	nd	32.8	nd	nd	nd	nd
P2-1	MPLN845	nd	58.2	6.4	1.6	5.7	2.9	nd	nd	nd	17.8	nd	nd	nd	nd	nd	nd	2.2	5.2	nd	nd	nd	nd
P2-2	MPLN846	nd	42.8	16.3	3.1	3.7	nd	nd	nd	nd	26.9	nd	nd	nd	nd	nd	nd	nd	2	5.2	nd	nd	nd
P2-3	MPLN847	nd	41.1	20.2	3	4.2	nd	nd	nd	nd	26.3	nd	nd	nd	nd	nd	nd	nd	2.1	3.1	nd	nd	nd
P3-1	MPLN849	nd	26.1	2.5	6.4	nd	nd	2	nd	nd	14.1	nd	nd	nd	nd	nd	nd	nd	49.2	nd	nd	nd	nd
P3-2	MPLN850	nd	4.8	nd	3.6	0.9	nd	nd	nd	nd	71.5	nd	nd	nd	nd	nd	nd	nd	19.2	nd	nd	nd	nd
P3-3	MPLN851	nd	25.9	nd	8.8	nd	nd	nd	nd	nd	23.8	nd	nd	nd	nd	nd	nd	nd	41.5	nd	nd	nd	nd
P3-4	MPLN852	nd	20.1	nd	15	nd	nd	nd	nd	nd	21.1	nd	nd	nd	nd	nd	nd	nd	43.8	nd	nd	nd	nd

Table 4.1.3. *Summary of selected phase(s) X-ray diffraction analysis.*

Original sample name	MPL code	Silicates						Zeolites		Carbonates/hydrated carbonates				Phyllosilicates/clay minerals							Others		
		andradite	anorthite	diopside	K-feldspar	quartz	tremolite	analcime	phillipsite	aragonite	calcite	dolomite	pyroaurite	chlorite	kaolinite	lizardite-1M	lizardite-1T	'mica'	smectite	talc	brucite	halite	magnetite
A1-1-2	MPLN805	<0.5									99.6												
A4	MPLN814									8.0	88.7					3.3							
A6	MPLN826										91.3					8.7							
C3	MPLN834									7.5	90.8					1.7							

KEY
nd not detected;
'mica' undifferentiated mica species including muscovite, biotite, illite and illite/smectite etc

Despite repeated washing, dilution of the amount of suspended material and the addition of different dispersion agents, these samples continued to almost instantaneously produce large, centimetre scale-sized flocs (Figure 4.1.2). Such persistent behaviour is very unusual. For these samples, due to this pronounced flocculation effect, the size-separation process isolated fine-size fraction was therefore not necessarily <2 μm.

Figure 4.1.1. *Dramatic flocculation behaviour of selected samples from the Allas and Chrisovrysi Springs (samples A4-4-1, A5-2, C3-1, C3-2, C3-3 and C3-4)*

Figure 4.1.2. *Closer view of flocculated suspensions illustrating the centimetre scale-size of the generated clay flocs (sample C3-1 and C3-2).*

XRD analysis suggests that the clay mineral assemblages of the samples are composed of variable amounts of lizardite, smectite, kaolinite, illite, chlorite and talc.

In all cases the separated <2 μm fractions also contain a variety of non-clay minerals including quartz, albite, K-feldspar, calcite, zeolite and pyroaurite.

The following criteria were used to identify and quantify the clay mineral assemblages:

- Lizardite was identified by its characteristic air-dry d_{001} spacings of *c.*7.3 and 3.65Å which remain invariant after glycol-solvation and heating. Quantification was based on the area beneath the lizardite d_{001} peak on the ethylene glycol trace. Peak intensity ratios and Newmod-modelling suggests relatively little Fe-substitution in the lizardite structure (less than one Fe atom per three octahedral sites). Modelling also suggests a range of average mean defect-free distances of between 15 and 50 layers (7Å units) and a size range of up to 80 layers.
- Smectite was identified by its typical air-dry d_{001} spacing of *c.*14.5Å which expands to a similarly typical *c.*17Å on glycol-solvation and collapses under heating to 550°C for 2 hours to an 'illite-like' 10Å d_{001} spacing. Smectite was quantified from the area beneath the d_{001} peak.
- Illite was identified by its characteristic air-dry d_{001} spacing of *c.*10.0Å which remains invariant after glycol-solvation and heating. Quantification was based on the area beneath the illite d_{001} peak on the ethylene glycol trace. Newmod-modelling suggests a range of crystallite-size distributions with mean defect-free distances of between 9 and 15 layers (10Å units) and a size range of between 1 to 65 layers.
- Chlorite was identified by its characteristic air-dry and glycol-solvated basal spacing peaks at 14.2, 7.1, 4.73 and 3.54Å and the presence of a peak at *c.*13.9Å after heating at 550°C. XRD peak intensities and Newmod-modelling suggests an Mg/Fe- chlorite composition with an average mean defect-free distance of 8 layers (14Å units) and a size range of 1 to 28 layers. Where possible, chlorite quantification was based on the area beneath its d_{001} peak on the ethylene glycol trace. However in many cases, considerable peak overlap made such measurements difficult.
- Kaolinite was identified by its characteristic air-dry basal spacings of *c.*7.1 and 3.58Å which remain invariant after glycol-solvation but which disappear after heating at 550 °C due to the meta-kaolinite's X-ray amorphous state. Quantification of kaolinite was based on the area beneath its d_{001} peak on the ethylene glycol trace. Newmod-modelling suggests a range of crystallite-size distributions with mean defect-free distances of between 8 and 45 layers (7Å units) and a size range of between 1 to 90 layers.
- Talc was principally identified and quantified by its characteristic basal spacing peak at 9.35 Å which remains invariant after glycol-solvation and heating. Modelling suggests a mean defect-free distance of 7 layers (9.4Å units) and a size range of between 1 to 20 layers.

The clay mineral assemblages of the samples collected from the Allas and Chrisovrysi Springs sites (sample series numbered A* and C*) are predominantly and often solely composed of the serpentine-group mineral, lizardite. Traces of smectite, kaolinite, illite and chlorite were also identified in some of these samples. Example <2 μm XRD traces for this clay mineral assemblage are shown in Figure 4.1.3.

Table 4.1.4. *Summary of <2 μm clay mineral X-ray diffraction analyses*

Original sample name	MPL code	%clay mineral						Non-clay minerals	Comments
		Lizardite	Smectite	Kaolinite	Illite	Chlorite	Talc		
A1-2	MPLN807	89	nd	5	3	3	nd	quartz	
A2-1	MPLN808	87	1	5	4	3	nd	quartz	
A2-2	MPLN809	86	2	7	2	3	nd	quartz	
A3-1	MPLN810	100	nd	nd	nd	nd	nd	pyroaurite, quartz	
A3-2	MPLN811	89	1	3	4	3	nd	quartz, pyroaurite	
A3-3	MPLN812	100	nd	nd	nd	nd	nd	pyroaurite, quartz	
A4-1	MPLN813	90	1	4	3	3	nd	quartz	
A4-2-1	MPLN815	96	nd	nd	1	2	nd	quartz, pyroaurite	
A4-2-2	MPLN816	94	nd	2	nd	4	nd	quartz, pyroaurite	
A4-4-1	MPLN821	100	nd	nd	nd	nd	nd	quartz	flocculated
A4-4-2	MPLN822	93	nd	5	2	1	nd	quartz, pyroaurite, calcite	
A5-1	MPLN824	100	nd	nd	nd	nd	nd	pyroaurite, quartz	
A5-2	MPLN825	100	nd	nd	nd	nd	nd	quartz	flocculated
C2-1	MPLN827	96	4	nd	nd	nd	nd	quartz	
C2-2	MPLN828	100	nd	nd	nd	nd	nd	quartz	
C3-1	MPLN829	100	nd	nd	nd	nd	nd	quartz	flocculated
C3-2	MPLN830	100	nd	nd	nd	nd	nd	quartz	flocculated
C3-3	MPLN831	100	nd	nd	nd	nd	nd	quartz	flocculated
C3-4	MPLN832	100	nd	nd	nd	nd	nd	quartz	flocculated
D2	MPLN837	nd	76	14	4	5	nd	quartz, calcite	
T2	MPLN839	nd	93	2	6	nd	nd	quartz, calcite, anorthite, zeolite	
T3	MPLN840	nd	99	1	nd	nd	nd	quartz, calcite	
T4	MPLN841	nd	95	5	nd	nd	nd	calcite, quartz	
T5	MPLN842	nd	98	2	nd	nd	nd	quartz, calcite	
T6	MPLN843	nd	96	4	nd	nd	nd	calcite, quartz	
T7	MPLN844	nd	97	3	nd	nd	nd	calcite, quartz	
P2-1	MPLN845	nd	60	4	35	nd	nd	calcite, quartz, zeolite	
P2-2	MPLN846	nd	60	nd	nd	nd	40	calcite, quartz, zeolite	+11.3 Å broad peak (unidentified mineral)
P2-3	MPLN847	nd	46	nd	nd	nd	54	calcite, quartz, anorthite, zeolite	
P3-1	MPLN849	nd	100	nd	nd	nd	nd	calcite, quartz, anorthite	
P3-2	MPLN850	nd	100	nd	nd	nd	nd	calcite, quartz, anorthite	
P3-3	MPLN851	nd	100	nd	nd	nd	nd	calcite, quartz, anorthite	
P3-4	MPLN852	nd	100	nd	nd	nd	nd	calcite, quartz, anorthite	

Interestingly the samples exhibiting the dramatic and persistent flocculation behaviour are characterised by mono-clay-mineralic assemblages of pure lizardite. This is atypical behaviour for lizardite but it is likely to be the result of surface charges produced by the high pH + high Ca chemistry environment However, the clay mineral assemblages of the remaining samples collected from the Waterfall site (sample D2), the road cutting on the F812 between Trimiklini and Agios Mamas (sample series numbered T*) and the Parsata area are smectite-dominated, often at very high (>90 %) concentration levels. Measurements of the d_{060} spacing on the random powder traces proved difficult due to profuse peak overlap in this region but the indicated spacings of c.1.50 Å suggest that the smectite is dioctahedral and probably a montmorillonite. Where other subordinate clay minerals are present, these comprise kaolinite, and rarely illite or talc. Example <2 µm XRD traces for this clay mineral assemblage are shown in Figure 4.1.4.

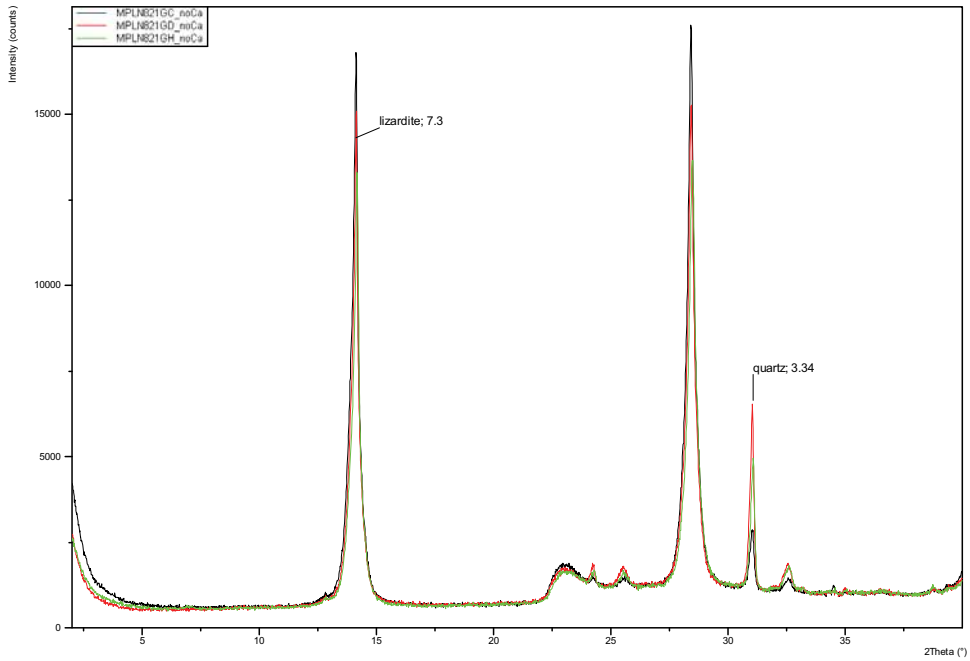

Figure 4.1.3. *Example <2 µm XRD traces, black trace (air dry), red trace (glycol-solvated), green trace (heated 550˚C/2 hours), sample A4-4-1, Allas Springs.*

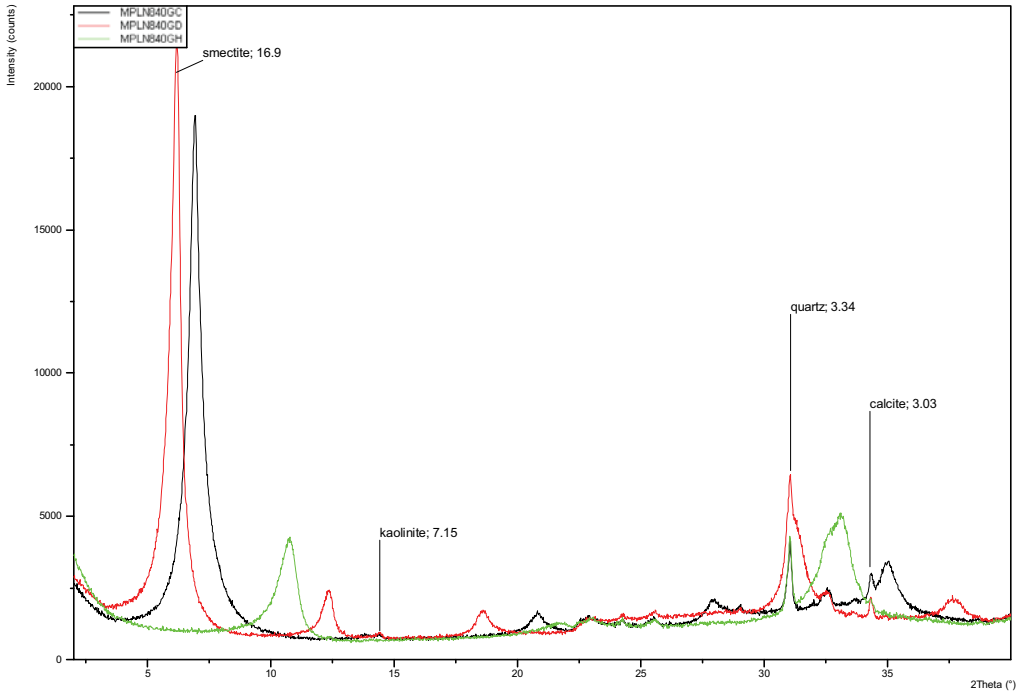

Figure 4.1.4. *Example <2 µm XRD traces, black trace (air dry), red trace (glycol-solvated), green trace (heated 550˚C/2 hours), sample T3, road cutting on the F812 between Trimiklini and Agios Mamas.*

4.2 Petrographical analysis

Note that all the images here are presented at the end of the section. Further, more detailed, descriptions of the samples are provided in appendix 5.

4.2.1 Allas Springs area

Travertine deposits

Travertine deposits were examined from sites A1-1/A1-3 at the Allas Springs area (samples A1-1 (MPLN805 and MPLN806) and A4 (sample A4 (MPLN814).

Flowstone coating the serpentinised harzbergite outcrop at A1-1 (sample MPLN805) comprises finely laminated calcium carbonate dominated by calcite, forming subvertical ribs (with occasional stalactites) locally up to c.100 mm thick at their thickest points. The calcite laminae are between 0.3 and 1.5 mm thick, with abundant vuggy porosity between component laminae (Figure 4.2.1). The calcite layers in the outer layers of the travertine are typically characterised by interlocking anhedral crystals of calcite. These are often prismatic; elongated in the c-axis direction perpendicular to the lamination (Figure 4.2.2). Deeper layers in the travertine are much more porous. These layers preserve a fragmented or “brecciated” carbonate fabric, comprising irregular (often deformed) “sheets” and “globular masses of micritic calcite containing abundant organic inclusions that are cemented by later inclusion-free calcite (Figure 4.2.3). The later calcite forms euhedral microcrystals that line the pores, producing a very vuggy

fabric (Figure 4.2.3). These organic inclusion-rich layers are also present in the later layers of travertine, although they are much less extensively developed. SEM observations also show that organic biofilm may line some of these intercrystalline vuggy pores (Figure 4.2.4)

Detailed BSEM observations show that the organic inclusions within the travertine are biogenic (Figure 4.2.5). They include:

- Clusters of rounded cellular features, with cell-sizes between 1-5 μm. These closely resemble coccoid (spherical) bacterial cells and spirochete bacterial chains
- Elongate cells 1-5 μm in size, and strings of these features resembling rod-like bacterial and bacterial chains. Some of these chains may form spiral or twisted structures that resemble spirochaete bacteria
- Fragments of tiny thread-like or worm-like (sometimes seen to be multicellular) organic structures. Seen in section, each fragment may be only between 5-20 μm in length but together, some fragments may form parts of a sinuous worm-like organism that may reach 50-100 μm in length. In some cases, the have more rounded and broader terminations at one end that may represent a "head-part". Other fragments terminate in sharply pointed ends that may represent a "tail". Larger rounded, globulose or amoeboid cellular features up to 50 μm are also visible.

The cell-walls of these structures have been largely replaced by calcite, and in many cases, the volume contained within the cell wall may be filled or partially-filled by calcite (Figure 4.2.6). However, in many cases, the bulk of the cell volume remains as an unmineralised cavity, which may or may not contain relicts of very fine grained organic matter (Figure 4.2.6).

Some of the preserved coccoid and rod-like features appear to illustrate "cells" undergoing mytosis (cell-division) (Figure 4.2.6). It is postulated here that these features represent fossilised bacterial biofilm or bacterial mats, closely associated with the formation of the travertine and probably very similar to the orange and red-brown modern biofilm that is observed on the external surface of the travertine at the present day (see Figure 2.3 and Figure 2.4). The worm-like or thread-like structures possibly represent nematode worms that could have been grazing on the bacteria and biofilm. Similarly, the amoeboid structures may represent amoebae living within and feeding on the biofilm and bacteria. The fragmented or brecciated fabric observed in the calcite may have developed as a result of shrinkage cause by drying out of the biofilm during periods of drought in the past when the springs may have ceased to flow.

The excellent preservation of these features within the travertine deposit at site A1-1 indicates that a complex microbiological community has developed and was able to thrive in this highly alkaline environment. It contrast markedly with the relative paucity of bacterial activity previously observed in hyperalkaline groundwaters from the Maqarin Natural Analogue Site (Alexander 1992; Linklater 1998; Smellie 1998). The difference in biological activity may be at least partially due to the difference in nutrient availability: the Maqarin groundwater system is very poor in organic nutrients – the

principal carbon source resides within kerogenous material within the Cretaceous and Tertiary host rocks, and this is not easily available to microorganisms (see also discussion in West et al. 1995). In contrast, the A1-1 site at Allas Springs is heavily forested, with an abundance of partially decomposed plant remains in the soil litter layer covering the forest floor, which could provide a much more readily available supply of organic nutrients for microbial activity. The travertine deposits found at the A4 site higher up the Argaki tou Karvouna (Allas Springs) valley also lack evidence of any preserved microbial community. Unlike A1-1, this site is situated on barren rock slopes high up on the mountainside, with little or no vegetation or soil cover to provide a source of organic nutrients. The low nutrient environment at A4 appears unable to support a significant microbiological activity, in contrast to that seen in the forested area lower down the valley at site A1-1.

The travertine carbonate-cemented organic-rich soil litter layer covering the ground surface around the A1-1/A1-3 site (sample MPLN806) is extremely porous (Figure 4.2.7). It comprises abundant loosely packed and partially-decayed pine needles, leaves of deciduous plants, woody twigs and fragments of branches, impregnated and cemented by pale buff-coloured, very fine, micritic and microcrystalline calcium carbonate, dominated by calcite. The travertine varies from unbedded plant debris cemented by calcium carbonate to crudely layered travertine with bands of denser calcium carbonate and bands of more plant debris-rich material.

Much of the plant debris has been petrified by calcite mineralisation. Fine micritic calcite forms a microporous cement binding the plant debris (Figure 4.2.7). Much of this micrite occurs as dense pellets or peds 0.2-1 mm diameter. The peds themselves may be loosely-packed or aggregated in a very open grain fabric. Microcrystalline calcite penetrates and often completely fills the cell cavities within the woody material, pine needles and deciduous leaves (Figure 4.2.8). Much of the original organic cell wall material is very well preserved where the plant cells have been completely filled by calcium carbonate. However, where the calcium carbonate has not completely impregnated the cells, the cell walls can be seen to be breaking down to a more diffuse organic material. Similar microbiological fabrics to those observed in the travertine coating the harzbergite surfaces are also found in this petrified organic litter.

The travertine from the A4 site (sample MPLN814) is very also finely laminated (Figure 4.2.9), with laminae ranging from 0.1-5 mm, often grouped in discrete bands of similar laminae up to 10 mm thick (Figure 4.2.9), similar to travertine coating the fractured harzbergite surfaces at the A1-1 site . The lamination is highlighted in thin section by very fine concentrations of fine clay- and silt-grade detrital sediment. The travertine is composed largely of calcite with minor aragonite (Table 4.1.3), and comprises interlocking c-axis elongated anhedral prismatic crystals of calcite that have grown with the c-axis orientated perpendicular to the lamination, giving the travertine a “fibrous” fabric. Some laminations have high contents of a white powdery aragonite, locally present with fan-like forms (Figure 4.2.10). There is significant porosity along intercrystalline boundaries within the calcite layers. This travertine contains none of the microbiological fabrics seen in travertine from the A1-1.

BSEM observations show that entrained silicate sediment within the travertine is largely composed of clay to fine sand-grade serpentine mineral fragments (identified by XRD as lizardite-1M) and coarser fragments of serpentinite (Figure 4.2.11). This serpentinitic detritus shows no evidence of alteration or replacement by the carbonate along grain boundaries (Figure 4.2.11). In addition to laminae containing serpentinitic detritus, this travertine also contains discrete laminae along which unusual "spherical structures" are concentrated along the surface of the underlying lamina (Figure 4.2.12a). The majority of these spherical features are voids, some of which may be partially filled by calcite or aragonite cement (Figure 4.2.12a). Some features have been completely filled by calcite and are only seen as ghost-like features outlined by a fine dirt fringe within the calcite matrix of the travertine. These voids are remarkable uniform in size (typically, between 20-50 μm diameter and sometimes occur as "clusters" of 2-3 spheres (Figure 4.2.12a). Very rare spherical silicate particles were also found within these spherule-rich layers (Figure 4.2.12b). The particles are highly altered and partially replaced by very fine authigenic clay with a smectitic composition (Na,Ca,Al,Fe-silicate). These particles are interpreted to be altered glass spherules, probably of volcanic dust or aerosol origin, deposited periodically on the surface of the travertine. The particles have the same shape and size as the voids seen in the same laminae. The voids therefore interpreted to result from the dissolution of the glass within the travertine, as a result of interaction with the alkaline groundwater.

Alteration of harzbergite and serpentinite

The wallrock of the fractured the harzbergite coated by travertine in Site A1-1 is composed largely of serpentine minerals, containing relicts of an original coarse grained fabric of olivine (forsterite) and enstatite, with subordinate sphene and chromite (Figure 4.2.13a). The olivine and enstatite are almost completely altered, occurring as corroded relicts within a brecciated fabric cemented and replaced by fine grained serpentine, with fine grains of Fe-Co-Ni oxide disseminated within the serpentine matrix along the margins of the relict olivine crystals. This alteration fabric is cross-cut by a cross-hatch fabric of finely spaced microfibrous veinlets of later serpentine.

The surface of the serpentinised harzbergite in contact with the travertine coating shows little evidence of interaction with the high-pH groundwater. There is no evidence of corrosion of the mineral surfaces in contact with the travertine, nor of any replacement by calcium carbonates. However, BSEM-EDXA reveals that close to the serpentinised harzbergite surface, the travertine contain very fine layers of high Mg-calcite (e.g. Figure 4.2.13a), which EDXA indicates contains 9-30 mole % $MgCO_3$ in solid-solution. These Mg-calcite layers in the travertine only occur within 0-0.5 mm of the serpentinised harzbergite surface. At distances >0.5 mm the calcium carbonate in the travertine is low Mg calcite. Although, there is no obvious etching of the serpentine, olivine and enstatite surfaces in contact with the travertine, the very localized Mg-rich chemistry of the early travertine layers would appear to indicate that there was some initial interaction between the serpentinite rock and the Ca-rich hyperalkaline groundwater, before the deposition of the calcium carbonate (travertine) coating possibly isolated the rock surface from further interaction with the groundwater.

Further downstream at the A1-2/A1-4 sites, the serpentinite is much more highly microfractured and altered, producing a soft rock with small residual blocks of more competent serpentinite within a "clayey" matrix of serpentine minerals. XRD analysis shows that this rock is predominantly a mixture of lizardite-1M and lizardite-1T (see Table 4.1.1). Unfortunately, the rock disaggregated on sampling and petrogaphic thin sections could only be prepared from loose rock fragments. Consideration should be given in future to the use of soil sampling techniques - using Kubiena soil tins or short core tubes pushed into the soft altered rock – in order to obtain intact/undisturbed samples for petrographical analysis from this type of material. Petrographic analysis shows that the original primary igneous minerals have been almost entirely replaced by serpentine. Only rarely are residual fragments of clinopyroxene (diopside-hedenbergite), orthopyroxene (enstatite) and olivine (forsterite) preserved. In addition, fragments of partially-altered Cr-Mg-bearing andradite garnet are also present in the serpentinite. The presence of andradite and clinopyroxene, in addition to olivine and orthopyroxene suggests that the original peridotite bedrock in the Allas Springs locally varied in composition from harzbergite (A1-1 site) to lherzolite or wehrlite (A1-2, A3 sites). The original olivine is now pseudomorphed by a brecciated fabric of very fine Mg-rich serpentine cut by a fine meshwork of more ferroan cross-fibre serpentine veins (e.g. Figure 4.2.13b). The fracture walls defining the serpentine blocks sometimes display some evidence for the dissolution of the earlier, finer grained serpentine (Figure 4.2.13b). Secondary quartz may be present locally, as fine euhedral crystals partly filling dissolution sites after the early serpentine (Figure 4.2.14). Some dissolution cavities also contained tiny euhedral crystals of a very minor to trace Mg-Fe carbonate phase, which may represent pyroaurite.

The alteration characteristics of the serpentinite examined from SiteA5 (sample MPLN825) are broadly similar to those observed at A1-2. However, pyroaurite is much more abundant as an alteration product (Table 4.1.1). Detailed SEM-EDXA of serpentinite fracture surfaces that were in contact with the high-pH groundwater, showed the formation of hexagonal plates of pyroaurite from fibrous lizardite (Figure 4.2.15, see also appendix 5).

The serpentinite scree and fractures in the serpentinite at Site A6 are heavily mineralised with calcite and aragonite (e.g. sample MPLN826). Again, the host rock is almost entirely composed of serpentine minerals, with minor iron oxides, titanite and traces of chromite, olivine, enstatite and clinopyroxene. The calcite forms an early coarsely crystalline coating lining fracture walls and intergranular pores in the scree material. Later needles of aragonite form a fringe resting on the earlier calcite. Traces of finely crystalline dolomite were locally found resting on the calcite and lining possible mineral dissolution sites (see appendix 5).

4.2.2 Chysovrysi Springs area

Highly altered serpentinite closely associated with alkaline groundwater seeps at Site C3 were examined. As with the altered serpentinite at the Allas Springs, it was not possible to sample intact rock material during this study. Only disaggregated rock fragments could be collected for petrographical analysis. Petrographic observations showed that the serpentinite host rock is very similar to that seen at the Allas Springs. It

comprises completely serpentinised peridotite, composed mainly of serpentine minerals with no primary igneous olivine, clinopyroxene or orthopyroxene now remaining.

The serpentinite shows minor evidence of dissolution of fine-grained serpentine along the walls of late open fractures penetrating to depths of between 0-20 μm. Calcite is the principal secondary mineral present in these late fractures cutting the altered serpentinite surfaces (Figure 4.2.17). The calcite may enclose or include euhedral crystals of an earlier Mg-Fe carbonate mineral, which can also be seen as fine crystalline coatings on the wallrock (Figure 4.2.16 and Figure 4.2.17). This Mg-Fe carbonate possibly corresponds to the small amount of pyroaurite identified by XRD in the bulk rock (Table 4.1.1).

Weakly consolidated sediment or soil regolith associated with tufa-filled fissures directly above the spring site at Site C2 were also examined in thin section. It is a poorly-sorted gravel comprising comprising angular silt to gravel grade clasts of serpentinite within a clay grade matrix of serpentine. Traces of fine grained iron oxides are disseminated through the serpentine matrix. No evidence of alteration of either serpentine matrix nor of the serpentinite clasts was evident adjacent to the tufa.

4.2.3 Trimiklini area

A sequence of samples was examined from the basalt pillow lavas at the base of the exposure through the overlying clay-rich sediment (see appendix 3 for details).

The basalt at the base of the sediment is highly altered and argillised. In thin section, it displays well-preserved laths of clinopyroxene (augite) with a very fine grained groundmass of secondary smectite (Figure 4.2.18). The augite laths typically have a feathery morphology and show little sign of alteration. Smectite entirely replaces the original lath-like plagioclase crystals, which are now only evident as “dirt-fringed” outlines in the smectite groundmass. The interstitial matrix between the pyroxene and plagioclase has also been entirely replaced by smectite. Much of this matrix may originally have been glassy.

The basalt is cut by numerous tufa-filled fractures, similar in texture to the tufa deposits observed in association with active high pH springs elsewhere in the Troodos area (e.g. Allas Springs, Chrysovrysi Springs areas). These fills have a finely laminated fabric of micritic calcite, often with fine bands of entrained sediment (Figure 4.2.18). The tufa veins cut, and therefore post-date the smectite fabric. No evidence of smectite alteration was observed adjacent to these tufa veins.

The sediment overlying the altered basalt pillow lava superficially appears to be clay-rich (see Figure 2.16). However, petrographic analysis shows that it is in fact largely highly altered lithic arenite (sandstone) (Figure 4.2.19). It comprises major coarse sand-grade angular detrital fragments of altered basalt and altered basalt minerals, with minor to major fresh sand-grade angular fragments of pyroxene (identified by XRD as diopside) and calcic plagioclase (identified by XRD as anorthite), and iron oxides (magnetite, ilmenite). The rock fragments have been strongly argillised and are almost

now entirely composed of smectite. XRD analysis shows that smectite is now a major component of the rock.

The sediment is only poorly consolidated and is seen in the field to be cut by tufa-filled fractures contiguous with the tufa-filled fractures cutting the underlying pillow lava. Unfortunately, the samples disaggregated during field collection and intact samples of argillised lithic sandstone in contact with tufa could not be collected. However, some fragments of tufa material with argillised lithic clasts attached were seen in thin section. The tufa clearly cuts across smectitised structures in the clast. No evidence could be seen for alteration of the smectite adjacent to the tufa coatings.

Any future sampling should consider collecting sandstone intact with fracture fills using soil-sampling techniques such as Kubiena tins or multi-barrel drillcores, in order to preserve these fabrics for more detailed petrographic analysis.

4.2.4 Parsata area

A sequence of samples was examined across the contact between altered autobrecciated basalt pillow lava and interstitial sediment between the basalt pillows (see section 2.6 and appendix 3 for details). The sequence is cut by tufa-lined fractures.

Although in the field the basalt appears to be highly altered and weathered, it is much less altered than the pillow lava at the Trimiklini site. In thin section it can be seen to be only partially altered, and comprises laths of relatively fresh labradorite and augite (Figure 4.2.20). The interstitial matrix, which may originally have been glassy, has either dissolved away to produce a very microporous rock, or has been replaced by a saponitic smectite matrix (Figure 4.2.20). Some of this smectite appears to have replaced possible rounded olivine crystals. Fine smectite lines the dissolution cavities and may be accompanied by microcrystalline quartz.

Detailed SEM observations were made of subsamples of the surfaces of altered basalt adjacent to a tufa-lined fractures, and were compared to altered basalt clasts from within the centre of basalt clasts. Dissolution micropores within the centres of basalt clasts are lined by delicate boxwork and spherulitic aggregates of platey smectite (Figure 4.2.21). However, adjacent to surfaces in contact with the tufa, the smectite fabrics appear to have collapse (Figure 4.2.22), which may indicate that it suffered some alteration by reaction with the fluids that precipitated the tufa.

The tufa fabrics appear to have more than one generation of calcite. The early calcite lining the fractures is typically micritic or microcrystalline and often laminates. However, traces of a later fibrous or needle-morphology calcite lines open cavities. This calcite closely resembles the needle morphology of calcite associated with calcium oxalate or calcium carbonate precipitation around plant roots in rhizolithic calcretes (e.g. Wright et al. 1995; Becze-Deák et al. 1997), and may therefore be of soil origin rather than precipitated from hyperalkaline groundwater.

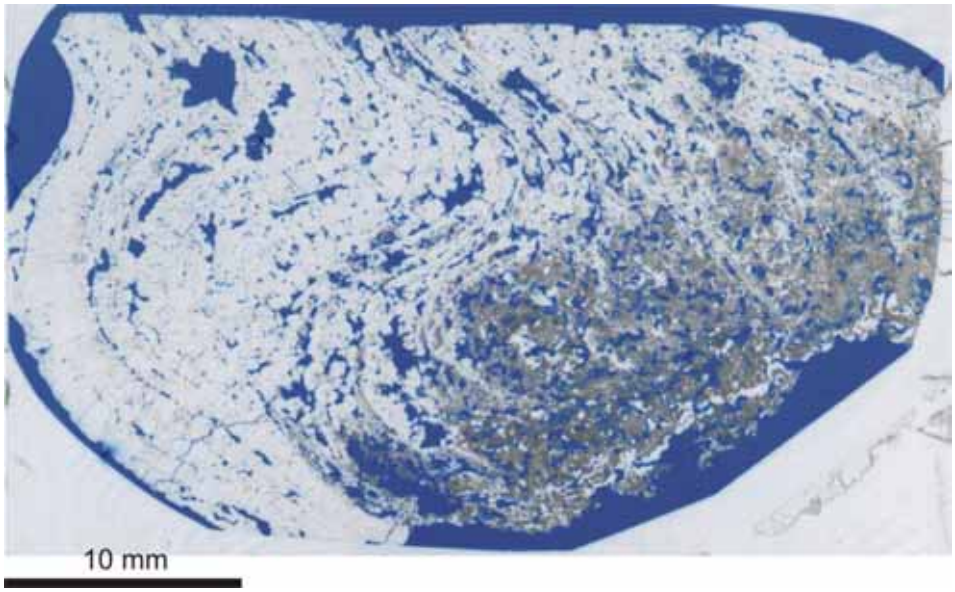

Figure 4.2.1. *Thin section through finely laminated travertine (LEFT - outer surface; RIGHT - inner surface) from active spring. Shows undulose to mammilated layering, with abundant vuggy porosity in layers parallel to the carbonate laminae. Euhedral calcite lines the walls of the cavities. The inner region is stained brown largely due to the presence of disseminated organic material. Sample MPLN805A, Allas Springs site A1-1.*

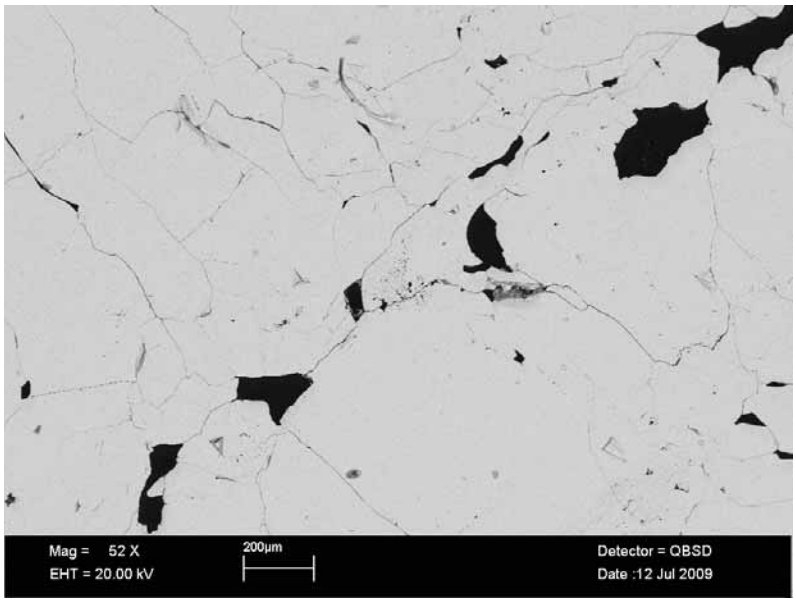

Figure 4.2.2. *BSEM photomicrograph of an area typical of many of the outer (later) layers of the travertine deposit, showing interlocking elongated (prismatic) subhedral to anhedral calcite crystal with fine vuggy intracrystalline porosity along the boundary between adjacent laminae. Calcite lining the cavities displays euhedral faces. Sample MPLN805A, Allas Springs site A1-1.*

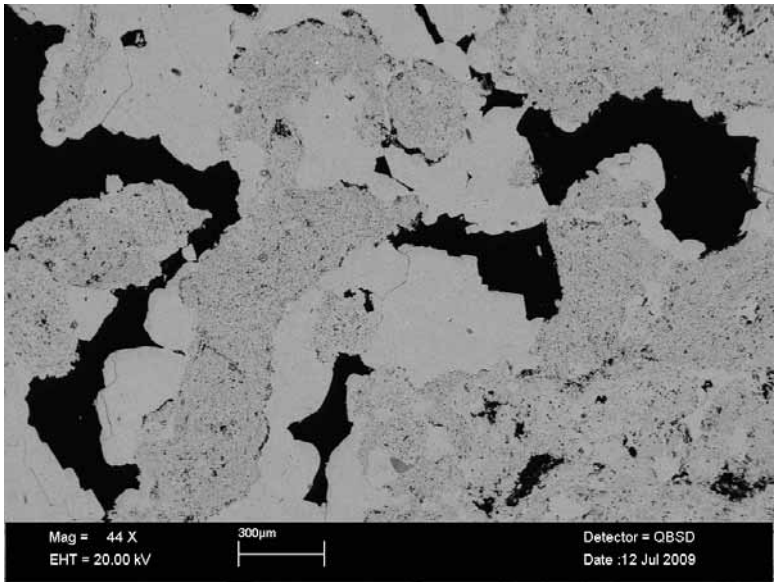

Figure 4.2.3. *BSEM photomicrograph of an area corresponding to the microporous inner (earlier) layers of the travertine. The duller calcite contains abundant inclusions of organic material, and appears to form a "fragmented" or "brecciated" fabric that has been cemented by later clean calcite with euhedral crystal faces lining the vuggy pores. Sample MPLN805A, Allas Springs site A1-1.*

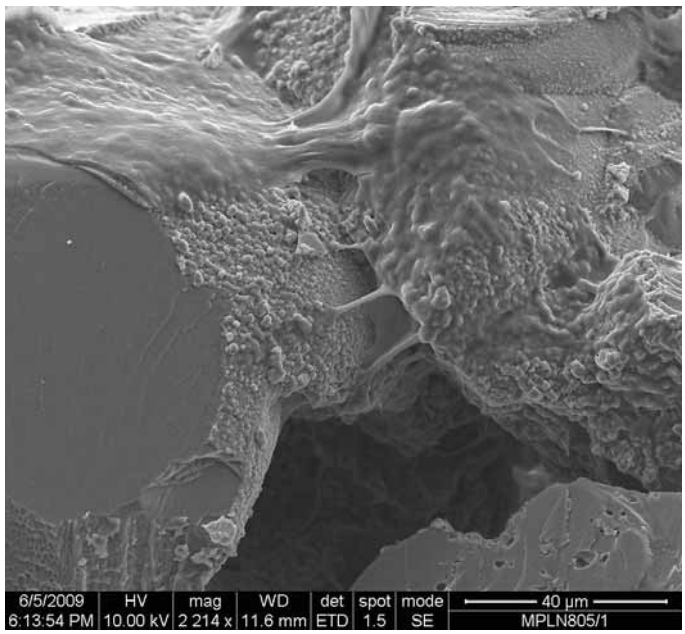

Figure 4.2.4. *SEM (SEI) photomicrograph showing organic biofilm coating calcite surfaces within intercrystalline porosity in the travertine. Sample MPLN805A, Allas Springs site A1-1.*

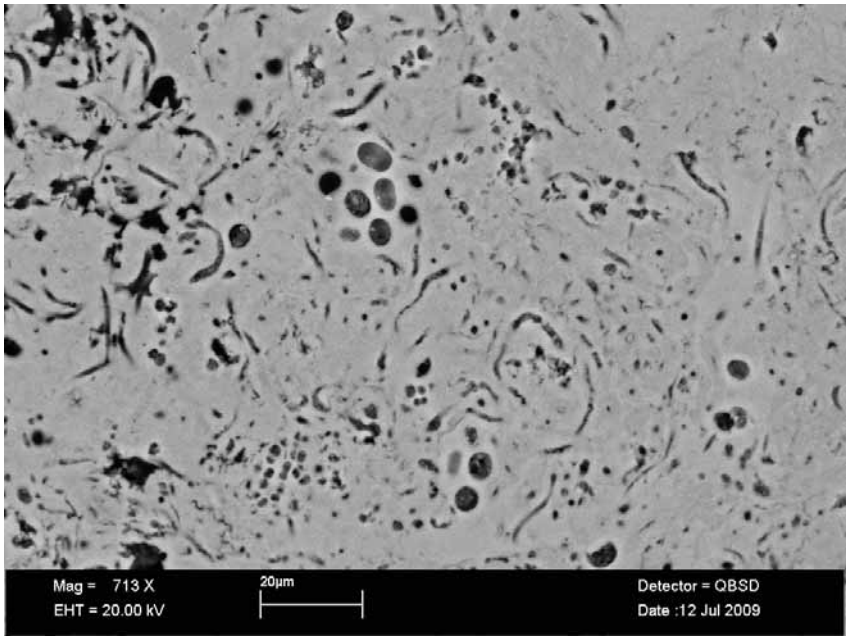

Figure 4.2.5. *BSEM photomicrograph showing detail of biogenic structures that comprise the organic inclusions preserved within travertine. The features include clusters of cellular features that resemble clusters of coccoid bacterial cells, rod-like bacteria, and fragments of minute worm-like organism that possibly represent nematodes . Sample MPLN805A, Allas Springs site A1-1.*

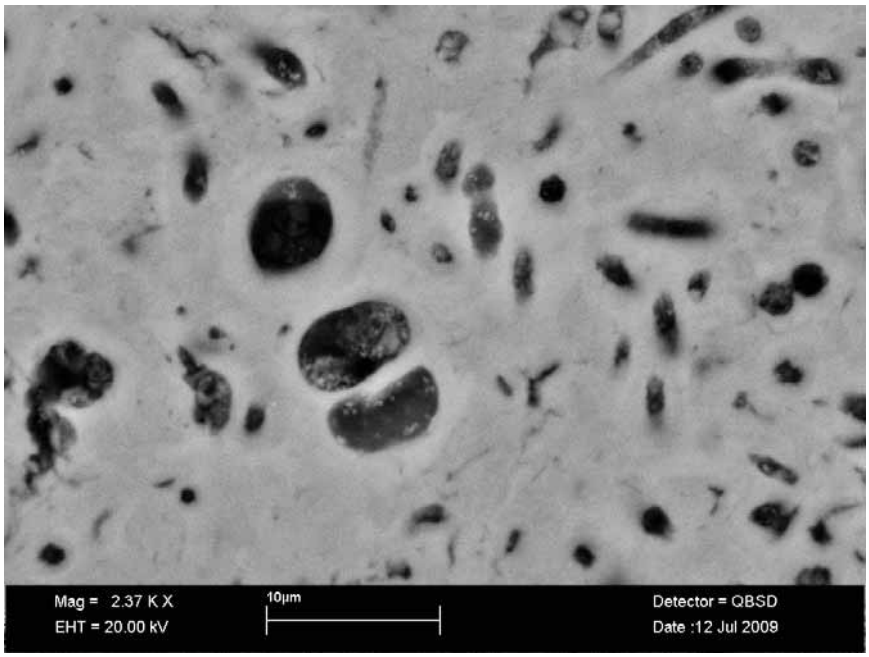

Figure 4.2.6. *BSEM photomicrograph showing detail of coccoid and rod-like biogenic structures that comprise the organic inclusions preserved within travertine. The image shows a probable preserved coccoid bacterial cell that appears to have been undergoing mytosis (cell-division). Sample MPLN805A, Allas Springs site A1-1.*

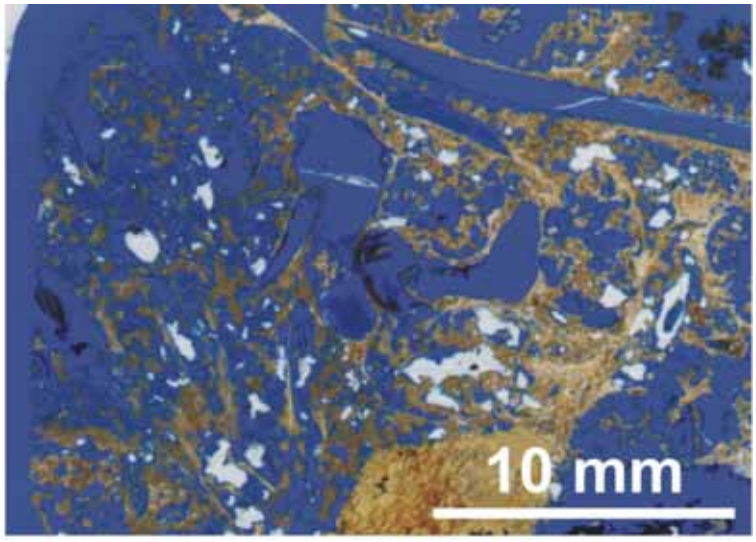

Figure 4.2.7. *Transmitted light photomicrograph of petrified plant debris (soil organic litter layer) within travertine deposit. The porosity largely exists within porous plant remains. Fine micritic calcite cements between the plant fragments. Sample MPLN806, Allas Springs site A1-1.*

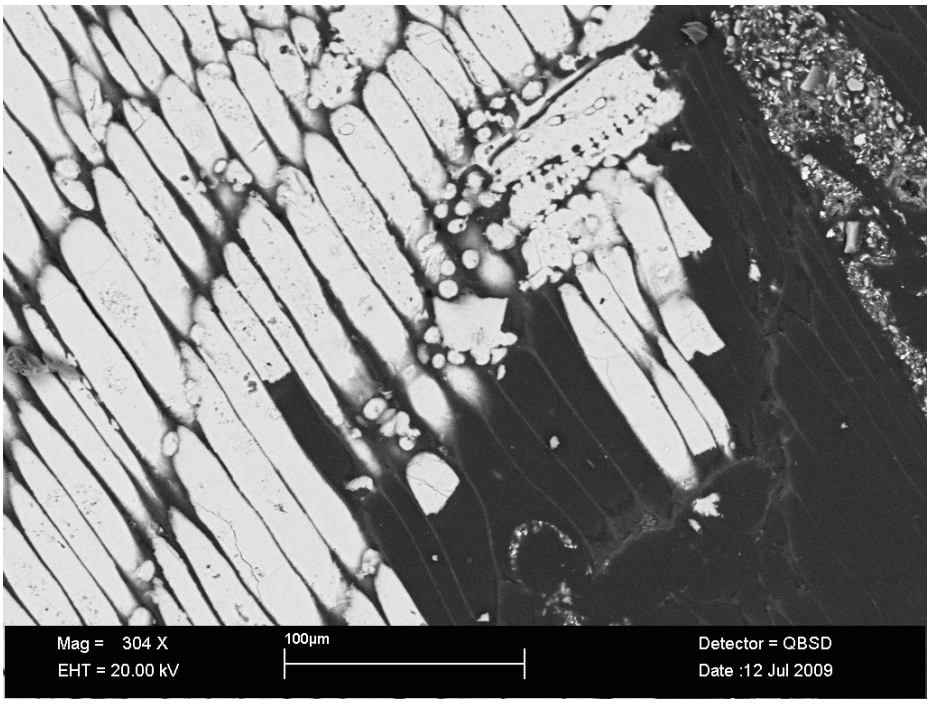

Figure 4.2.8. *BSEM photomicrograph showing detail of the cellular fabric of part of a pine needle preserved within the extensive travertine deposit cementing forest leaf litter around the A1-1 spring discharge site. Calcium carbonate (bright) fills the intracellular cavities. The organic walls of the cells are still preserved, although in places (lower right hand area) some of the cell walls appear to become diffuse as they break down. Sample MPLN806, Allas Springs site A1-1.*

Figure 4.2.9. *Transmitted light photomicrograph of a thin section through finely laminated travertine. Laminae are undulating, and are made up of interlocking elongated anhedral crystals of calcite that are orientated perpendicular to the lamination. Blue resin reveals significant porosity along crystal boundaries. The lamination is picked out by very fine detrital mineral debris (very fine dark laminae). Sample MPLN814, Allas Springs site A4.*

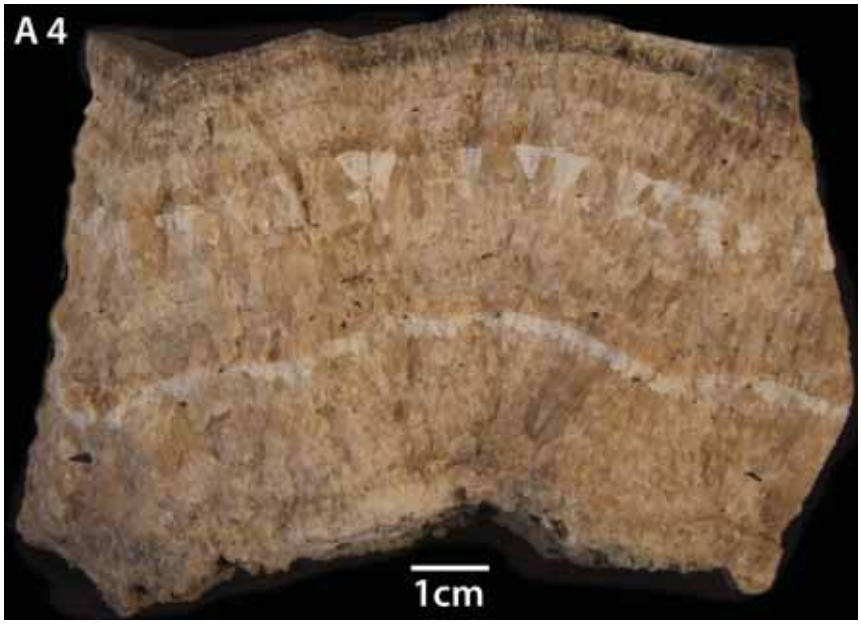

Figure 4.2.10. *Photograph of a section through a block of travertine, showing mammilated fine laminated structure with buff-coloured calcite layers and white powdery aragonite layers. Sample MPLN814, Allas Springs site A4.*

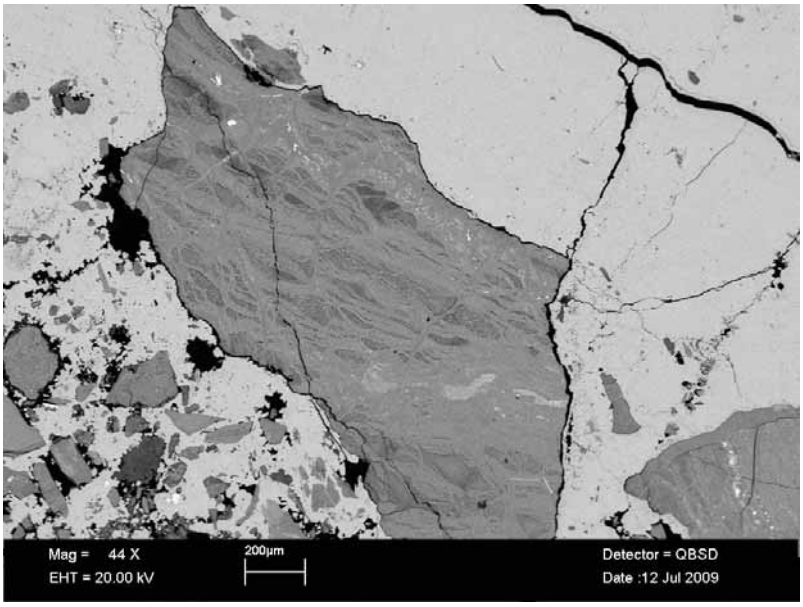

Figure 4.2.11. *BSEM photomicrograph showing fragments of serpentinite and serpentine entrained within detrital sediment-rich layers in the calcite matrix of the travertine. The silicate mineral fragments show no evidence of alteration in contact with the calcite (white). Sample MPLN814, Allas Springs site A4.*

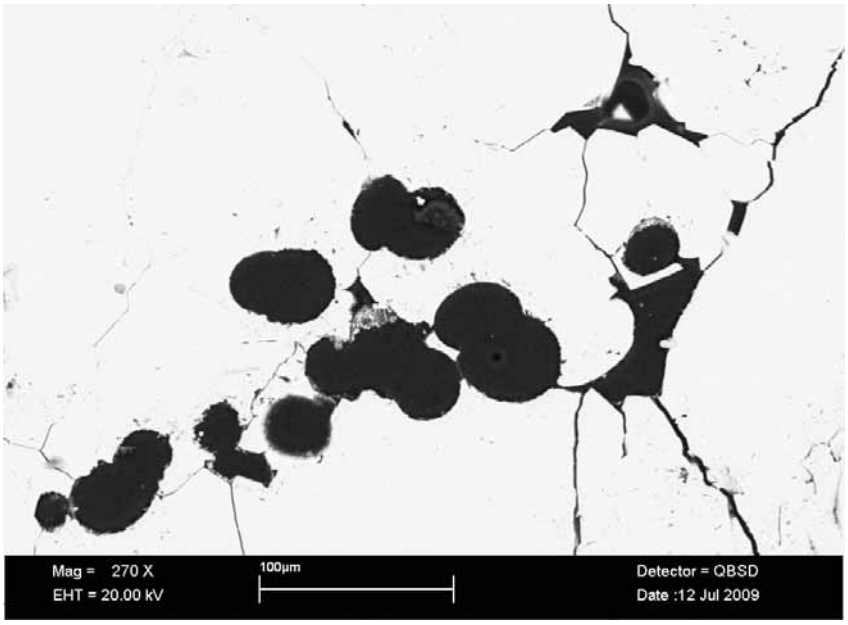

Figure 4.2.12a. *BSEM photomicrograph showing and example of the concentration of unusual spherical voids found within some travertine laminae. Some voids are partially filled by euhedral calcite cement. Sample MPLN814, Allas Springs site A4.*

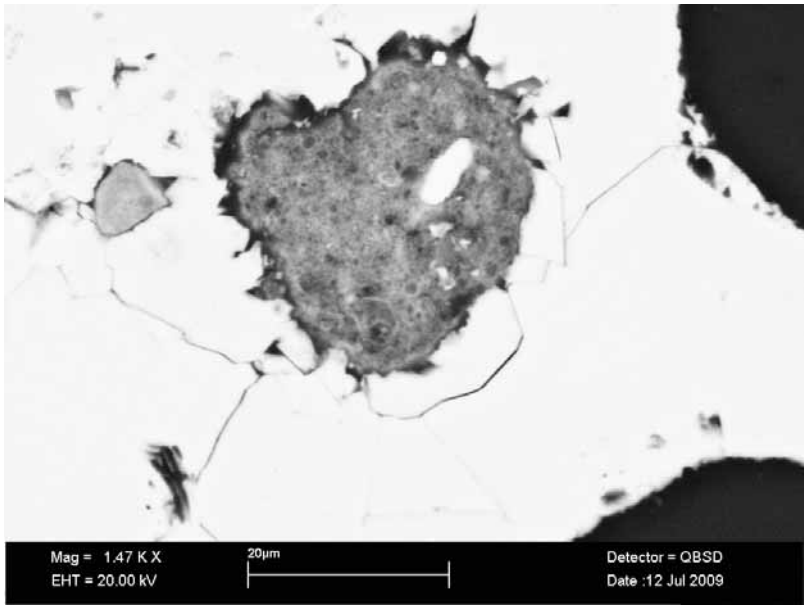

Figure 4.2.12b. *BSEM photomicrograph showing an altered glass spherule partially replaced by authigenic smectitic clay and entrained within a travertine laminae. Sample MPLN814, Allas Springs site A4.*

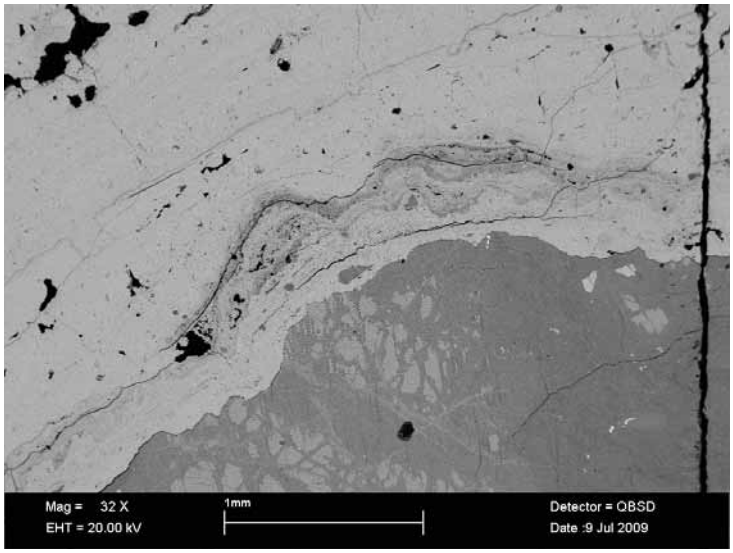

Figure 4.2.13a. *BSEM photomicrograph showing the contact between travertine (light grey) and altered harzbergite (bottom) with relict brecciated olivine in a fine grained matrix of lizardite. Fine bands of high Mg-calcite (dull grey) occur within the travertine, close to contact with the harzbergite. Sample MPLN805, Allas Springs site A1-1.*

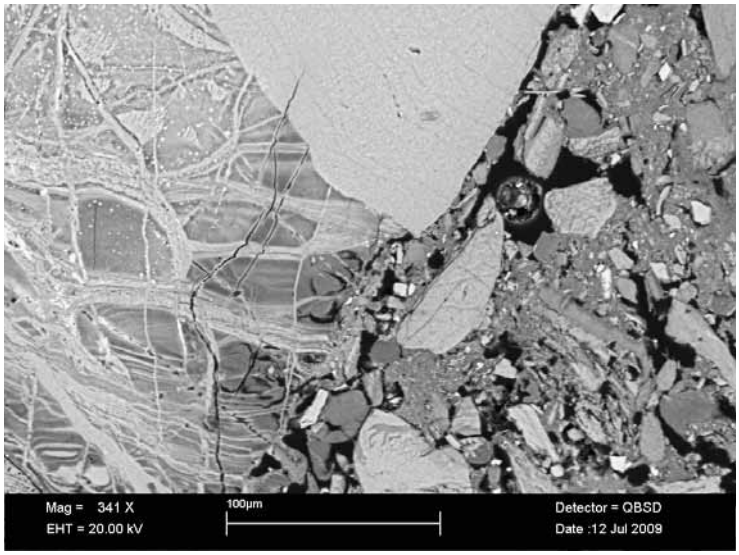

Figure 4.2.13b. *BSEM photomicrograph of the fractured margin of a block of altered serpentinite. A meshwork fibrous lizardite veins (light grey) cut an earlier serpentine groundmass (dull grey). The early serpentine displays dissolution at the margins of the block which have been exposed to high pH groundwater. Sample MPLN808, Allas Springs site A1-2.*

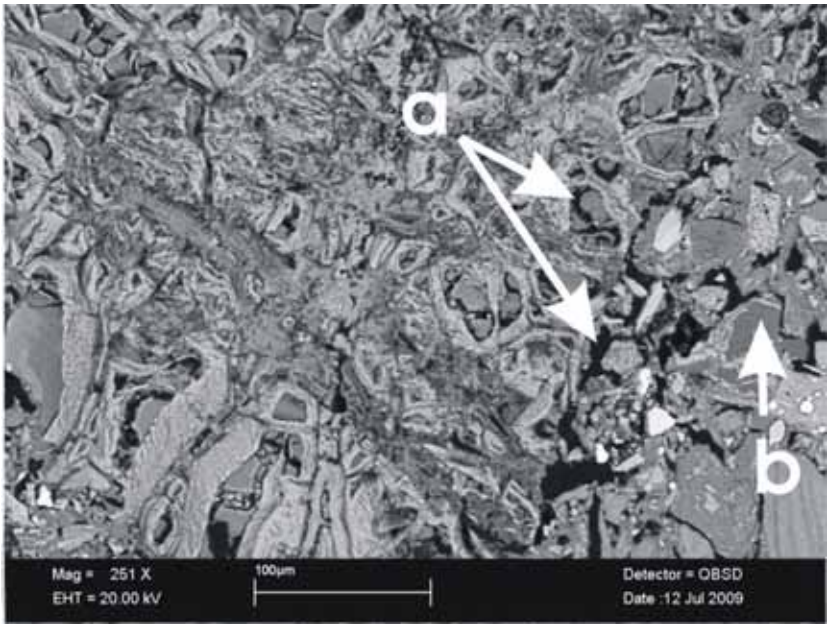

Figure 4.2.14. *BSEM photomicrograph of the fractured margin of a block of altered serpentinite. The early fine grained serpentine (dull grey) has been locally dissolved (a) and secondary quartz (b) is locally precipitated in dissolution sites. Sample MPLN808, Allas Springs site A1-2.*

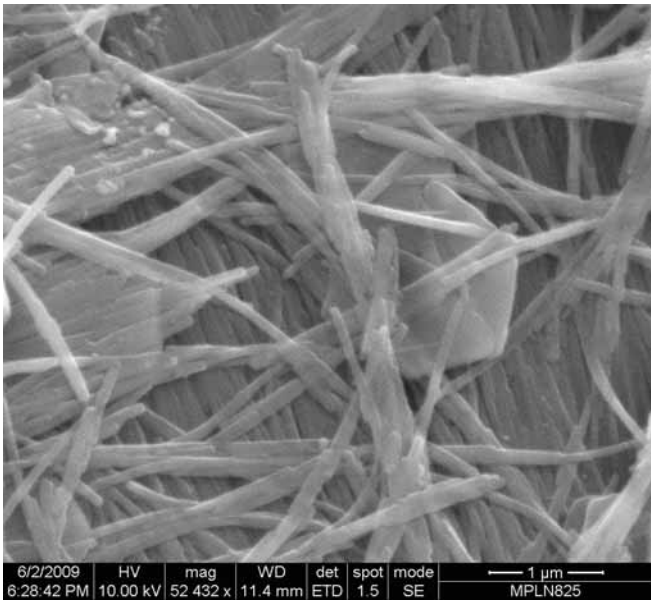

Figure 4.2.15. *SEM photomicrograph showing hexagonal plates of pyroaurite forming from, and replacing fibrous lizardite on fracture surfaces of altered serpentinite in contact with high-pH groundwater. Sample MPLN825, Allas Springs site A5.*

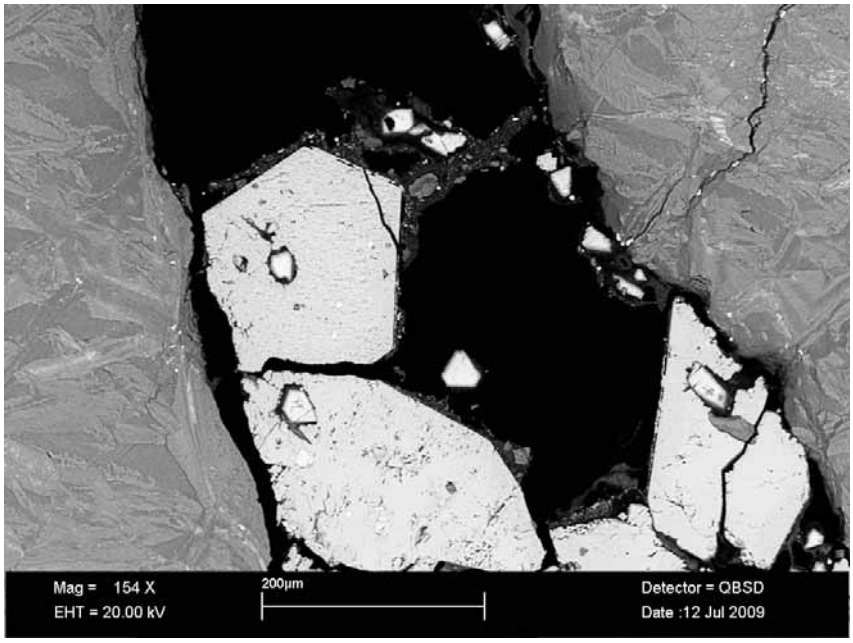

Figure: 4.2.16. *BSEM photomicrograph showing equant euhedral crystals of calcite lining fractures in serpentinite. Small hexagonal plates of pyroaurite are included within the calcite and also are present on the fracture walls. Sample MPLN831, Chrisovrysi Springs site C3.*

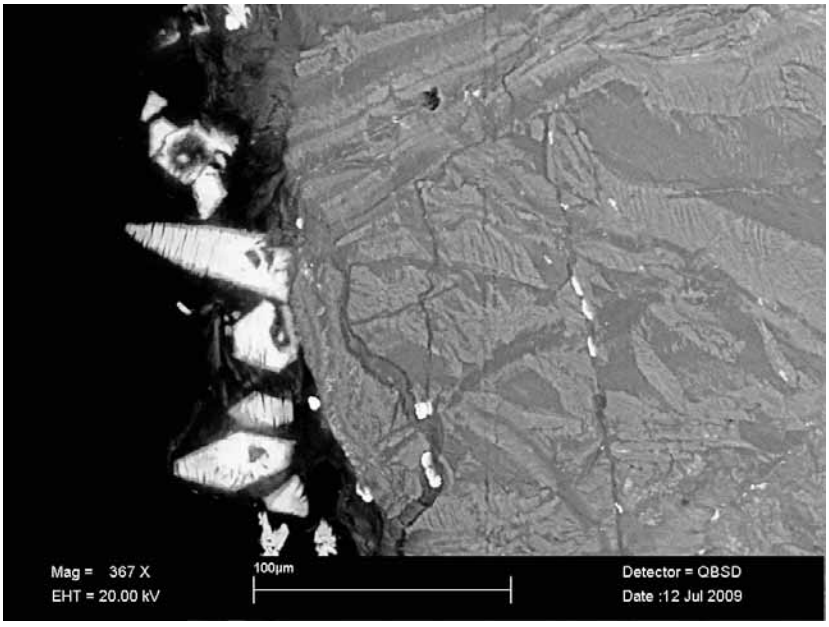

Figure: 4.2.17. *BSEM photomicrograph showing euhedral crystals of pyroaurite lining fracture walls in serpentinite. Sample MPLN831, Chrisovrysi Springs site C3.*

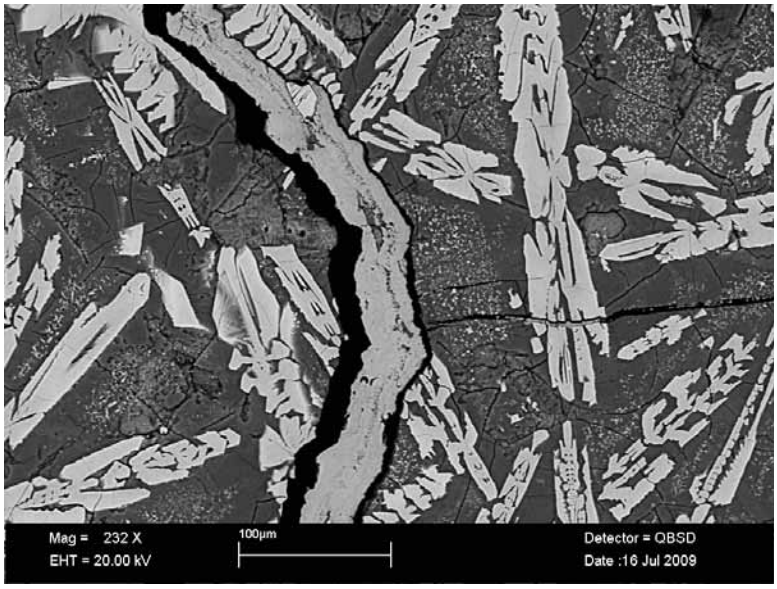

Figure: 4.2.18. *BSEM photomicrograph of polished section though highly altered basalt pillow lava, cut by a sub-vertical vein of finely laminated calcite (tufa-filled fracture). The rock contains well-preserved euhedral laths of augite) clinopyroxene (white) in a fine grained groundmass of secondary smectite (dark grey). Fine disseminated iron oxide (fine bright grain) is disseminated within the smectite Sample MPLN838, Trimiklini site.*

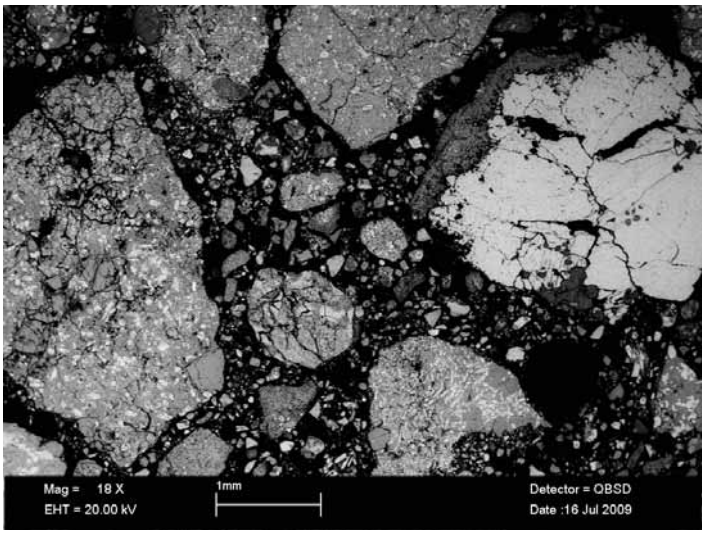

Figure: 4.2.19. *BSEM photomicrograph of polished section though highly altered coarse lithic arenite. The rock contains highly argillised detrital clasts of altered basalt and basaltic mineral fragments, within a silty matrix. Fine disseminated iron oxide (fine bright grain) is disseminated within the smectite Sample MPLN840, Trimiklini site.*

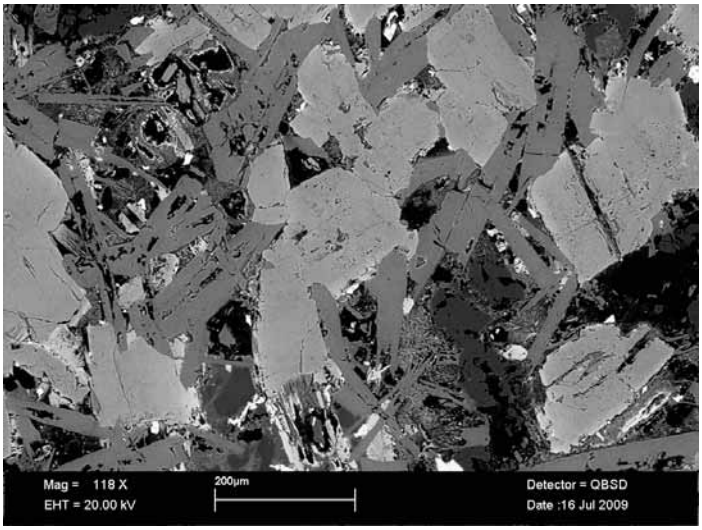

Figure: 4.2.20. *BSEM photomicrograph of partially altered basalt. The rock contains largely unaltered laths of labradorite (mid grey) and subhedral blocky crystals of augite (light grey). The interstitial regions between these minerals are porous and partially filled with secondary smectite and fine quartz. Sample MPLN847, Parsata site.*

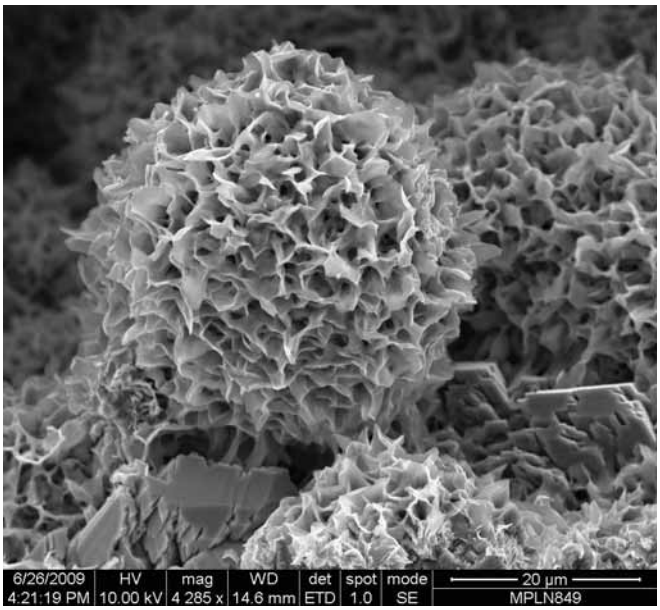

Figure: 4.2.21. *BSEM photomicrograph showing delicate authigenic smectite spherical boxwork aggregate of platey crystallites within dissolution cavity in altered basalt. Taken from centre of a basalt fragment away from contact with tufa vein coatings. Sample MPLN849, Parsata site.*

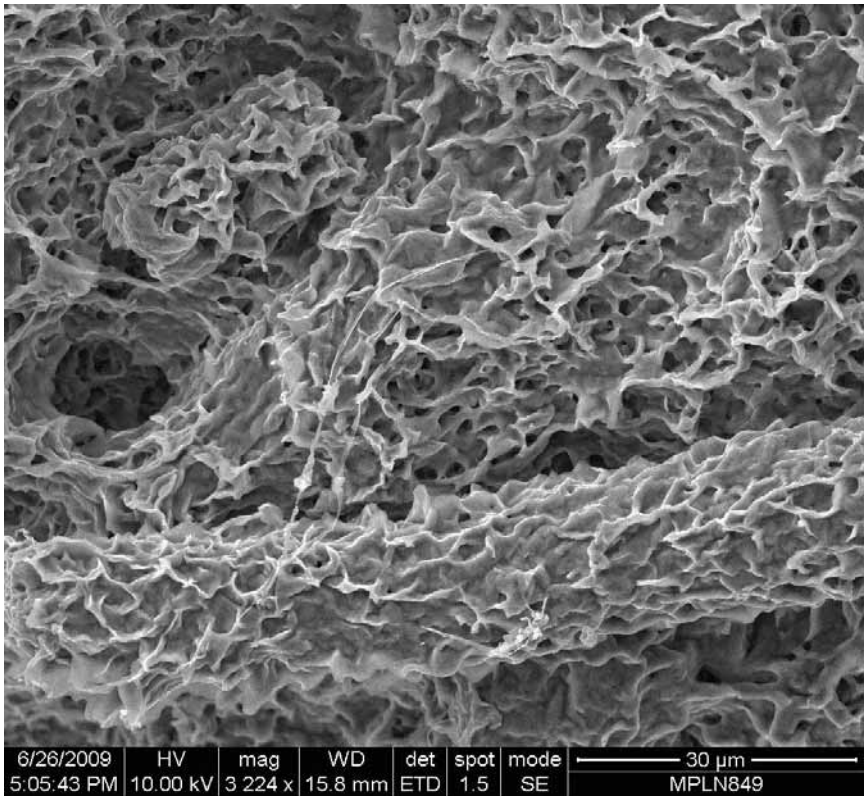

Figure: 4.2.22. *BSEM photomicrograph from another fragment of altered lava. Here the smectite lines a very large pore surface, probably exposed at the outside of the fragment. This shows a relatively subdued relief, suggesting collapse. Fibres on surface are most likely biofilm or biogenic filaments. Sample MPLN849, Parsata site.*

4.3 Hydrochemistry

4.3.1 Major element chemistry

General overview

The full groundwater raw data are presented in appendix 6 and a selection of the major element concentrations is presented in Table 4.3.1.

Table 4.3.1. *Selected major element concentrations for the groundwater samples (all concentrations mgL^{-1}).*

Sample	Field pH	Lab pH	Ca^{2+}	Mg^{2+}	Na^{+}	K^{+}	CO_3^{2-}	HCO_3^{-}	Cl^{-}	SO_4^{2-}	NO_3^{-}
A4-1	n.d.	9.77	3.20	58.7	747	31.4	127	152	1093	87.2	0.343
A4-2	n.d.	9.90	3.43	58.4	893	40.5	161	121	1342	106	1.82
A4-3	n.d.	9.71	3.37	58.8	921	40.7	140	154	1321	106	2.40
A5	9.8	9.22	1.34	64.2	224	9.76	n/a	307	346	27.7	1.98
A3	9.84	9.29	1.32	63.9	238	10.2	50.5	203	369	30.5	2.22
A2	9.69	9.04	1.61	65.5	172	7.33	38.5	232	254	22.8	1.66
A1-1	11.9	11.3	37.2	0.101	1435	63.1	n/a	272	2177	101	<1.5
A1-3	10.01	9.31	12.2	0.554	1337	60.1	54.1	96.4	1926	114	10.3
A1-2	9.26	8.82	4.87	48.3	502	23.7	25.8	288	699	50.7	3.90
A1-4	9.78	9.27	11.2	5.73	1214	54.0	61.2	124	1748	78.5	8.33
A6	9.67	9.60	2.22	50.7	921	42.9	102	150	1383	97.0	7.31
E1-1	9.5	9.48	1.07	56.4	75.3	2.62	52.2	190	92.7	7.128	1.03
C2	9.58	8.90	1.69	67.9	4.79	<0.5	23.7	255	8.361	3.207	0.580
C1	9.41	8.85	1.80	68.3	4.68	<0.5	n/a	309	8.486	3.272	0.640
C3	9.69	9.11	1.67	92.7	5.14	0.926	44.5	311	18.2	2.484	1.86
P1	11.42	10.3	36.5	0.021	116	<0.5	27.6	<10	80.9	149	<0.03
D2	8.25	8.21	154.7	69.3	82.8	1.01	n/a	413	204	151	<0.03

Allas Springs

There are a large number of samples from this area and they are grouped in related systems

A4-1 to A4-3: This is the highest site, the spring (A4-1) emerging at the contact between the harzbergite and the overlying altered gabbro. The laboratory pH here is 9.77 (no functioning pH electrode was available during sampling), but by comparison with the other samples, the field pH is probably just >10. The water is not untypical for ophiolites (cf. Table 1.3), but the Na and Cl levels are somewhat high, possibly reflecting the presence of relict seawater in the host rock. Certainly the Br/Cl ration of this water is 2.2×10^{-3}, somewhat lower than the seawater ratio of 3.3×10^{-3} (Kreitler and Bledsoe, 1993), but this may simply reflect loss of Br to microbial processes (e.g. Upstill-Goddard and Elderfield, 1988). Both Mg and K are somewhat higher than usual too.

Samples A4-2 and A4-3 show indications of reaction along the flow path, both having lost Ca (presumably to the tufa precipitates), K, Na and Si and gained Mg. Interestingly,

both also show significant gains of Cl, which might indicate other springs charging the stream from within the scree which covers much of the slopes (this could also explain the increased pH in A4-2). All three waters are oxidising, with the oxidant levels (e.g. NO_3^-) increasing with flow distance.

A5: This water seeps out of the scree/colluvium at the valley wall and so has presumably undergone some degree of reaction and chemical change from the original rock-buffered state. Nevertheless, the pH remains relatively high at 9.80 (field). It is a much less saline groundwater with lower concentrations of Ca and K, but higher Mg than A4-1.

A3: Is very similar to A5, but with a lower HCO_3^- concentration, presumably indicating less atmospheric interaction.

A2: Is very similar to A3, suggesting that their ultimate source under the scree is the same.

A1-1 to A1-3: A1-1 is the most saline sample collected yet and also has the highest pH at 11.9 (field value). This sample is collected immediately as it leaves a fracture in the harzbergite (see Figure 2.4) and is presumed to be correct as the electrode was set against pH 10 and 14 standards and the value is temperature corrected. The Ca is high and the Mg low, reflecting the fact that little atmospheric or sedimentary reaction has taken place. The Br/Cl ratio is 2.9x10, rather more close to the seawater ratio than any of the other Allas Spring samples, but the Na concentration is lower than seawater, reflecting reaction in the host rock.

The chemistry of sample A1-3 reflects reaction in the soil and forest litter downhill from A1-1. Not surprisingly, the forest litter here is cemented with thick (20-30 cm) tufa deposits (see appendix 1 and comments in section 4.2). Sample A1-2, collected downflow of A1-3, shows signs of further reaction, including decreased pH, Ca, Na and K levels and higher Mg and bicarbonate. Interestingly, the overall chemistry of A1-2 is most similar to the A4 samples, clearly suggesting that they too have undergone interaction with the rock and scree.

A1-4: Is more saline (Cl=1748 mgL^{-1}) than A4-1 and has higher Ca, Na, NO_3^- and Br levels (although the Br/Cl ratio is the same as A4-1), possibly suggesting less reaction within the scree where it was collected. Compositionally, it lies between A1-2 and A1-3.

A6: Despite being collected the furthest away from the springs, sample A6 still shows clear signatures of its origin, with elevated pH, low Ca and high Cl concentrations. Interestingly, Schopka and Derry (2009) show that large rivers draining ophiolite ultramafics in the Philippines have consistently higher pH than those draining volcanic rocks in the area, hinting that these contributions may be important to defining water chemistry, at least on a local scale. Certainly, it proved possible to track down hyperalkaline seeps in the thickly forested slopes of the Zambales ophiolite in Luzon by following the pH trends in the small streams draining the area (Alexander et al. 2008a).

E1: Apart from the elevated pH (9.67 in the field), there is little about the chemistry of the sample which would immediately identify it as ophiolitic sourced. The low Ca and

high Mg concentrations imply reaction with the scree materials and the stable isotope signature (see Figure 4.3.1) reflects local precipitation, indicating that dilution with young surface water has also played a role.

Chrisovrysi Springs

C1 to C3: Sample C1 is effectively the same as sample C2, so confirming the field observation that the C1 spring is probably supplied by the C2 cistern (see appendix 1). Both display high pH values (around 9.5) and low Ca concentrations, but these are likely to be due to storage for some time in the cisterns, so allowing some degree of atmospheric equilibration. The relatively high Mg concentrations imply some degree of reaction with the sedimentary cover before collection in the concrete cisterns and this is consistent with the original spring which seems to have flowed through the sediments and soils at the site before being captured by the cisterns in the 1960s (the cistern in the forefront of Figure 4.3.1 bears a 1962 date). Although physically close to the Allas Springs (only ~2 km apart), the high salinities which characterise the Allas area are absent in these waters.

Sample C3 is slightly removed from the cistern system and was collected from seeps into a stream. The water emerged from heavily altered serpentised harzbergite (serpentinite), so the chemistry and high pH (9.69 in the field) are not surprising. The chemistry is similar to that of C1 and C2, although the higher Mg may indicate more reaction with sediments at the sampling site. Interestingly, although the Cl concentration is low, the Br/Cl ratio (3.02×10^{-3}) is near that of seawater.

P1: This sample comes from groundwater below bentonite/bentonite analogue (at the Parsata farm borehole) and it is likely that the sampling interval is in the altered PLV here (to be checked in future). The field pH of 11.42, low Mg and K concentrations are typical of ophiolite hyperalkaline groundwaters (cf. Table 1.3). The Ca levels are as high as A1-1, indicating little or no reaction with the atmosphere, even if the field dissolved oxygen measurement appears to indicate oxidising conditions (in disagreement with the Fe and Mn data – see section 4.3.2). Cl concentration is low (80.9 mgL^{-1}), but the Br/Cl ratio is that of seawater. In general, it appears that this groundwater is equilibrated with the PLV (see below), as would be expected from the sampling depth (probably some 10-15 m below the base of the bentonite), and suggests that careful drilling and sampling at or near this locality could provide samples from the bentonite reaction zone. Interestingly, this sample also has the highest silica concentration, almost twice that of the next highest, sample A1-2, possibly indicating clay reaction at depth.

D2: This sample was collected at one of the most spectacular sites in Cyprus with the 30 m high waterfall encrusted in 30-40 cm thick tufa a seemingly sure sign of hyperalkaline groundwaters. Although fluctuations in pH in the stream which supplies the waterfall suggest that there are some form of hyperalkaline groundwaters entering the stream, it seems that the flow during the sampling period was not sufficient to have a significant impact on the stream chemistry. However, the presence of soils in and around the stream suggest that it may be worth sampling again in the future.

Figure 4.3.1. *The original spring at site C2 (Chrisovrysi Springs) is under the old roof and groundwater looks to have flowed through the soils at the site (numerous tufa veins can be seen through the soil here).*

4.3.2 Redox and trace element chemistry

Redox

The redox state of all the samples is, not surprisingly, generally oxic (appendix 6) with most samples showing field dissolved oxygen levels of >3 mg L^{-1}. For example, for all samples apart from P1, the sulphur is predominantly present as sulphate and the reduced sulphur is at or near the detection limit. Even for P1, which has the highest total sulphur content, the reduced sulphur constitutes less than 1 % of the total.

With the NO_3^-/ NO_2^- pair, the NO_2^- is generally below detection and the NH_4^+ dominates. Interestingly, in P1, all three species are below the detection limits, possibly suggesting that the nitrogen system in the surface spring samples is reflecting atmospheric and soil input. For the Fe pair, reduced Fe is below the detection limit in all cases and oxidised Fe is below 0.070 mg L^{-1}. Total Mn is also generally below the detection limit.

Clearly, to more fully assess the redox state of these groundwaters, downhole sampling and collection of gas samples (to better represent the *in situ* conditions) is required.

Trace elements

The trace element concentrations are almost uniformly below detection. Only in the case of Li and B are there significant deviations above background. For example, at Allas Springs, most samples have a B/Cl ratio of between and 4.2-4.4x10^{-3}, somewhat greater than that of seawater (3.3x10^{-3}; Kreitler and Bledsoe, 1993). Interestingly, the Li/Cl ratios of these same samples all lie very close to 2.9x10^{-3} (cf. seawater with ~8.4x10^{-6}; Presley et al. 1973).

Davis and Elderfield (2004) note that Li is preferentially leached during early stages of high temperature serpentinisation of ocean crust and that the Li/Cl and B/Cl ratios provide a useful guide to the fluid/rock mass ratios (when the ophiolite Li and B concentrations are known). This being the case, it may be worth measuring these parameters at appropriate boreholes to assess the impact of varying fluid/rock mass ratios on the source hyperalkaline groundwater chemistry (i.e. before reaction with the bentonite/bentonite analogue).

4.3.3 Stable isotopes and tritium

The groundwater stable isotope and tritium data are presented in Table 4.3.1 and the δD vs. $\delta^{18}O$ plot is shown in Figure 4.3.1. It can be clearly seen that the samples plot between the Mediterranean Meteoric Water Line (MMWL; from IAEA, 2005) and the Global Meteoric Water Line (GMWL; from Craig and Gordon, 1965). The all-sample regression line is $\delta D = 5.92 * \delta^{18}O + 4.99$ ($R^2 = 0.84$) whereas removing sediment-hosted samples D2 and P1 produces a regression line of $\delta D = 1.93 * \delta^{18}O - 23.55$ ($R^2 = 0.32$). In comparison, rainfall data for the Eastern Mediterranean show:

Kouris catchment, Cyprus (Boronina 2003; Boronina et al. 2005)

$\delta D = 6.6 * \delta^{18}O + 10.9$

Alexandria, Egypt (IAEA, 2005)

$\delta D = 6.56 * \delta^{18}O + 11.14$ ($R^2 = 0.90$)

Sidi Barrani, Egypt (IAEA, 2005)

$\delta D = 5.83 * \delta^{18}O + 10.10$ ($R^2 = 0.77$)

Jacovides (1979) and Boronina (2003) analysed 234 groundwaters from the Kouris catchment area in southern Cyprus and distinguished two water types:

- ophiolite samples with isotopically depleted groundwater
- overlying sediments with isotopically enriched groundwater

Within analytical uncertainty, they found that 52 % of groundwaters in the ophiolites and 10 % in the sediments fell on the local MMWL regression line. The rest of their samples were displaced below the local regression line around a line of a slightly smaller slope (m = 5.9), i.e. very similar to that observed for the all-sample line here. Allison et al. (1983) suggested that partial evaporation from soils and dilution by subsequent recharge could induce a move towards a line parallel to and below the local regression line and this is certainly observed by Boronina (2003) for the Kouris catchment area.

It is tempting to suggest that the shallower slope and isotopic enrichment observed when the sedimentary data (i.e. samples D2 and P1) are removed from this dataset may be indicating an additional mechanism (e.g. significant evaporation; Gibson et al. 1999;

Baskaran et al. 2005), but the few data and subsequent weak correlation (R^2 = 0.32) means that this may be purely spurious. Certainly, there is nothing as comparable in the much larger dataset of Boronina (2003; see Figure 3.6 in that report).

Boronina (2003) also reports an altitude gradient of -2.2 ‰ per 100 m for δ^2H and -0.34 ‰ per 100 m for $\delta^{18}O$. Although the comparison is difficult to make here as the samples are not from one catchment, for the general area around the Allas and Chrisovrysi Springs (which covers only a few square kilometres), the δ^2H gradient is -1.09 ‰ per 100 m and the $\delta^{18}O$ gradient is -3.41 ‰ per 100 m. The Allas Springs area alone has a δ^2H gradient of -1.09 ‰ per 100 m and the $\delta^{18}O$ gradient is -2.90 ‰ per 100 m. While this may reflect some input from recent precipitation (see comments below), it is presumably also a reflection of the more complex flow system in the area with supply from greater elevation locally. Interestingly, the P1 stable isotope signature suggests a lower altitude source (extrapolating from the data of Boronina, 2003, would suggest 200-300m above the borehole) for the groundwater, perhaps implying a relatively local input.

Jacovides (1979) and Boronina (2003) have reported over 140 ^3H data for Cyprus (Table 4.3.2) and, although the range is rather large (with the highest rainfall data presumably a reflection of atmospheric bomb testing in the 1960's), most recent values have not been too high. Boronina (2003) reported that, in general in the Kouris catchment area, the ophiolite-sourced groundwaters were relatively young, probably <35 a, whereas the sediment-sourced groundwaters tended to be >45 a, but this does not would appear to be reflected in the small number of samples available here. Both the direct from ophiolite sample A1-1 and the sample from below the bentonite/bentonite analogue (P1) show the lowest tritium activities, suggesting that the other samples include some degree of young precipitation which is missing from these groundwaters.

However, as Boronina (2003) did not discuss the groundwater chemistry in anything but a superficial manner, it is difficult to judge the meaning of this apparent age difference[4]. In the context of the samples reported here, it could be taken to show that the sub-bentonite hyperalkaline groundwaters (such as sampled at Parsata) are indeed older and representative of a deeper groundwater flow system trapped under the bentonite/ bentonite analogue.

[4] It is of note that although Boronina (2003) is a doctoral thesis, the raw hydrochemical data have not been published with the isotopic data, which would seem to be an opportunity lost.

Table 4.3.1. *Stable isotope and tritium data from the sampled groundwaters.*

Sample ID	$\delta^{18}O$	$\delta^{2}H$	Tritium activity
	‰VSMOW	‰VSMOW	TU
A1-1	-6.99	-38.4	<1
A4-1	-6.80	-35.3	4.5 ± 0.4
C2	-7.59	-39.1	5.2 ± 0.4
C3	-6.56	-34.7	3.9 ± 0.4
P1	-4.99	-22.4	<1

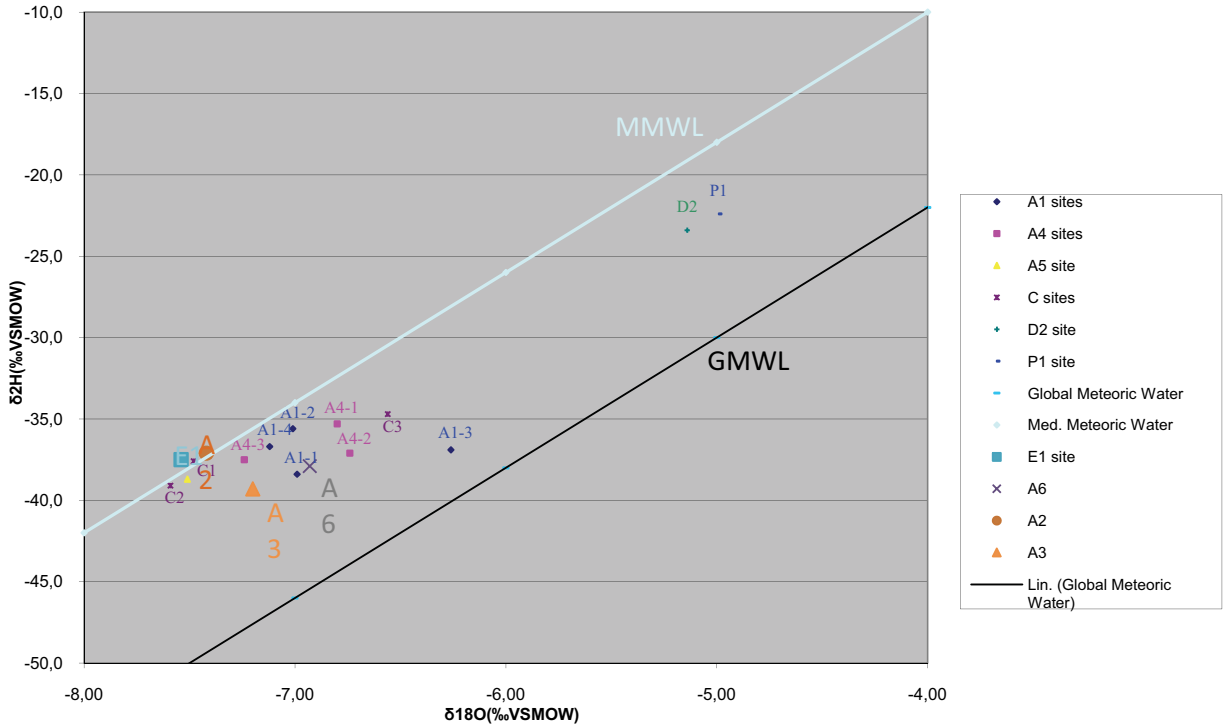

Figure 4.3.1. *δD vs $\delta^{18}O$ in the sampled groundwaters (GMWL from Craig and Gordon 1965, MMWL from Gat, 1971).*

Table 4.3.2. *^{3}H in precipitation and groundwaters in Cyprus.*

	Number of samples	Range of ^{3}H activities (TU)
Precipitation		
1960 - 1974	64	14 - 2300
1998 - 2002	12	2.8 – 4.3
Groundwaters		
1972 - 1978	74	0.6 - 62
1998 - 2002	125	0.7 – 22.5

Examination of the groundwater chemistry of the Allas Springs samples from site A4 shows that the pH increases and the Cl concentration drops with distance away from the spring (Table 4.3.1) and this suggests that there is probably some dilution from low chlorinity snow meltwater[5] along the course of the stream. This would probably be enough to provide the observed ^{3}H signal in the spring samples.

[5] The Troodos area received its first significant snowfall in a decade in the winter of 2008-2009 and the snowline was just above the springline during the sampling period.

5 DISCUSSION

5.1 Groundwater

The groundwater chemistries are fully relevant to the project aims, with the range observed lying within the range of low alkali cement leachates (Table 5.1). However, in future, appropriate methodologies are required to obtain samples which have had no atmospheric contact. While simple sampling of springs and boreholes is appropriate for this reconnaissance study, it has the drawback of making any current assessment of the redox state of the system irrelevant. Sampling from springs also has the limitation that contact of the groundwater with the atmosphere induces rapid and widespread precipitation of secondary carbonates which can mask the more repository relevant mechanisms (for example, it may shield the host rock and bentonite from further reaction). Appropriate sampling is certainly not easy (cf. discussions in Laaksoharju et al. 1993; Laaksoharju 2008; Kunimaru et al. 2009), but can be most suitably carried out downhole in dedicated boreholes (discussed further in section 6.3).

Table 5.1. *Comparison of the groundwater chemistry (samples from Parsata and Allas Springs) with representative low alkali cement leachates (data from Vuorinen et al. 2005).*

	pH	Na	K	Ca	Mg	Cl
ALL-MR f63	11.0	42	7.3	20	<0.5	52
P1	11.42	116	<0.5	36.5	0.021	80.9
OL-SR f63	10.0	4400	150	4300	0.56	13000
A1-3	10.01	1337	60.1	12.2	0.554	1926

Nevertheless, the data from the Allas and Christovrysi Springs clearly indicate that groundwaters of relevant chemistries are being produced in the ophiolite and so will be available at more appropriate sites, such as the Parsata farm spring. The tritium data for samples A1-1 (sampled directly from a fracture in the harzburgite) and P1 (borehole through the bentonite) suggest significant residence times for the hyperalkaline groundwaters. Unfortunately, directly relevant local data on the tritium content of precipitation are not currently available and these have to be accessed for a fuller assessment of groundwater residence times (see comments in section 6.3).

The stable isotope data tend to suggest that the precipitation altitudes are somewhat higher than the current springs, but more importantly suggest that groundwaters associated with the bentonites/bentonite analogues (i.e. P1 and D2) are from distinctly

different systems than those higher on the Troodos Massif. Indeed, re-examination of the data of Boronina (2003) possibly indicates a similar effect, in agreement with the presence of the implied transform faults to the south and south-west of the Troodos Massif (C. Constantinou, *pers. com.,* February 2009). This being the case, more focus should be given to sites in the Mamonia and Circum Troodos Terrains (cf. Figure 1.2) in future.

Here, the more appropriate combination of hyperalkaline groundwater and bentonite/bentonite analogue is certainly available and the groundwater chemistry is fully relevant to the repository environment. Additionally, the P1 site would appear to confirm the conceptual model (Figure 5.1) of the aquiclude role of the bentonite/bentonite analogue, effectively 'trapping' the hyperalkaline groundwater below the bentonite.

5.2 Rock and bentonite/bentonite analogue

Although no petrological observations of active high-pH groundwater-rock interaction could be made from the samples collected to date, there is nevertheless evidence of "fossil" hyperalkaline groundwater interaction at the Trimiklini and Parsata sites. At these two sites, fracture-mineralising tufa, similar to that seen in the active hyperalkaline springs area, penetrates smectite-rich material: either hydrothermally-altered basaltic pillow lavas (Parsata) or poorly-consolidated Tertiary or Quaternary sediments containing >90 % smectite (Trimiklini). The basalt assemblages, in particular, provide some evidence of the interaction of potential hyperalkaline groundwater and smectite. Early diagenetic smectite forms from the hydrothermal alteration of basaltic glass fragments within horizons of autobreccia at the top of the pillow lavas. This is very similar to the fossil reactions observed at the Saile quarry site in the Philippines (see Arcilla et al. 2009; Honrado et al. 2009) where secondary smectite is found throughout a wide swathe of altered pillow lavas and autobreccia.

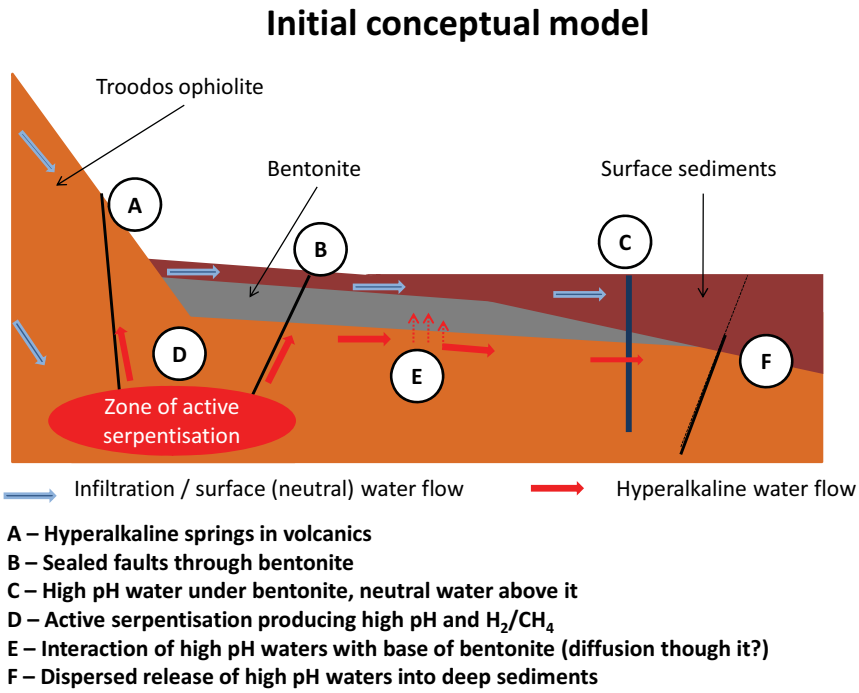

Figure 5.1. *Initial conceptual model of the hyperalkaline groundwater/bentonite reaction zones (after Alexander et al. 2008a).*

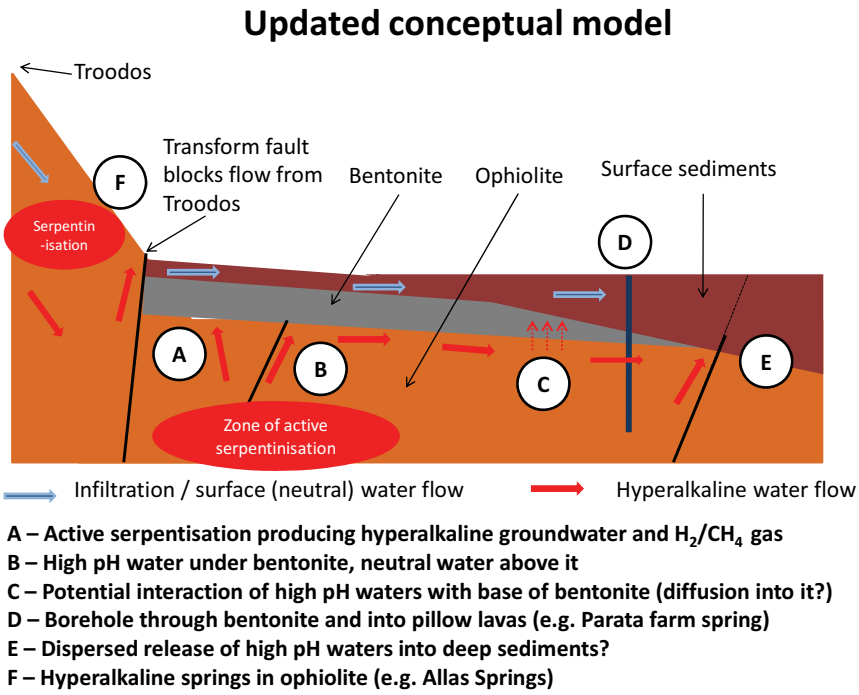

Figure 5.2. *Updated conceptual model of the hyperalkaline groundwater/bentonite reaction zones.*

At the Trimiklini and Parsata sites, petrographic evidence suggests that, adjacent to the tufa-mineralised fractures, this early diagenetic smectite shows evidence of significant morphological change, accompanied by possible dissolution and very fine new mineral formation. However, the tufa mineralisation is complicated by later carbonate mineralisation, associated with the formation of authigenic calcite or calcium oxalate needles, resembling rhizolithic carbonate formation by fungal activity associated with plant roots (e.g. Wright et al. 1995; Becze-Deák et al. 1997). A key element of any future research will be to confirm the link between these tufa-fracture fills and a hyperalkaline groundwater origin for the alteration of smectite. However, it is quite clear that these areas offer significant potential for studying the interaction between high-pH groundwater and smectite-rich sediments.

Mineralogical and petrographic analyses show that the active hyperalkaline groundwater-rock interaction and alteration of serpentinised harzbergite and lherzolite (serpentinite) at the Allas and Christovrysi Springs is dominated by interaction of the groundwater with serpentine minerals (principally 1M and 1T forms). There is little evidence of smectite or other relevant clays at these sites, by which reaction of bentonite/bentonite analogue can be studied.

The principal alteration product of the interaction of the high-pH groundwater with the serpentinite is the formation of the complex Mg-Fe hydroxycarbonate mineral, pyroaurite ($Mg_6Fe_2(SO_4, CO_3)(OH)_{16}.4H_2O$). This phase is isostructural with "green rust" (Taylor and McKenzie, 1980) formed during the corrosion of steel, and also has significant ion-exchange properties and the potential to incorporate heavy metal cations (Seida et al. 2001). This phase may therefore have implications for the retardation of radionuclides in a repository environment, but this is currently outwith the scope of this study.

It appears that all of the solid materials (including soils and clay-sized material) at the Allas and Christovrysi Springs are dominated by serpentine minerals, making clear that almost complete serpentinisation of the original ophiolite lithology (in this area at least) has happened to a previously unsuspected degree. As such, further solid-phase studies at these sites would probably yield little relevant information. Nevertheless, these sites are of use in understanding the production of the hyperalkaline groundwaters (e.g. Milodowski et al. 2009) and have provided additional information for the development of an updated conceptual model (see Figure 5.2).

5.3 Updated conceptual model

The new information collected in Phase II has provided a better understanding of specific sites and has greatly improved the conceptual model of the overall system (Figure 5.2). It now seems likely that hyperalkaline groundwater system of the Troodos Massif is discontinuous with that of the Mamonia and Circum Troodos Terrains, the systems being separated by the Arakapas and Years Transform Faults to the south and southwest of the massif. As such, the hyperalkaline groundwaters identified under the bentonite/bentonite analogue at several sites across Cyprus (e.g. Parsata farm spring) are probably related to separate ophiolite source rocks. Regardless of the source, in these

terrains it seems likely that any active reaction zone will need to be accessed by drilling through to the base of the bentonite/bentonite analogue where the hyperalkaline groundwaters appear to be trapped.

5.4 Other points

Although not a primary focus of the current study, it is interesting to note the relatively high microbial activity observed in association with the hyperalkaline groundwaters. This reflects the findings in the hyperalkaline systems in the Philippines where microbial activity is so marked in some areas that microbial mats have been used as a visual field guide to potential hyperalkaline springs (Alexander et al. 2008b). This is in contrast to the results from the OPC natural analogue in Jordan and the ophiolite natural analogue in Oman, where microbial activity was shown to be low (Bath et al. 1987; West et al. 1995; Smellie 1998; Pitty 2009), possibly due to a lack of nutrients in the system. It remains to be seen if the higher activities noted here and in the Philippines are based on a greater availability of nutrients or are a reflection of the slightly lower pH of the system.

6 CONCLUSIONS AND RECOMMENDATIONS

The two, short, reconnaissance campaigns were extremely useful from the viewpoint of answering many of the questions set at the beginning of Phase II and these are addressed in section 6.1 below. Additional points which could be addressed at the sites are covered in section 6.2 and section 6.3 includes some suggested areas of focus for any future studies.

6.1 Main questions addressed

- *Are the groundwaters accessible and of an appropriate chemistry?* Yes, waters in the range of pH9.5 to 12 have been collected and their chemistries lie well within the range of relevance to low alkali cement leachates (cf. Table 1.3).

- *Are there widespread bentonite/bentonite analogue terrains of the appropriate mineralogy?* Yes, significant areas of the island are 'bentonitic' in the wider sense and extensive deposits of 'true' bentonite deposits also exist.

- *Are there other, smectite-rich sediments and soils where hyperalkaline reaction could also be studied?* Yes, as can be seen in the mineralogical data for the Trimiklini and Parsata areas where smectitic clays dominate the mineralogy of the sediments (up to 100% in some samples). The seemingly all-encompassing serpentinisation of the Allas and Christovrysi Springs areas, and the predominance of basic and ultrabasic bedrocks would seem to rule them out of further study, but the observations on the groundwater chemistry at these sites has supported the development of the conceptual model.

- *Are there options for water sampling with minimum contact with air?* Yes, simple borehole sampling has already been carried out (at the Parsata site) and any future sampling should use boreholes and suitable downhole sampling equipment (see also comments in the discussion).

- *How easy will be sampling profiles of bentonite/bentonite analogue and host rock reaction?* Fossil systems have already been sampled very simply (e.g. Trimiklini road cutting) and can be better constrained using more appropriate soil/unconsolidated sediment sampling techniques (employing Kubiena soil tins, for example) or hand-held corers (cf. Alexander et al. 2008a). This would enable samples to be collected with the minimum of disturbance to the mineral fabrics. Hand-held corers could also be used to sample reacting fractures in the host rock at Allas Springs (NB as the bentonite can be taken as representative of an unfractured diffusive system, the focus could be on an advective fractured system for the host rock).

  With respect to procuring bentonite/bentonite analogue samples from an active hyperalkaline groundwater system, it appears that the only possibility will be to drill into the reaction zone (using a triple-barrel corer to minimise sample disturbance) as the bentonite ore appears to be a very efficient aquiclude (as has

been observed in the Philippines: see Yamakawa et al. 2008, for example). This will be tested in the Philippines during a September, 2009, field campaign and will provide good experience for the project team in advance of doing anything similar in Cyprus. Currently, the best site would appear to be at or near the Parsata Spring, but the conceptual model suggests that any existing borehole drilled through the bentonite/bentonite analogue which contains hyperalkaline groundwater would be a relevant target – for example in the area around the Sarama Springs (site 029, Figure 2.1 and appendix 1). In general, the Mamonia Terrain would be expected to yield the best results.

- *Are indicators of the timescale of hyperalkaline leachate/bentonite and leachate/host rock interaction available?* In essence, yes, but it has not been possible to examine this aspect here due to lack of appropriate samples (see comments above). However, assuming samples from a bentonite/hyperalkaline leachate reaction zone can be collected, various dating methods could be applied. For example, measuring natural decay series disequilibria in a profile across the bentonite/bentonite analogue interface, looking at both the bulk clay and at mineral separates, would allow assessment of timescales of alteration. Note that this should include measurement of ^{226}Ra ($t_{1/2}$ = 1.608 ka) to assess very young perturbations in what is likely to be a complex system.

  Other parameters should include the porosity and mineralogy distribution of the profile, which would allow a clear focus on the areas of most importance (e.g. in and around areas of reduced porosity) and supporting evidence such as stable isotopes in the groundwater and clay (cf. discussion of clay alteration at the Khushaym Matruk site in Jordan in Pitty, 2009). This is discussed further in section 6.3.

- *Are there options for coastal sampling locations where potential bentonite/hyperalkaline fluid reaction under saline conditions could be studied?* Probably. Although not discussed in the report, one site, Petra tou Romiou (Aphrodite's Rock) on the south coast of Cyprus (see site 030 in appendix 1) was examined briefly in failing light. Extensive bentonite and bentonite analogue deposits exist in the area and heavily altered PLV is exposed on the shore and in gullies – but no groundwaters (springs or wells) could be examined in the time available.

  Two additional sites were identified, one in discussion with the GSD and another from the literature since the second field campaign. Both lie on Chrysochou Bay (west Cyprus), one to the NE of the small town of Polis, the other to the NW. The first are a series of reportedly hyperalkaline springs between Argaka and Gialia on the eastern side of the bay (about 20 km due north of the Sarama Springs) and the second are a series of reportedly hyperalkaline springs (e.g. Fontana Amorosa and the Baths of Aphrodite) on the Akamas Peninsula on the western side of the bay. Both areas contain extensive bentonite/bentonite analogue deposits on PLV and their coastal location offers the potential for saline environments. Although the Allas Springs waters are

saline, they are still much more dilute than seawater and so are not really a viable alternative to a coastal site.

- *Presence of gas (hydrogen and/or methane) in many relevant waters?* Although only one site has previously been reported to emit gas (Neal and Shand 2002), most of the cistern-contained springs examined here would also appear to do so (indeed, active degassing of the water could be heard at several sites). Previous (e.g. Abrajano et al. 1988) and recent (C. Arcilla, *pers. comm.,* June 2009) work in the Philippines shows the hyperalkaline groundwater-associated gases to be widespread and associated with low-temperature serpentinisation, so it may be worth considering this as a test of the gas-impermeability of the bentonite ores. Ongoing work in the Zambales ophiolite in the Philippines has shown very little evidence for gas diffusion through the bentonites, even when present in only thin beds (note this will be examined further during a September, 2009, field campaign). Clearly this not a direct technical analogy of the repository environment (high gas pressures in compacted bentonite), but it could be used as an illustrative example of the barrier qualities of bentonite.

  Gas transport of radionuclides away from a repository (either directly on bubbles or, for example, as $^{14}CH_4$) are both of concern (e.g. Nagra, 2002; JAEA, 2007). The gas (H_2 and CH_4) which is evolved during serpentinisation could be a good analogy for gas- induced radionuclide transport in these systems if appropriate sampling can be carried out.

- *Good support infrastructure available at reasonable cost?* Yes, as long as the field work is conducted outwith the main tourist season, living costs are very reasonable as are flights from Europe (and most main cities have direct flights to Cyprus several times a week, even in winter). In addition, a massive road improvement scheme over the last 5-10 years means that the transport infrastructure is as good as anywhere in Europe.

- *Existence of a national Geological Survey (the GSD) or mining company for local support?* The GSD have been enormously helpful in every way possible and it is hoped that this will continue. Although the project is well outside their remit, it is recognised that associating younger GSD staff with the project allows them to be trained in areas outwith their normal responsibility. Further, involvement of more senior staff in external project publications allows them access to another audience than those they deal with routinely and this should be encouraged during any subsequent work.

- *Lack of political sensitivity to field work?* Absolutely no problem (apart from over-zealous hunters on Sunday mornings and Wednesday afternoons). Although the GSD is unable to offer direct support for drilling etc, they can recommend experienced companies when required by the project. And the direct involvement of younger GSD staff in the field work has been invaluable in aiding site access.

6.2 Additional areas

In addition to bentonite alteration, other features and processes of relevance to the use of low alkali cements in radioactive waste disposal could be studied in parallel to the main focus. These include:

- examination of the behaviour of microbes in the hyperalkaline leachates (cf. West et al. 1995). The travertines preserve (i.e. "fossilise") abundant biofilm with bacterial cell and other microbiological material of various forms, including: individual and clusters of coccoid cells and rod-shaped cells, spirochaete and single chain forms; cells in the act of mytosis (splitting); and amoeboid cells and nematode-like organisms that may have been grazing on the biofilm/bacteria. These features indicate that complex active microbial assemblages can survive in these high-pH conditions.

- cellulose breakdown: travertines formed at the spring discharge sites (particularly those within the forested areas at Allas Springs) enclose remnants of woody plant debris, which potentially enable analogous observation of the interaction between cellulose wastes and high-pH groundwater. Observations show that the cellular cavities of the woody tissues have been partially filled by calcium carbonates (aragonite, high- and low-Mg calcites). There is some evidence that the cell walls are gradually broken down, but that much of cell wall material is actually preserved intact.

- potential sealing of host rock fractures through reaction with the hyperalkaline groundwaters. Clearly the thick tufa deposits at the surface seal fractures and soils, but is this also the case at depth, away from atmospheric CO_2?

- sealing of the matrix – directly related to the above point. If fractures in host rock do at least become coated with secondary reaction products, will this seal off the matrix and 'close down' matrix diffusion?

6.3 Focus of any future studies

The overall concensus from the two reconnaissance campaigns is that appropriate sites exist in Cyprus where the core project aims (and additional, lower priority, targets) can be met. This being the case, it is suggested that Phase III should be initiated with the following boundary conditions:

- The project duration should be 1.5 years, so as to provide data as soon as possible. Although intensive, this can be done assuming the main focus remains bentonite/bentonite analogue reaction
- Comprehensive, quality assured documentation will be given high priority and regular reports will ensure all information obtained is distributed to all partners as quickly as possible
- Final project report would be complemented by production of at least one reviewed technical paper

Specific technical boundary conditions include:

- Focussing on the Mamonia Terrain, identify 2 or 3 appropriate sites for sampling the base of the bentonite/bentonite analogue. 'Appropriate' also means areas where permission is likely to be given to drill and this will be discussed thoroughly with the GSD. It is clear that sites such as Parsata offer the ideal combination of appropriate hyperalkaline groundwaters in contact with bentonite/bentonite analogue and these areas will be the focus of future work
- Drill boreholes through the bentonite/bentonite analogue to access the reaction zone. Samples of bentonite and underlying host rock to be collected by triple-barrel corers (to minimise disturbance) and interface to be packed off to allow controlled groundwater sampling[6]
- Sample 1 'fossil' system for comparison – both the Triniklini and Parsata sites have abundant smectite (up to 100 % in some samples) and evidence of 'fossil' flow systems
- Analysis of solid and liquid phase samples, with the protocols based on those reported here (see also comments below)
- Solid phase sampling should include a section across the base of the bentonite/bentonite analogue and/or across any fracture in the bentonite/ bentonite analogue[7]
- Assess potential indicators of the age of reaction processes in the bentonite/ bentonite analogue. In addition to 'standard' radiochemical and mineralogical methods, this could include palaeomagnetic tools (cf. Pitty 2009). One of the key issues to be addressed at an early stage in the research will be to establish the precise nature and origin of any bentonite reaction. The value of the analogue will depend significantly on determining whether the palaeo- or ongoing bentonite alteration is definitively related to interaction with hyperalkaline groundwater, or results from hydrothermal alteration or weathering-related processes. This will require specialist petrological and geochemical expertise focussing on the recognition and characterisation of mineralogical features characteristic to alkali-rock interaction, and the ability to define and differentiate alteration related to different hydrogeological and hydrogeochemical regimes.

  Another particular interest will be establishing profiles from a zone of interaction (e.g. the base of the bentonite) back into the unaltered material. This will allow definition of the degree of change and also the mode of fluid transport – was it diffusive, as would be expected?

  Samples should first be petrographically characterised in detail. Standard and polished petrographic thin-sections will be prepared and these will initially be examined using an optical petrographic microscope. Materials will be stabilised

[6] Note that this needs to be done as soon as possible after the start of the project to allow the borehole to recover, otherwise the groundwater samples will be too disturbed to be of any use.

[7] In the Saile quarry site in the Philippines, reaction has been observed in fractures and microfractures in the basal layers of the bentonite (C.Pascau, *pers. comm.,* June, 2009)

by impregnation with epoxy resin prior to thin section preparation and a coloured dye (normally blue) will be added to the epoxy-resin to enable porosity characteristics to be more readily visualised under the optical petrographic microscope.

Samples that have potentially been altered by hyperalkaline groundwater will be characterised in greater detail by higher-resolution petrographical observations using backscattered scanning electron microscopy (BSEM). Mineralogical identification of phases observed under BSEM will be aided by qualitative and quantitative microchemical analyses using either energy-dispersive X-ray microanalysis (EDXA) or wavelength-dispersive X-ray microanalysis (WDXA). Consideration should also be given to using higher-resolution analytical transmission electron microscopy (ATEM) to characterise clay mineral alteration, particularly smectite, where the particle size is likely to be at the limits of the special resolution of SEM-based techniques Cathodoluminescence microscopy will also be used, where appropriate, to further observe and characterise the different generations of carbonate or other fluorescent mineral precipitates that may be present[8].

Samples will also be prepared as stub-mounts for examination in the scanning electron microscope by secondary electron imaging (SEI). SEI observations will be used to characterise morphological relationships, and to examine features related to rock-water interaction at mineral and fracture surfaces for evidence indicative of hyperalkaline groundwater alteration, secondary precipitates and dissolution that may impact on hydrogeological and rock mass transport properties.

Quantitative chemical compositions of hyperalkaline alteration products will be determined by EDXA or WDXA, and ATEM should be considered for microchemical characterisation of altered clay minerals and very fine grained reaction products likely to be encountered. Samples of background (i.e. unaltered) bentonite/bentonite analogue and altered bentonite/bentonite analogue that has reacted with hyperalkaline groundwater will be analysed by X-ray diffraction analysis (XRD) to characterise changed in both bulk mineralogical characteristics and changes in clay mineralogy. Quantitative whole rock mineralogy will be determined by Rietveld modelling of XRD profiles from material prepared as randomly orientated XRD mounts. Clay mineralogical characteristics will be quantified using NEWMOD modelling of XRD profiles recorded from orientated mounts of separated < 2 micron fraction material.

Bulk chemical composition of background and altered bentonite/bentonite analogue samples will be determined by X-ray fluorescence spectroscopy (XRF). Major element XRF analysis will be performed on material prepared as fused glass beads. Trace element XRF analyses will be performed on material prepared as pressed powder pellets.

[8] To be expected when the hyperalkaline groundwaters and bentonite porewaters mix.

In the case of fossil hyperalkaline interaction sites, a key requirement will be to establish the link between now-inactive travertine/tufa and associated mineralogical alteration of the host rocks and sediments, and past hyperalkaline groundwater. This will be important in order to differentiate this type of rock-water interaction from alteration associated with some other process (e.g. calcrete formation or old hydrothermal activity). Stable isotope analysis ($\delta^{13}C$ and $\delta^{18}O$) and $^{87}Sr/^{86}Sr$ analysis of carbonate fracture fills and related alteration products should be included as potential tracers of the reaction pathway, and compared with analyses of the isotopic composition of presently-active hyperalkaline groundwaters

Comparison will be made between these observations and the nature of secondary phases (such as CSH minerals, zeolites etc) and changes in physical properties predicted from experimental studies or from geochemical modeling of hyperalkaline groundwater-rock interaction.

Of importance is to try and establish timescales of alteration and this will be approached by means of natural decay series measurements. Critical here will be to look at the entire decay chain from ^{238}U down to ^{226}Ra as this will allow definition of timescales between several million and 10s of thousands of years. Appropriate modelling of the raw data also allows an assessment of whether the alteration has been a simple, single phase reaction or a multi-phase, multi-event alteration. This should be supported by a systematic study of the Sr ($^{87}Sr/^{86}Sr$), C ($\delta^{13}C$) and O ($\delta^{18}O$) isotopic systems as these can all provide additional information on the conditions under which alteration took place and the nature of the reacting fluid(s). Consideration should also be given to the potential use of modern electron spin resonance, optical stimulated luminescence and cosmogenic isotope dating techniques for potentially dating travertine deposits and vein fillings that may not be conducive to conventional radiometric dating techniques, which can be appropriate to dating over archaeological to short geological timescales

Additionally, dating the groundwaters is required for any attempt to assess bentonite/bentonite analogue reaction times: the data currently available imply reasonable ages for the hyperalkaline waters, but this needs to be better supported with a wider range of analytical techniques (e.g. natural decay series, ^{14}C, $^{39}Ar/^{85}Kr$). Access to the raw data of Jacovides (1979) and Boronina (2003) would also allow better definition of the tritium ages of the groundwater.

Modelling of bentonite reaction processes and integration of data with that currently available from ongoing laboratory studies.

Further development of the conceptual model as more data become available. The initial conceptual model (Figure 5.1) has already been updated (Figure 5.2) and this will continue as a better understanding of the system is gained. This will allow the full relevance of the analogy to be understood and more effectively fed into the repository performance assessment.

7 ACKNOWLEDGEMENTS

The authors would like to thank the Project Funding Partners of the Cyprus Natural Analogue Project (CNAP) Phase II, namely the NDA (UK), Posiva (Finland) and SKB (Sweden), for their moral support and financial backing. In addition, we would like to warmly thank all our colleagues at the Geological Survey Department of Cyprus (GSD) for their immense help and support. Very special thanks to Dr Eleni Georghiou Morisseau (Acting Director of the GSD) and Dr Costas Constantinou (Head of the Hydrogeological Section, GSD).

REFERENCES

T.A.Abrajano, N.C.Sturchio, J.K.Bohlke, G.L.Lyon, R.J.Poreda and C.M.Stevens (1988). Methane-hydrogen gas seeps, Zambales Ophiolite, Philippines: Deep or shallow origin? *in*: M. Schoell, Origins of Methane in the Earth. Chem. Geol., 71, 211-222.

H.Ahokas, P.Hellä, et al. (2006). Control of water inflow and use of cement in ONKALO after penetration of fracture zone R19. Posiva Working Report 2006-45, Posiva, Olkiluoto, Finland.

W.R. Alexander (ed) (1992) A natural analogue study of the Maqarin hyperalkaline groundwaters. I. Source term description and thermodynamic database testing. Nagra Technical Report, 91-10, Nagra, Wettingen, Switzerland.

W.R.Alexander (2009). Groundwater colloid sampling and characterisation. Ch 2 *in* S.W.Swanton, W.R.Alexander, J.A.Berry and M.Kelly. Review of the behaviour of colloids in the geosphere. NDA Technical Report, NDA 09-XX, NDA-RWMD, Harwell, UK (*in press*).

W.R.Alexander and F.B.Neall (2007). Assessment of potential perturbations to Posiva's SF repository at Olkiluoto caused by construction and operation of the ONKALO facility. Posiva Working Report 2007-35, Posiva, Olkiluoto, Finland.

W.R.Alexander, A.Gautschi and P.Zuidema (1998). Thorough testing of performance assessment models: the necessary integration of *in situ* experiments, natural analogues and laboratory work. Sci. Basis Nucl. Waste Manag. XXI, 1013-1014.

W.R.Alexander, L.E. McKinley and I.G.McKinley (2007). Chapter 10: A Look to the Future *in* W.R.Alexander and L.E.McKinley (*eds*). Deep geological disposal of radioactive wastes. Elsevier, Amsterdam, The Netherlands.

W.R.Alexander, I.G.McKinley, C.A.Arcilla, Y.Takahashi, H.Kawamura, M.Yamakawa and K.Aoki (2008a). Hyperalkaline Natural Analogue Potential in the Philippines. Proc. 2nd East Asia Forum on Radwaste Management (EAFORM) Conference, 20-23 October 2008, Tokyo, Japan. RWMC, Tokyo, Japan.

W.R.Alexander, C.A. Arcilla, I.G.McKinley, H.Kawamura, Y.Takahashi, K.Aoki and S.Miyoshi (2008b). A new natural analogue study of the interaction of low-alkali cement leachates and the bentonite buffer. Sci Basis Nucl Waste Manag XXXI, 493-500.

G.B.Allison, C.J.Barnes, M.W.Hughes and F.W.J.Leaney (1983). Effect of climate and vegetation on oxygen-18 and deuterium profiles in soils. Isotope Hydrology. IAEA, Vienna, Austria.

C.A.Arcilla, C.S.Pascua, E.Vargas, M.L.L.Honrado, W.R.Alexander, K.Namiki, N.Fujii, M.Yamakawa, T.Sato and I.G.McKinley (2009). Reaction pathways for rising hyperalkaline groundwater in a bentonite mine in the Philippines. Proc. Goldschmidt

2009 Conference, Davos, 22-26 June, 2009. Geochim Cosmochim Acta, Goldschmidt Conference Abstracts, A50

A.Atkinson (1985). The time-dependence of pH within a repository for radioactive waste disposal UKAEA Tech. Rep. AERE-R11777, Harwell, Oxon, GB.

I.Barnes and J.R.O'Neill (1969). The relationship between fluids in some fresh alpine-type ultramafics and possible modern serpentinisation, western United States. Geol. Soc. Amer. Bull., 80, 1947-1960.

I.Barnes, J.B.Rapp, J.R.O`Neil, R.A.Sheppard and A.J.Gude (1972). Metamorphic assemblages and the direction of flow of metamorphic fluids in four instances of serpentinisation. Contrib. Min. Pet. 35, 263-276.

S.Baskaran, T.Ransley and R.S.Brodie (2005). Tools for assessing groundwater-surface water interactions: a case study in the Border Rivers catchment, Murray-Darling Basin. Bureau of Rural Sciences, Canberra, Australia.

A.H.Bath., N. Christofi, C. Neal, J.C. Philp, M.R. Cave, I.G. McKinley and U.Berner (1987). Trace Element and Microbiological Studies of Alkaline Groundwaters in Oman, Arabian Gulf: A Natural Analogue for Cement Pore Waters. BGS Report FLPU 87-2, BGS, Keyworth, UK.

L.M.Bear (1960). The geology and mineral resources of the Akaki-Lythrodondha area. Geological Survey Department Memoirs No. 3, GSD, Lefkosia, Cyprus.

J. Becze-Deák, R. Langohr and E.P. Verrechia (1997) Small-scale secondary CaCO3 accumulations in selected sections of the European loess belt. Morphological forms and potential for paleoenvironmental reconstruction. Geoderma, 76, 221-252.

A.V.Boronina (2003). Application of numerical modelling, isotope studies and streamflow observations for quantitative description of hydrogeology of the Kouris catchment (Cyprus). ETH PhD Thesis No. 15338, ETH, Zürich, Switzerland.

A.V.Boronina, W.Balderer, P:Renard and W.Stichler (2005). Study of stable isotopes in the Kouris catchment (Cyprus) for the description of the regional groundwater flow. J.Hydrol. 308, 214 – 226.

M.H.Bradbury and B.Baeyens (2002). Porewater chemistry in compacted, re-saturated MX-80 bentonite: physico-chemical characterisation and geochemical modelling. PSI Report 02-10, PSI, Villigen, Switzerland.

N.Y.Bragin, L.G.Bragina, K.G.Kaleda and K.A.Krylov (2005). The Sedimentary Cover of the Troodos Massif. Ch. 1H (pp41-48) *in* Geological Framework of the Levant Volume I: Cyprus and Syria. Historical Productions-Hall, London, UK, ISBN 965-7297-02-8.

L.G.Bragina and N.Y.Bragin (1996). Stratigraphy and radiolarians of the type section of the Upper Cretaceous Perapedhi Formation (Cyprus). Stratigraphy and Geol. Correlation, 4, 38-45, Moscow (*in Russian*).

A.Brogniart (1813). Essai de classifacation mineralogique des roches melanges, Journal des Mines, v. XXXIV, 190-199 (*in French*).

N.A.Chapman, I.G.McKinley and J.A.T.Smellie (1984). The Potential of Natural Analogues in Assessing Systems for Deep Disposal of High-Level Radioactive Waste; Nagra Technical Report NTB 85-41, Nagra, Wettingen, Switzerland.

G.E.Christidis (2006). Genesis and compositional heterogeneity of smectites. Part III: Alteration of basic pyroclastic rocks—A case study from the Troodos Ophiolite Complex, Cyprus. Amer. Min. 91, 685-701.

H.Craig (1961). Isotopic variations in meteoric waters. Science 133, 1702–1703.

H.Craig and L.Gordon (1965). Deuterium and Oxygen-18 variations in the ocean and the marine atmosphere *in* Stable isotopes in oceanographic studies and paleotemperatures. Spoleta. pp.9–130.

E.E.Davies and H.Elderfield (*eds*) (2004). Hydrogeology of the Oceanic Lithosphere, Cambridge University Press, Cambridge, UK.

I.D.Gass, C.J.MacCleod, B.J.Murton, A.Panayiotou, K.O.Simonian and C.Xenophontos (1994). The Geology of the Southern Troodos Transform Fault Zone. Geological Survey Department Memoir No.9, GSD, Lefkosia, Cyprus.

J.R.Gat (1971). Comments on stable isotope method in regional groundwater investigations. Water Resources. Research, 7, 980-993.

Geotimes (1972). Penrose Conference report. Geotimes, pp24-25, Am. Geol. Inst., Alexandria, USA.

J.J.Gibson, T.W.D.Edwards and T.D.Prowse (1999). Pan-derived isotopic composition of atmospheric water vapour and its variability in northern Canada. Journal of Hydrology 217, 55-74.

M.R.Gillespie and M.T.Styles (1999). BGS Rock Classification Scheme. Volume 1: Classification of Igneous Rocks. British Geological Survey Research Report (2nd Edition), RR99-06, 52pp. British Geological Survey, Keyworth, Nottingham, UK.

J.I.Goldstein, D.E.Newbury, P.Echlin, D.C.Joy, C.Fiori and E.Lifshin (1981). Scanning Electron Microscopy and X-Ray Microanalysis. Plenum Press, New York.

GSD (1959). 1:31,680 Geological Map of the Xeros-Troodos Area (Sheet 2), Geological Survey Department Maps, GSD, Lefkosia, Cyprus.

C.R.Hallsworth and R.W.O'B.Knox (1999). BGS Rock Classification Scheme. Volume 3: Classification of Sediments and Sedimentary Rocks. British Geological Survey Research Report, RR99-03. British Geological Survey, Keyworth, Nottingham, UK.

A.Haworth, S.M.Sharland, P.W.Tasker and C.J.Tweed (1987) Evolution of the groundwater chemistry around a nuclear waste repository. Sci. Basis Nucl. Waste Manag., XI, 425-434

S.Hillier (1999). Use of an air-brush to spray dry samples for X-ray powder diffraction. Clay Minerals, 34, 127-135.

S.Hillier, K.Suzuki and J. Cotter-Howells (2001). Quantitative determination of Cerussite (lead carbonate) by X-ray powder diffraction and inferences for lead speciation and transport in stream sediments from a former lead mining area of Scotland. Applied Geochemistry, **16**, 597-608.

M.L.L.Honrado, C.S.Pascua, E.Vargas, C.A.Arcilla, W.R.Alexander, K.Namiki, N.Fujii, M.Yamakawa, T.Sato and I.G.McKinley (2009). Smectite and zeolite formation from the pyroclastic deposits of the Aksitero Formation, Philippines. Proc. Goldschmidt 2009 Conference, Davos, 22-26 June, 2009. Geochim Cosmochim Acta, Goldschmidt Conference Abstracts, A547

IAEA (2005). Isotopic composition of precipitation in the Mediterranean Basin in relation to air circulation patterns and climate. Final report of a coordinated research project, 2000-2004. IAEA-TECDOC-1453, IAEA, Vienna, Austria.

ICDD (2008). CDD PDF-4+ 2008 database, International Centre for Diffraction Data (ICDD), 12 Campus Boulevard, Newton Square, PA, USA.

J.Jacovides (1979). Environmental isotope survey (Cyprus), Final report on I.A.E.A., research contract No: 1039/RB, Technical Report, Ministry of Agriculture and Natural Resources, Department of Water Development, Nicosia, Cyprus, 82 p.

JAEA (2007). Second progress report on R&D for TRU waste disposal in Japan. JAEA Review 2007-010/FEPC TRU-TR2-2007-01, JAEA, Tokai, Japan.

O.Karnland, U.Nilsson, S.Olsson and P.Sellin (2005). Laboratory experiments with compacted bentonite in contact with highly alkaline solutions, R&D on Low-pH cement for a geological repository. Ch. 3 *in* Bäckblom, G. (2005) (*ed*). ESDRED: supporting documents of the first training workshop: proceedings of the 2nd low pH workshop, Madrid, 15-16 June, 2005. ANDRA Unpubl. Internal Report, ANDRA, Paris, France.

W.C.Knight (1898) Bentonite. Engineering & Mining Journal, 66, p491.

C.W.Kreitler and B.E.Bledsoe (1993). Geochemical techniques for identifying sources of ground-water salinization. CRC Press, London, UK.

T.Kunimaru, K.Ota, W.R.Alexander and H.Yamamoto (2009). Horonobe Underground Research Laboratory Project: Quality assurance audit of hydrochemical data from surface-based investigations. Proceedings of the Annual Meeting of the Atomic Energy Society of Japan (23rd – 25th March 2009), AESJ, Tokyo, Japan (*in Japanese*).

M.Laaksoharju (2008). (*ed*) Hydrogeochemistry Forsmark Site descriptive modelling SDM-Site Forsmark. SKB Report R-08-07, SKB, Stockholm, Sweden.

M.Laaksoharju, J.A.T.Smellie, P.Ruotsalainen and M.Snellman (1993). An approach to quality classification of deep groundwaters in Sweden and Finland. SKB Report TR-93-27, SKB, Stockholm, Sweden.

C.M.Linklater (ed) (1998). A natural analogue study of cement-buffered, hyperalkaline groundwaters and their interaction with a repository host rock. Phase II. Nirex Science Report, S/98/003., United Kingdom Nirex Limited, Harwell, UK.

C.J.MacLeod (1990). Role of the Southern Troodos Transform Fault in the rotation of the Cyprus microplate: evidence from the Eastern Limassol Forest Complex. *In*: J. Malpas, E. M. Moores, A. Panayiotou and C. Xenophontos (*eds*.), Ophiolites: Oceanic Crustal Analogues, Proceedings of the Symposium Troodos 1987, Nicosia, 1987, Cyprus, p. 75-85.

I.G.McKinley (1989). Applying natural analogues in predictive performance assessment (1): principles and requirements; (2): examples and discussions. Risk analysis in nuclear waste management, pp.357-396, Klewer Academic Publ., The Netherlands.

I.G.McKinley, A.H.Bath, U.Berner, M.Cave and C.Neal (1988) Results of the Oman analogue study. Radiochim Acta, 44/45, 311-316.

R.Metcalfe and C.Walker (2004). Proceedings of the International Workshop on Bentonite-Cement Interaction in Repository Environments 14–16 April 2004, Tokyo, Japan. NUMO Tech. Rep. NUMO-TR-04-05, NUMO, Tokyo, Japan.

W.M.Miller, W.R.Alexander, N.A.Chapman, I.G.McKinley, and J.A.T.Smellie (2000). Geological disposal of radioactive wastes and natural analogues. Waste management series, vol. 2, Pergamon, Amsterdam, The Netherlands.

A.E.Milodowski, C.A.Constantinou, W.R.Alexander, M.Rigas, C.Tweed, P.Sellin, P. Korkeakoski, S.J.Kemp and J.C.Rushton (2009). Reaction of bentonite in low-alkali cement leachates: preliminary results from the Cyprus Natural Analogue Project. ICEM'09 Conference, Liverpool, UK, October, 2009 (*submitted*).

J.B.Moody (1976). Serpentinisation: a review. Lithos, 9, 125-138.

D.M.Moore and R.C. Reynolds (1997) X-Ray Diffraction and the Identification and Analysis of Clay Minerals, Second Edition. Oxford University Press, New York.

Nagra (2002). Project Opalinus Clay – Safety Report. Nagra Technical Report NTB 02-05, Nagra, Wettingen, Switzerland.

C.Neal and G.Stanger (1983). Hydrogen generation from mantle source rocks in Oman. Earth Planet. Sci. Lett., 66, 315–320.

C.Neal and P.Shand (2002). Spring and surface water quality of the Cyprus Ophiolites. Hydrol. Earth System Sci., 6, 797-817.

ONDRAF (2001). SAFIR 2, Safety assessment and feasibility interim report 2, ONDRAF/NIRAS Technical Report NIROND 2001-05E, ONDRAF/NIRAS, Brussels, Belgium.

K.Ota, T.Kunimaru and W.R.Alexander (2009). A quality assurance programme for rock matrix porewater hydrochemistry: an example from JAEA's Horonobe underground research laboratory, Japan. Geochemistry: Exploration, Environment, Analysis (*submitted*).

PANalytical (2006a). X'Pert HighScore Plus V2.2a software, PANalytical B.V., Almelo, The Netherlands.

PANalytical (2006b). PANalytical Epsilon 5 version 2.0A, 2006. PANalytical B.V., Amelo, The Netherlands. http://www.panalytical.com/index.cfm?pid=609

PANalytical (2008). PANalytical SuperQ version 4.0o, 2008 (including Protrace application package). PANalytical B.V., Amelo, The Netherlands
http://www.panalytical.com/index.cfm?pid=190

T.M.Pantazis (1967). The geology and mineral resources of the Pharmakas-Kalavasos area. Geological Survey Department Memoirs No. 8, GSD, Lefkosia, Cyprus.

S.M.Pate, I.G.McKinley and W.R.Alexander (1994). Use of natural analogue test cases to evaluate a new performance assessment TDB *in* Proceedings of the 5th NAWG workshop, Toledo, Spain, September 1992. H. von Maravic and J.A.T. Smellie (*eds*). CEC Report EUR 15176 EN, pp321-331.

J.C.Petit (1992). Reasoning by analogy: rational foundation of natural analogue studies. Appl. Geochem. (Suppl. Issue 1), 9-12.

B.J.Presley, C.Petrowski, and I.R.Kaplan (1973). Ch 31.2. Interstitial water chemistry: DSDP Leg 13, pp809-811. Deep Sea Drilling Project Initial Reports, IODP, Housten, USA (doi:10.2973/dsdp.proc.13.1973).

R.C.Reynolds and R.C.Reynolds (1996). Description of Newmod-for-Windows™. The calculation of one-dimensional X-ray diffraction patterns of mixed layered clay minerals. R.C.Reynolds Jr., 8 Brook Road, Hanover, USA.

A.H.F.Robertson and N.H.Woodcock (1979). Mamonia Complex, Southwest Cyprus: evolution and emplacement of a Mesozoic continental margin. Geol. Soc. Am. Bull., 90, 651-655.

A.H.F.Robertson, J.E.Dixon, et al. (2003). Edinburgh University School of GeoSciences Honours Geology and GPG excursion to Cyprus Field Guide. Unpubl. internal note, The School of GeoSciences, University of Edinburgh, UK.

H.H.Schopka and L.A.Derry (2009). Chemical weathering rates of ultramafic to intermediate rocks in the Philippines. Appl.Geochem. (*submitted*).

Y.Seida, Y.Nakano and Y.Nakamura (2001). Rapid removal of dilute lead from water by pyroaurite-like compound. Water Res., 35, 2341-2346.

P.Sellin, F.Karlsson, L.Werme, K.Spahiu and I.Puigdomenech (2003). Effect of pH on the safety of KBS-3 deep repository and the confidence in safety assessments. Proceedings of a workshop on Qualification of Low pH Cement for a Geological Repository, Oct 15-16, 2003, Stockholm. SKB, Stockholm, Sweden.

K.O.Simonian and I.G.Gass (1978). Arakapas fault belt, Cyprus: a fossil transform fault. Geol. Soc. Am. Bull., 89, 1220-1230.

J.A.T.Smellie, A.B.MacKenzie and R.D.Scott (1985). An analogue validation study of natural radionuclide migration in crystalline rocks using uranium series disequilibrium: preliminary results; Sci. Basis Nucl. Waste Manag. IX, pp.91-98.

J.A.T. Smellie (ed) (1998). Maqarin natural analogue study: Phase III. SKB Technical Report, TR-98-04, Svensk Kärnbränslehantering (SKB), Stockholm, Sweden.

R.L.Snyder and D.L.Bish (1989). Chapter 5 Quantitative analysis (pp. 101-144). In: Bish, D.L., Post, J.E. (*Eds*), *Modern Powder Diffraction, Reviews in Mineralogy*, Volume 20, Mineralogical Society of America, USA.

A. Streckeisen (1973). Plutonic Rocks. Classification and nomenclature recommended by the IUGS Subcommision on the Systematics of Igneous Rocks. Geotimes, 18 (10), 26-30

R.M.Taylor and R.M.McKenzie (1980). The influence of aluminium on iron oxides. VI: The formation of Fe(II)-Al(III) hydroxychlorides, sulphates, and carbonates as new members of the pyroaurite group and their significance in soils. Clay Miner., 28, 179-187.

H.Umeki (2009). Holistic assessment to put mobile radionuclides in perspective. Proc. MOFAP'07, January 16-19 2007, La Baule, France (*in press*).

R.C.Upstill-Goddard and H.Elderfield (1988). The role of diagenesis in the estuarine budgets of iodine and bromine. Continental Shelf Research 8, 405-430.

U.Vuorinen, J.Lehikoinen, H.Imoto, T.Yamamoto and M.Cruz Alonso (2005). Injection Grout for Deep Repositories, Subproject 1: Low-pH cementitious Grout for Larger Fractures, Leach Testing of Grout Mixes and Evaluation of the Long-Term Safety. Posiva Working Report 2004-46, Posiva, Olkiluoto, Finland.

I.M.West (2007). Geology of the Salt Lake and Coast of the Akrotiri Peninsula, Cyprus. National Oceanography Centre, Southampton, UK. Internet site. http://www.soton.ac.uk/~imw/Cyprus-Akrotiri-Lake-Coast.htm. Version: 16 January 2007.

J.M.West, P.Coombs, S.J.Gardner and C.A.Rochelle (1995). The microbiology of the Maqarin site, Jordan - a natural analogue for cementitious radioactive waste repositories. Sci.Basis Nucl. waste Manag. XVIII, pp181-188.

J.West, W.R.Alexander, K.Kaku, I.G.McKinley and A.Shimmura (2002). Communication of nuclear power concepts to stakeholders - the use of nature's own laboratories. Proceedings for NUCEF 2001 - Scientific Bases for Criticality Safety, Separation Process and Waste Disposal. 31 Oct to 2 Nov 2001, Tokai, Japan. Japan Atomic Energy Research Institute Report JAERI Conf 2002-004. pp 47 – 54

R.A.M.Wilson and F.T.Ingham (1959). The geology of the Xeros-Troodos area. Geological Survey Department Memoir Number 1, Nicosia, Cyprus.

V.P.Wright, N.H.Platt, S.B.Marriott and V.H.Beck (1995) A classification of rhizogenic (root-formed) calcretes, with examples from the Upper Jurassic-Lower Cretaceous of Spain and Upper Cretaceous of southern France. Sedimentary. Geology, 100, 143-158.

M.Yamakawa, W.R.Alexander, I.G.McKinley, C.A.Arcilla, Y.Takahashi and K.Namiki (2008). The potential in the Philippines for studying natural analogues of the interaction of low-alkali cement leachates and bentonite barriers in a radioactive waste repository. Proc. Japan-Korea Joint Meeting, 30th April – 1st May, 2008, Tokyo. RWMC, Tokyo, Japan.

LIST OF APPENDICES

Short overview of all sites examined during the reconnaissance campaign in December, 2008.

A table listing all sites examined is presented below and a short description of each site (with photographs where appropriate) is provided.

Grid UTM, Datum WGS 84

Site	GPS No	Date	Zone	Easting	Northing	Altitude (m)
Allas Springs (trackway)	1	27-Nov-08	36 S	0492157	3867233	1238
Chrisovrysi Spring (alt. Chrisovrysy Spring)	2	27-Nov-08	36 S	0493102	3865570	1306
Pashalivadi (alt. Pashialivadi or Livadhitou Pasha)	3	27-Nov-08	36 S	0489893	3865729	1659
Para Pedi	4	27-Nov-08	36 S	0486363	3858065	886
F819 road cutting, between Agios Mamas and Trimiklini	4a	27-Nov-08	36 S	0493124	3857357	646
Kalavasos-Parsata road	5	30-Nov-08	36 S	0525666	3850496	149
Parsata Dam	6	30-Nov-08	36 S	0525512	3850935	171
Parsata-Layia road cutting, c.2 km north of Parsata	7	30-Nov-08	36 S	0523623	3854496	403
Parsata village, valley top - dry spring	8	30-Nov-08	36 S	0524196	3853887	401
Parsata valley bottom	9	30-Nov-08	36 S	0523801	3853732	318
Parsata valley bottom	10	30-Nov-08	36 S	0523936	3853795	345
Layia well locations	11	30-Nov-08	36 S	0522450	3856066	394
Layia-Ora road cutting	12	30-Nov-08	36 S	0521825	3856209	413
Arakapas road cutting	13	30-Nov-08	36 S	0508764	3856116	419
Ayos Mamas road cutting near artesian well	14	30-Nov-08	36 S	0495973	3856391	521
Ayos Mamas artesian well location	15	30-Nov-08	36 S	0495940	3856399	516
Dry waterfall with major travertine-flowstone deposit	16	30-Nov-08	36 S	0496698	3853598	400
Pedoulas, war memorial spring upper valley	17	01-Dec-08	36 S	0484451	3869810	986
Pedoulas valley bottom, potential sping location	18	01-Dec-08	36 S	0484497	3870514	842
Pedoulas valley bottom, potential sping location	19	01-Dec-08	36 S	0484484	3870698	827
Allas Springs, stream	20	01-Dec-08	36 S	0492026	3867150	**1327***
Allas Springs, stream near source	21	01-Dec-08	36 S	0492033	3867145	**1326+**
Allas Springs, stream reappears from scree	22	01-Dec-08	36 S	0492092	3867213	1279
Allas Springs, Cistern 1	23	01-Dec-08	36 S	0492099	3867264	1275

Allas Springs, Cistern 2	24	01-Dec-08	36 S	0492125	3867229	1260
Allas Springs, Cistern 4	25	01-Dec-08	36 S	0492154	3867226	1268
Kalasavos-Asgata, road cutting below military camp	26	02-Dec-08	36 S	0522541	3850378	234
Asgata-Monagroulli road, road cutting	27	02-Dec-08	36 S	0522648	3847913	290
Pambajera Hill, disused quarry near Monagroulli	28	02-Dec-08	36 S	0520890	3847088	214
Sarama Springs, possible borehole location	29	02-Dec-08	36 S	0456036	3867962	214
Petra tou Romiou (Aphrodite's Rock) on the south coast of Cyprus	30	02-Dec-08	nd	nd	nd	Sea level

** note this should be c.10m lower*
+ note this should be c.10m higher

Site 001: Allas spring, Troodos Massif (0492157, 3867233 +/-6m) Alt 1238m. pH (GSD meter) of 12.5, cond 6.9 mS cm^{-1}, T=10°C. pH papers registered 11. Spring discharge collected in cistern on forest track, pH measured on cistern discharge. Source in ultrabasics in cliffs above site. NB stream discharging from site gave pH 11 with papers – no precipitates in stream – measured 30 m upstream from cistern. This site was revisited for a detailed study, see site 20 for description.

Site 002: Chrysovrysi spring, Troodos Massif. (0493102, 3865570 +/-8m). Alt 1306. Road side spring discharging through decorative Victorian cistern (commemorates opening Nicosia-Limassol road in 1901). pH (GSD meter) of 9.22, cond 0.44 mS cm-1, T=12.9°C. pH paper gave pH 8. Supposed high Mg, Cl<30 mgL^{-1}. Spring sourced in hills above, in gabbros and ultrabasics, on south side of same ridge as Alles spring (north side). Water collected by pipe from hill above.

As in the Allas Springs area, the geological map of the Xeros-Troodos area (GSD, 1959) also defines the bedrock here as bastite-serpentine within enstatite-olivinite, but which would now be re-classified as serpentinite or serpentinised pyroxene-peridotite, or more specifically as serpentinised harzbergite (Streckeisen, 1973; Gillespie and Styles, 1999). The 1:31,680 scale geological map (GDS, 1959) records this area to be intensely affected shearing and brecciation along both and east-west grain and northwest-southeast grain. The serpentinite can be seen to be locally very intensely veined and mineralised by veins of asbestiform serpentine minerals. These veins are often banded providing evidence of multiple generations of fracturing and mineralisation. The intensity of asbestiform serpentine vein mineralisation is manifest most strongly at Amiandos, in the southwest of the area, where large-scale economic deposits of chrysotile asbestos mineralisation were mined from 1904-1988.

Site C1
Sampling site C1 was a decorative limestone cistern by the roadside (Figure 2.1), located on the B9 road from Platania to Troodos Square (Troodos Resort). This is not an

actual spring location point but discharges water that to be piped from large concrete collecting tanks associated with a series of spring discharges about 50 m higher up the hillside (Site C3). Temperature, dissolved O_2, pH and conductivity were measured directly on-site at the time of collection, in water samples collected directly by dipping into the cistern. No rock or soil samples were collected from this site

Site C2
Sample site C2 is located on the hillside about 50m above the B9 road and the C1 site. High pH spring water is piped from several seepages and collected in a series of large concrete cisterns or tanks (Figure 2.2) that are used for local water supply. As at the Allas Springs, the cisterns are fitted with gas vents and appeared to be emitting gas. The springs pervasively seep through steeply-inclined fractures in intensely fractured, sheared, deformed and highly altered and pervasively-serpentinised harzbergite (serpentinite), and along the interface between buff-coloured clayey soil (regolith) on boulder-to-gravel-grade serpentinite-harzbergite scree resting on the fractured serpentinite bedrock. Tufa-like calcareous deposits partially filled the fractures in the soil-regolith above the seeps.

Samples of groundwater were collected by opening a plastic pipe outlet in the largest cistern (Figure 2.3). The pipe was opened and the water allowed to flow through the pipe for 5 minutes before sampling in order to flush any standing water in the pipe. Temperature, dissolved O_2, pH and conductivity were measured directly on-site at the time of collection. Samples of soil and serpentinite clasts were sampled in contact with the calcareous fracture mineralisation in the soil/colluvium associated with these springs.

Site C3
Site C3 is located within a small stream gully draining the hillside about 20 m above the B9 road and about 20 m north of C1 (Figure 2.4). Here numerous small groundwater seepages discharge along the walls and bed of the gully, feeding the flow of water in the stream. The orientation of the gully broadly follows the dominant northwest-south-east shear direction indicated on the geological map (GSD, 1959), and is roughly parallel to some of the major shear-zones filled by very soft pale green, serpentinitic fault gouge observed in the serpentinite exposed in the stream bed.

The bedrock comprises very highly sheared and altered serpentinite cut by a very fine millimetre-to centimetre-scale meshwork of fractures mineralised by “soapy”, pale green to white, and very fine grained serpentine. These reactivated along vein margins or are cut by later unmineralised hairline fissures, typically with apertures < 0.5 mm and fracture spacings of the order of a 1-10 mm. The serpentine fracture mineralisation is sheared and fracture surfaces are highly polished. High-pH groundwater seeps along the reactivated margins of sheared serpentine veinlets and cross-cutting unmineralised fractures, and through finely comminuted serpentinitic fault gouge in narrow shear zones up to 200 mm wide (Figure 2.5). High-pH groundwater also seeps along the interface between the bedrock and the overlying serpentinite-serpentinised harzbergite scree. Where the seeps occur the serpentinite bedrock is thoroughly altered and in many places is very poorly consolidated with a consistency of soft “putty”. Thin deposits of travertine coat rock surfaces locally where the high-pH groundwater discharges. Locally,

the scree may cemented by calcium carbonate to form a carbonate-cemented conglomerate along the interface with the bedrock.

Groundwater samples were taken by collecting water into glass tritium bottles directly from discharging fractures in the highly altered serpentinite (Figure 2.6). Temperature, dissolved O_2, pH and conductivity were measured directly on-site at the time of collection, in water samples collected directly by dipping into the cistern. The altered rock associated with these springs was so poorly consolidated that it was not possible to collect intact rock samples. The altered rock was therefore collected as bulk disaggregated fragmented material. It is recommended that a future sampling campaign should consider trying to collect undisturbed intact altered rock material using soil sampling techniques employing Kubiena soil tins.

Figure 2.1. *Site C1. Decorative limestone cistern used for public drinking water discharges spring water fed via plastic pipes from large concrete collecting tanks located on the hillside about 50 m above.*

See photo C2-1e.JPG in appendix 7

Figure 2.2. *Site C2. Large concrete cisterns collects spring water seeping through colluvium and scree resting on highly sheared and finely fissured, altered, and serpentinised harzbergite (serpentinite) exposed in the rock wall at the back of the corrugated iron shed seen in this photograph. The "crook-shaped" pipe vents gas from one of the cisterns.*

See photo C2-1f.JPG in appendix 7

Figure 2.3. *Site C2. The authors sampling groundwater discharging from a plastic pipe draining a large concrete cistern that collects spring water seeping through colluvium and scree resting on highly sheared and finely fissured, altered, and serpentinised harzbergite (serpentinite). The picture also shows one of the authors using a portable field colourimetric kit for determination of dissolved oxygen.*

Figure 2.4. *Site C3. Small stream bed and gully in scree resting on highly sheared and altered serpentised harzbergite (serpentinite). Thin white deposits of travertine coat the surfaces of many serpentinite boulders.*

Figure 2.5. *Site C3. Sampling high-pH groundwater directly from a discharging fissure in highly sheared, fractured and altered serpentinised harzbergite.*

Site 003: Pashiavalli (Livadhitou Pasha) (0489893, 3865729 +/-4 m). Alt 1659 m. Wooden cistern collecting dripping water at side of main Troodos Limassol road. pH (GSD) 8.98, T=9.3 °C, cond 0.66 mS cm^{-1}.

Site 004: Near Para Pedi (0486363, 3858065 +/-6m) Alt. 886 m. Road cutting with sequence of PLV (pillow lavas) cut by late veining of low T hydrothermal alteration (i.e. tufa-like infills, see later).

Site004a: Situated by F812, between Agios Mamas and Trimiklini (0493124, 3857357 +/-5m). Alt. 646 m. Road cutting and disused quarry showing section of highly brecciated PLV, cut by fractured with tufa-like secondary alteration. Lavas overlain by well-bedded calc mudstone and siltstone and thin beds of chalky conglomerate, bed thickness 5-50 cm. Channel forms observed, mapped as Vis (fine grained interlava volcanogenic sediments). Filled fractures reach up into sediments from PLV.

Site 005: Kalavasos to Parsata road (0525666, 3850496 +/-5m). Alt 149 m. Road cutting (100m vertical exposure: Fig 5-1) showing brecciated PLV passing up into autobreccia comprising PLV breccia and sediment matrix. Appears highly fractured, pillows show altered, reddened margins (Fig 5-2). Cut by vertical fractures (strike N015°, dip 90+/-10°) with calcareous fills. Surfaces of lava exposed with vertical and sub-horizontal fractures coated by up to 5mm thick, creamy, microporous travertine. Stream below site is dry. Above the PLV is heavily damaged calci-limestone with limestone conglomerate on top (angular clasts; Fig 5-3).

Site 006: Parsata Dam vicinity (0525512, 3850935+/- ?) alt 171m. Seepage from south side of road cutting, ground damp but no free water seen. Drains north into small valley below dam (which is approx. 1km north of site). Recent seepage with possible traces of carbonate precipitates.

Site 007: Road cutting approx 2km south of Parsata. (0523623, 3854496+/-4m). Alt. 403m. Site near hilltop showing faulted contact between sheeted dyke complex and zeolite to lower greenschist facies PLV with dykes. Extensively fractured with abundant tufa-like coatings on fractures. Faulted contact forms valley below which includes farm with pond (borehole fed?).

Several stages of alteration recognised:

- early hydrothermal alteration of PLV and sheeted dykes with reddening and chloritisation
- early siliceous white veining (zeolite?)
- onion skin weathering of basalt
- late tufaceous white coatings on late, irregular network of extensive fractures which X-cuts the onion skin weathering. Parsata spring not found, but it may be located in an extension of the faulted valley further to the west and remains to be checked in the February field visit.

Site 008: Parsata village. Gully with spring, now dry, no flow, but ground damp. (0524196, 3853887+/-?). Alt 401m. Line of boreholes from below road down into the valley (Fig 8-1), 2 and 3 close together on made ground. Capped.

Figure 5-1. *Road cutting showing brecciated PLV.*

Figure 5-2. *Fractured PLV with altered margins.*

Figure 5-3. *Angular clasts in limestone.*

Figure 8-1. *Capped borehole on edge of valley below Parsata village.*

site 009: Boreholes (0523802, 3853732). Just to north of boreholes, fracture running E-W with valley, roughly following the trend of the transform fault. PLV (brecciated) to N.

Site 010: Parsata, in valley. Brecciated PLV, heavily altered, cut by 30-90° dipping fractures with 3cm filling of fine white tufa (Fig 10-1). Horizontal tufa filled fractures too. Just north of borehole 2 (0523936, 3853795+/-4m). Alt. 345m.

Figure 10-1. *Heavily altered PLV.*

Site 011: Layia (0522450, 3856066+/-4m) Alt. 394m. PLV, borehole located about 10m from road. Corresponds to hyperalkaline wells recorded by GSD, one of which is supposedly artesian. One well in garden (maybe water running), second nearby at side of road. Tufa alteration in veins in PLV at road side.

Site 012: Layia to Ora road (0521825, 3856209+/-?). Alt. 413m. Well exposed layered gabbro cut by NE-SW fault and juxtaposed against PLV, with PLV atop the gabbro. Ground damp in valley bottom along which fault runs, but no free water. Gabbro extensively cut by many low-angled (25-45° dip to NW) fractures (shear?) filled with tufa. Umbers and patchy ochrous alteration iassociated with fracture zones in gabbro.

Site 013: Road cutting north of Arakapas (0508764, 3856116+/-?). Alt. 419m. Extensively altered gabbros/PLV (?) with well-developed, tufa-filled fractures, exposed at edge of small valley (Figs 13-1 & 2). Ground is damp at valley bottom, but no free-water.

Figure 13-1. *Extensively altered gabbros/PLV(?)*

..***Figure 13-2.*** *Close-up shows degree of replacement*

Site 014: Ayos Mamas (Agios Mamas). Near location of artesian borehole (0495973, 3856391+/-4m). Alt. 521m. Rocks around borehole heavily serpentinised with

tufaceous veining (Fig 14-1). Orthogonal joints, vertical and horizontal with spacings between 2-20cm. Gabbro and PLV/diabase appear to be disrupted by faulting (Fig 14-2). Gabbro separated from PLV by fault running along river.

Figure 14-1. *Gabbro in vicinity of Ayos Mamas well.*

Figure 14-2. *Rock in this area is heavily faulted with extensive low-temperature clayey and carbonate alteration.*

Site 015: Ayos Mamas (Agios Mamas). (0495940, 3856399+/-4m). Alt. 516. Location of artesian borehole (Figs 15-1 & 2). Borehole may be associated/on line of fault of site 14.

Figigure 15-1. *Artesian borehole at Ayos Mamas, stream.*

Figure 15-2. *Borehole from other side of stream (NBin foreground, borehole behind locked and on private property).*

Figure 16-1. *Tufa coated rock wall appears to be a hyperalkaline waterfall (currently almost dry).*

Site 016: Travertine site on dried waterfall in builder's yard (W side of road from Ayos Mamas to Limassol: 0496698, 3853598+/-5m). Kuoris valley. Extensive flowstone deposits on 50m high stepped cliff – currently a dry waterfall (Fig 16-1). Tufa was very damp, but no actual flow at moment. Highly altered serpentinised host rocks with tufa-coated joints. pH indicator papers pressed onto the damp travertine gave pH 8, but they normally under-read by 1 pH unit. Alt 400m. It was not possible to examine this site further due to failing light, but it certainly appears worth another visit in February.

Site 017: On road below Pedoulas. Spring with tap next to war memorial – Fig 17-1. (0484451, 3869810+/-4m) Alt. 986m. Approx 2/3 to 3/4 way up the valley, good flow from tap (Fig 17-2. pH paper gave pH 7, on meter pH 8.75, T=9.6°C, cond. 0.255 $mScm^{-1}$. Highly altered gabbro at site. As can often be seen in the Philipinnes, a fig tree marks the spring (useful field indicator). This site may provide an indication of the change in chemistry of the high pH groundwaters further down-gradient of the Allas Spring type groundwater sourced higher in the Troodos.

Figure 17-1. *War memorial below Pedoulas village.*

Figure 17-2. *Spring captured in tap.*

Site 018: Pedoulas spring possible boreholes (co-ordinates fit GSD data). (0484497, 3870514+/-4m) Alt. 642m. At back of valley in terraces, dense overgrowth, couldn't sample. Now capped and piped for irrigation. Stream behind is dry, might be that the well has captured the flow (Fig 18-1)? NB sites 17-18 lie on a lineament.

Figure 18-1. *Potential Pedoulas spring site (No. 1).*

Site 019: Second Pedoulas spring further down valley at side of fields (on track). (0484484, 3870698+/-4m). Alt. 827m. Fig. 19-1. As can be seen from Fig 19-2, area is heavily overgrown and it is difficult to be more certain without sampling (NB taps locked)

Figure 19-1. *Potential Pedoulas spring site (No. 2)*

Figure 19-2. *Area heavily overgrown.*

Site 019a: Water tanks further up road, south of Pedoulas (Fig 19a-1). Above site 17. pH 9.37 corr. to T=9.1°C. Cond. 0.328 $mScm^{-1}$.

Figure 19a-1. *Water tank – captured spring?*

Site 020: Alles hyperalkaline springs. In forest above Forestry Dept. office and picnic site (Platania). Approach is along a very narrow forest track to a point where several sources are collected in a series of cysterns. From the road, there is a steep climb of around 150 m up a tufa-coated gully (Figs 20-1 & 2) to the main spring.

The 1959 Cyprus Geological Survey Department geological map of the Xeros-Troodos area (GSD, 1959) originally defined the bedrock in this area as bastite-serpentine within enstatite-olivinite. Modern terminology would now re-classify this as serpentinite, serpentised pyroxene-peridotite, or more specifically as serpentinised harzbergite (Streckeisen, 1973; Gillespie and Styles, 1999). The 1:31,680 scale geological map (GDS, 1959) records the harzbergite in this area to be locally affected by intense shearing and brecciation with a dominant northwest-southeast grain. However, the shearing would appear to be less intense than in the Chrysovrysi Spring area (see site 2, above)

Last stretch to spring is very steep (Fig 20-3), so first samples taken around 20m below source – horizontal, tufa-filled fractures at top of harzburgite/base of altered gabbro (?). (0492026, 3867150+/-9m) Alt. 1327m. pH 11.49 corr to T=8.7°C, cond 9.93 $mScm^{-1}$. Tufa-filled horizon is broken up by vertical N-S faults separated every 5-10m or so. Precipitation on/near sources was 5-8cm thick, showing very fine multiple bands. Almost coloform in appearance (see Fig 20-4).

Figure 20-1. *Steep climb to main spring.*

Figure 20-2. *Tufa coats stream bed.*

Figure 20-3. *First groundwater sampling site viewed from below.*

Figure 20-4. *Typical heavy tufa precipitation around same spring (viewed from top left of Fig 20-3)*

Site 021: About 10m higher than 20, poor GPS fix (0492033, 3867145+/-19m). Alt. 1326m – wrong! pH11.2, corr. to T=9.4°C, cond 8.2 $mScm^{-1}$.

Site 022: Further down ravine where water re-appears through scree (disappears for approx. 50m). This is where the tufa (creamy) deposition stops (Fig 22-1). pH 10.20 corr to T=10.7°C, cond 8.25 $mScm^{-1}$. (0492092, 3867213+/-5m). Alt. 1279.

Figure 22-1. *Last of tufa in stream bed.*

Site 023: Cistern 1 (Fig 23-1), west side of ravine some 50m below main spring, piped from neighbouring ravine further west. (0492099, 3867264+/-6m) Alt. 1275m. Not possible to sample (locked), but gas (H_2 and/or CH_4?) being vented periodically.

Figure 23-1. *Cistern 1, collecting water from ravine further west.*

Site 024: Cistern 2 (Fig 24-1), east side of ravine. (0492125, 3867229+/-9m) Alt. 1260m. Below large tree (pine), tufa at base of tree/soil – water discharging through soil as well. cf Maqarin Station cutting? Rock under tree was heavily altered and appeared clay-rich. Could not sample cistern (locked), but pH paper pressed to damp soil above the cistern (see Fig 24-1) indicated the presence of alkaline water.

Figure 24-1. *Cistern 2.*

Cistern 3 and 4 on eastern side of spring, 3 was vented too. No sample possible as both locked.

Site 025: Cistern 4, eastern side. pH 9.69 corr to T=9.6°C, cond 2.259 $mScm^{-1}$. Both 3 & 4 seeping through bank. (0492154, 3867226+/-11m) Alt. 1268m (NB 25 is actually below 24, so altitude is incorrect).

Note that it seems likely that other sources are present at height as other seeps through the scree are present (to be checked in detail with the Forestry Dept.).

Site 026: Road cutting on Kalavasos to Asgata road adjacent to military camp. (0522541, 3850378 – NB done in car as it was a military controlled zone – no photos etc allowed). Alt. 234m. PLV and sediments with extensive travertine alteration.

Site 027: Road cutting on Asgata to Monagroulli road. (0522648, 3847913+/-4m). Alt. 290m. Highly altered PLV, intensely veined with carbonate/tufa and heavily oxidised

(Fig 27-1, 27-2). Basalt top is planed and overlain by bouldery-clay chalk, veins pass into chalk from PLV. Possibly channel fill of chalk into PLV (Fig 27-3).

Figure 27-1. *Road cutting outside Asgata.*

Figure 27-2. *Intensively veined PLV.*

Figure 27-3. *Chalk channel in PLV?*

Site 028: Pambajera Hill. Disused roadstone quarry, 300m NW of Asgata to Monagruilli road, located ca. 500m north of working quarry area. (0520890, 3847088+/-3m). Alt. 214. Exposes contact between top of PLV and chalky marl/bentonite (Fig 28-left). PLV extensively altered, thick tufa veins and possible travertine coatings (Fig 28-right). Ground damp between Pambajera Hill and adjacent lower hill – possibility of trenching here should be examined. Possible travertine caps Hill on top of bentonite. On GSD unpublished map (copy available in project depository), 1:5000, sheet 55/1.

Figure 28*-left. Foreground: heavily altered PLV. Background (top of image): chalky marl/bentonite with contact in between.* ***Figure 28****-right: Extensively altered PLV.*

Site 029: Sarama Springs.(0456036, 3867962). Alt. 214m. Attempt to find two springs, one hydrothermal, other gaseous. At GPS position, found two capped boreholes – springs? Boreholes 1113/2/3 (south side of field track), 1113/2/2 on other side of track. Also a small stream just to the south of the site would be worth investigating upstream of the farm (downstream is polluted with effluent). Area is heavily cultivated, no exposures of rock – but travertines seen in PLV at Sarama village, near top of valley. Bentonites widely distributed through valley (Fig 29-1). Site would be worth further, more detailed examination as this was cut short due to failing light.

Figure 29-1. *Topography typical of Sarama village area (view NW from Sarama village, west Cyprus, site 029 in Figure 2.1).*

Site 030: Petra tou Romiou (Aphrodite's Rock) on the south coast of Cyprus. This was a very short visit (due to failing light) where extensive bentonite deposits can be viewed in a coastal environment. On the shoreline (Fig 30-1) and immediately inland (Fig 30-2), bentonites and

Figure 30-1. *Petra tou Romiou (Aphrodite's Rock) on the south coast (southeast of Paphos) where bentonites (and slump/flood deposits) can be observed lying directly on heavily altered PLV.*

Figure 30-2. *Dry gully in sediments and PLV immediately inland from Petra tou Romiou, heading towards Agios Georgios. Poor photo quality is due to failing light.*

other sediments (slump or flood deposits) in direct contact with heavily altered PLV can be observed. No groundwater was observed and failing light curtailed any further investigations.

BGS Laboratory Code	Original sample number	Revised sample number		GPSLocation			X-Y error (m)	GPS Elevation (m)
Samples collected for chemical and stable isotope analysis								
12081-0001	A1-1	A1-1	Allas Springs: artesian discharge through fracture, with tufa deposit. Source of high pH groundwater for A1 site located on the western side of valley about 20-30 m above forest track	36 UTM S	0492173	38672	5	1270
12081-0002	A1-2	A1-2	Allas Springs: Spring discharge in eastern bank of scree/colluvium located close to forestry road, at confluence of small valley draining from A1-1 and main mountain stream draining northwards from high Troodos ridge. The spring discharge is collected in concrete cistern. Water collected from discharge at interface between colluvium/scree/soil and highly fractured bedrock surface	36 UTM S	0492174	3867229	5	1262
12081-0003	A1-3	A1-3	Allas Springs: Flowing water within pit dug in calcified soil profile/tufa deposit (calcified litter of pine needles, leaves, partially decomposed wood, branches and other plant debris). 0.5 m depth. Located ~midway between A1-1 and A1-2	36 UTM S	0492167	3867200	6	1263

Details of the groundwater sampling sites APPENDIX 2

BGS Laboratory Code	Original sample number	Revised sample number		GPSLocation			X-Y error (m)	GPS Elevation (m)
12081-0004	A1-4	A1-4	Allas Springs: ~3 m north of A1-2. Spring discharge in eastern bank of scree/colluvium located close to forestry road, at confluence of small valley draining from A1-1 and main mountain stream draining northwards from high Troodos ridge. The spring discharge is collected in concrete cistern. Water collected from discharge at interface between colluvium/scree/soil and highly fractured bedrock surface	36 UTM S	0492168	3867234	6	1262
12081-0005	A4-1	**E1-1**	Spring just below tree above main valley bottom. Field pH9.5. Photos A4-1a and b	36 UTM S	0492258	3867116	6	1255
field measurement	GPS16	**E3-1**	Stream in E1 valley, pH9.9	36 UTM S	0492273	3867120	2	1263
field measurement	GPS16	**E3-2**	10m downstream from E3-1, pH9.7		ditto	ditto		
field measurement	GPS20	**E5**	Main stream joins another tributary, combined pH9.5		0492285	3867168	6	1255
12081-0006	A4-2	**A4-3**	Main stream from A4-1, just before joins stream from spring to the west of A4-1	36 UTM S	0492065	3867179	7	1311
12081-0007	A4-3	**A4-2**	Sample site some 25-30m vertically below A4-1 (NB GPS shows it to be higher). Tufa samples - photo A4-2a	36 UTM S	0492037	3867159	2	1320
12081-0008	A4-4	**A4-1**	Highest spring, emits from horizontal joint between harzburgite and overlying altered gabbro. Massive, almost coliform tufa. Sample collected ~7m vertically below spring	36 UTM S	0491854	3867342	8	1225

BGS Laboratory Code	Original sample number	Revised sample number		GPSLocation			X-Y error (m)	GPS Elevation (m)
12081-0009	A5-1	A5	Allas Springs: Spring discharge in eastern bank of scree/colluvium located ~10 m upstream from A3 in main valley of the principal mountain stream draining northwards from high Troodos ridge. The spring discharge is collected in concrete cistern. Water collected from discharge above cistern, at interface between colluvium/scree/soil at the base of a large tree, and at the interface highly fractured bedrock surface	36 UTM S	0492131	3867220	6	1283
12081-0010	A6	A6	Allas Springs: Spring discharge in eastern bank of scree/colluvium located ~50 m downstream and below forestry road from A1-2, in main valley of the principal mountain stream draining northwards from high Troodos ridge. The spring discharges through scree, boulder at interface with fractured serpentinite bedrock. Fracture surfaces coated with tufa.	36 UTM S	0492178	3867279	10	1233
12081-0011	C1	C1	Chrisovrysi spring: water discharging from pipe into decorative cistern by roadside of main Troodos highway	36 UTM S	0493104	3865578	7	1305
12081-0012	C2	C2	Hillside above Chrisovrysi spring cistern. Discharge from soil-bedrock interface, within soil profile impregnated with carbonate. Water collected in series of large concrete cisterns close to source (state-controlled water supply), with pipes leading downhill to Chrisovrysi cistern. Water collected from flowing pipe after flushing for 3 minutes.	36 UTM S	0493023	3865493	7	1350

BGS Laboratory Code	Original sample number	Revised sample number		GPSLocation			X-Y error (m)	GPS Elevation (m)
12081-0013	C3	C3	Spring discharges in base and walls of small mountainside stream, through highly altered and fractured serpentinite, close to interface with colluvium and scree. Groundwater flows from fissures in altered bedrock. Associated with tufa coatings on rock surfaces exposed to atmosphere. The stream is ~20-30 m north of Cq.	36 UTM S	0493058	3865635	9	1317
12081-0014	AL-2-1	A2	Allas Springs: Spring discharge in eastern bank of scree/colluvium located ~16 m upstream from A1-1 in the valley of the main mountain stream draining northwards from high Troodos ridge. The spring discharge is collected in concrete cistern. Water collected from discharge above cistern, at interface between colluvium/scree/soil and highly fractured bedrock surface	36 UTM S	0492153	3867233	29	1264
12081-0015	AL-3-1	A3	Allas Springs: Spring discharge in eastern bank of scree/colluvium located ~10-15 m upstream from A2 in the valley of the main mountain stream draining northwards from high Troodos ridge. The spring discharge is collected in concrete cistern. Water collected from discharge above cistern, at interface between colluvium/scree/soil and highly fractured bedrock surface	36 UTM S	0492143	3867217	6	1266
12081-0016	D2	D2	Waterfall site: stream water from above high waterfall in west side of valley. Extensive travertine/tufa deposits. Gabbros and pillow lavas	36 UTM S	0496585	3853633	10	439

BGS Laboratory Code	Original sample number	Revised sample number		GPSLocation			X-Y error (m)	GPS Elevation (m)
12081-0017	P1	P1	Parsata Spring; Borehole in base of valley used by local farmer for irrigation of fields. Pumped by solar-powered electric pump. Valley now dry but locally significant tufa coatings on rocks in valley floor. Extensively flushed before sampling since farmer was using water (several hundreds of litres) for filling tanks for irrigation at time of sampling.	36 UTM S	0523555	3854131	4	321

BGS Laboratory Code	pH [temperature corrected]	Temperature [C)	Conductivity [mS/cm]	Dissolved O2 [mg/l]	Comments
Samples collected for chemical and stable isotope analysis					
12081-0001	12.19	8.5	6820	4	
12081-0002	9.26	10.2	295	3	
12081-0003	10.01	8.2	5690	3	
					Altitude is probably about 3-4 m higher
12081-0004	9.78	9	5150	3.5	
12081-0005				nd	
field measurement					
field measurement					
field measurement					
12081-0006				nd	
12081-0007				nd	
12081-0008	nd	nd	nd	nd	
12081-0009	9.8	9.5	1430	3	
12081-0010	9.67	9	4360	4	
12081-0011	9.41	11.8	421	4	
12081-0012	9.58	10	n.d.	5.5	
12081-0013	9.69	10	n.d.	5.5	
12081-0014	9.69	10.1	1260	5	
12081-0015	9.84	10.9	1445	4	
12081-0016	8.25	14.8	1394	6	
12081-0017	11.42	22.9	779	3	smell of H_2S

XRD CLAY ONLY			
CHEMICAL ANALYSIS			Y
THIN SECTION	Y	Y	
XRD SPECIFIC COMPONENT ONLY	Y		
XRD CLAY + BULK			Y
Comments	Sample of tufa (travertine) forming stalactites and flowstone coating the fracture surface of the harzburgite. Contains fragments of harzburgite within the tufa.	Forest litter and plant debris reacted with and cemented by travertine from discharging high pH groundwater. Consists of calcified litter of pine needles, leaves, partially decomposed wood, branches and other plant debris). 0.5 m depth	Highly altered (argillised) soil which has altered by interaction with high pH groundwater around discharge point
GPS Elevation (m)	1270	1270	1262
X-Y error (m)	5	5	5
GPS Location	38672	38672	3867229
	0492173	0492173	0492174
	36 UTM S	36 UTM S	36 UTM S
Location Description	Allas Springs: artesian discharge through fracture in harzburgite, with tufa deposit. Source of high pH groundwater for A1 site located on the western side of valley about 20-30 m above forest track	Allas Springs: artesian discharge through fracture in harzburgite, with tufa deposit. Source of high pH groundwater for A1 site located on the western side of valley about 20-30 m above forest track	Allas Springs: Spring discharge in stream bank, through soil and scree resting on fractured and highly serpentinised harzburgite.
Site	1-1A	1-1A	2-1A
BGS Laboratory No.	MPLN805	MPLN806	MPLN807
Original sample label	A1-1-2	A1-1-1	A1-2

XRD CLAY ONLY				
CHEMICAL ANALYSIS	Y	Y	Y	Y
THIN SECTION	Y	Y		
XRD SPECIFIC COMPONENT ONLY				
XRD CLAY + BULK	Y	Y	Y	Y
Comments	Soil and altered scree from north side of discharge point. Photo A2-1a	Soil from around seepage point (from above and south of seepage point).	Soil (reddish clay, black clasts plus some tufa) with organics developed on scree and associated with high pH seepage. Sampled to south of seepage, about 1m above the concrete base. Photo A3-1a	Altered scree/ultrabasic rock (fine material from below the boulder) associated with high pH seepage. Sampled to south of the seepage, ~1.5m above concrete base.
GPS Elevation (m)	1264	1264	1266	1266
X-Y error (m)	29	29	5	5
GPS Location	3867233	3867233	3867217	3867217
	0492153	0492153	0492143	0492143
	36 UTM S	36 UTM S	36 UTM S	36 UTM S
Location Description	Allas Springs: Spring discharge in stream bank, through soil and scree resting on fractured harzburgite. About 16 m south (upstream) of A1-2	Allas Springs: Spring discharge in stream bank, through soil and scree resting on fractured harzburgite. About 16 m south (upstream) of A1-2	Allas Springs: Spring discharge in stream bank, through fractured harzburgite and along interface between soil/scree and underlying fractured bedrock. About 10-15 m south (upstream) of A2	Allas Springs: Spring discharge in stream bank, through fractured harzburgite and along interface between soil/scree and underlying fractured bedrock. About 10-15 m south (upstream) of A2
Site	2A	2A	3A	3A
BGS Laboratory No.	MPLN808	MPLN809	MPLN810	MPLN811
Original sample label	A2-1	A2-2	A3-1	A3-2

XRD CLAY ONLY				
CHEMICAL ANALYSIS	Y	Y		
THIN SECTION				
XRD SPECIFIC COMPONENT ONLY				
XRD CLAY + BULK	Y	Y	Y	
Comments	Altered and fractured ultrabasic rock (with some tufa) associated with high pH seepage. Sampled within the flow, 0.5m above the concrete base.	Photo A4-1a shows sampling site (and that of sample A4-1-2). Green tufa and clasts. Sampling point 30cm to the right of the pen in photo A4-1b. Note that elevation is probably inaccurate due to position in a rock chimney. Photos A4-1-e-f area show general overview.	Clay next to the tufa (photo A4-1a)	Clay in flow zone (currently dry). Photo A4-1d.
GPS Elevation (m)	1266	1225	1225	1225
X-Y error (m)	5	8	8	8
GPS Location	3867217	3867342	3867342	3867342
	0492143	491854	491854	491854
	36 UTM S	36 UTM S	36 UTM S	36 UTM S
Location Description	Allas Springs: Spring discharge in stream bank, through fractured harzburgite and along interface between soil/scree and underlying fractured bedrock. About 10-15 m south (upstream) of A2	Allas Springs: Main high pH groundwater discharge, near upper source high up Allas Springs valley, with scree and bedrock coated with thick travertine	Just to west of stream bed in heavily altered rock	Immediately next to stream bed, currently dry but damp
Site	3A	4A	4A	4A
BGS Laboratory No.	MPLN812	MPLN813	MPLN822	MPLN823
Original sample label	A3-3	A4-1-1	A4-1-2	A4-1-3

XRD CLAY ONLY				
CHEMICAL ANALYSIS				
THIN SECTION	2			
XRD SPECIFIC COMPONENT ONLY	Y			
XRD CLAY + BULK				
Comments	Laminated travertine encrusting stream bed sediments. Contains entrained harzburgite and other ultrabasic rock fragments	Clay and tufa from under a boulder within the stream (damp). The altitude is probably correct here, more open terrain .	Clay and tufa within the stream (see photo A4-2a).	Tufa-covered clast from within the stream
GPS Elevation (m)	1225	1320	1320	1320
X-Y error (m)	8	2	2	2
GPS Location	3867342	3867159	3867159	3867159
	491854	492037	492037	492037
	36 UTM S	36 UTM S	36 UTM S	36 UTM S
Location Description	Travertine from stream bed	Alles Springs: in stream, about 25-30m downstream of the main spring	In stream, about 20m downstream from A4-2-1	as above
Site	4A	4A	4A	4A
BGS Laboratory No.	MPLN814	MPLN818	MPLN819	MPLN820
Original sample label	A4-1-4	A4-2-1	A4-2-2	A4-2-3

XRD CLAY ONLY				
CHEMICAL ANALYSIS				Y
THIN SECTION				
XRD SPECIFIC COMPONENT ONLY				
XRD CLAY + BULK	Y	Y		Y
Comments	Clay in stream	Sediments around burn	Clay-rich sediment in burn, 2 m vertically above A4-3-1	Soil (reddish clay with tufa skin on top) associated with alkaline spring. Sampled to the north and 0.5m above the cistern
GPS Elevation (m)	1311	1311	1311	n.d.
X-Y error (m)	7	7	7	6
GPS Location	3867179	3867179	3867179	3867220
	492065	492065	492065	0492131
	36 UTM S	36 UTM S	36 UTM S	36 UTM S
Location Description	Alles Springs: in stream, just before another stream joins on the west side. This originates from another tufa-covered seep at about the same altitude and to the west of A4-1. Note that this stream seems buffered at this point as no tufa in stream bed.	As above	As above, 2m upstream from A4-3-2	Allas Springs: Stream bank 10 m upstream of A3. High pH groundwater spring discharges through soil-covered scree and boulders at interface with altered and fractured bedrock at the base of tree roots
Site	4A	4A	4A	5A
BGS Laboratory No.	MPLN815	MPLN816	MPLN817	MPLN824
Original sample label	A4-3-1	A4-3-2	A4-3-3	A5-1

XRD CLAY ONLY				
CHEMICAL ANALYSIS	Y		Y	Y
THIN SECTION	Y	Y		Y
XRD SPECIFIC COMPONENT ONLY		Y		
XRD CLAY + BULK	Y		Y	Y
Comments	Altered bedrock (now blueish clay with rock clasts), sampled in water very close to water sampling point.	Tufa/travertine-cemented scree of ultabasic clasts from stream bed at contact with serpentinite bedrock	Soil/regolith directly above spring seepages. Photos C2-1a to d show the site. C2-1e shows old shed covering the original spring and C2-1f sampling from one of the cisterns (NB off-gassing from cisterns heard)	Soil and regolith clasts reacted with or coated by tufa.
GPS Elevation (m)	n.d.	n.d.	1350	1350
X-Y error (m)	6	10	7	7
GPS Location	3867220	3867279	3865493	3865493
	0492131	0492178	0493023	0493023
	36 UTM S	36 UTM S	36 UTM S	36 UTM S
Location Description	Allas Springs: Stream bank 10 m upstream of A3. High pH groundwater spring discharges through soil-covered scree and boulders at interface with altered and fractured bedrock at the base of tree roots	Tufa cemented scree, 50 m down valley, north of forest path and A1-1. Alkaline groundwater and stream discharges through the base of the scree at bedrock surface exposed in the stream bed. Discharges from fractured serpentinite with tufa coatings	Chrisovrysi Springs: hillside cisterns collecting alkaline groundwater. Located on high hillside above the decorative roadside cistern. Exposure of soil profile through which springs originally discharged. Cisterns all vented so possibly gas present.	Chrisovrysi Springs: hillside cisterns collecting alkaline groundwater. Located on high hillside above the decorative roadside cistern. Exposure of soil profile through which springs originally discharged
Site	5A	6A	2C	2C
BGS Laboratory No.	MPLN825	MPLN826	MPLN827	MPLN828
Original sample label	A5-2	A6	C2-1	C2-2

XRD CLAY ONLY		
CHEMICAL ANALYSIS	Y	Y
THIN SECTION		
XRD SPECIFIC COMPONENT ONLY		
XRD CLAY + BULK	Y	Y
Comments	Argillised or altered serpentinite (?clay + organic containing) from altered bedrock directly below the travertine coating and directly in contact with alkaline groundwater seep along scree-bedrock interface. Photo C3-1a is overview of site, C3-1b shows algal mat in contact with the groundwater and altered rock.	Altered serpentinite in direct contact with alkaline groundwater through fractures in bedrock within the stream. Photos C3-2a-j detail the site. C3-2b shows porous flow through the fully decomposed rock.
GPS Elevation (m)	1317	1317
X-Y error (m)	9	9
GPS Location	3865635	3865635
	0493058	0493058
	36 UTM S	36 UTM S
Location Description	Chrisovrysi Springs: Stream cutting through steep scree resting on highly fractured and altered serpentinite. Located about 50-100m up the hillside from the roadside (north from the cistern site "C1"). Groundwater discharges through highly altered and argillised fractured serpentinite just beneath (0-1 m) the contact with the scree, and feeds the flow in the stream. Photo C3-1a is overview of the site.	Chrisovrysi Springs: Stream cutting through steep scree resting on highly fractured and altered serpentinite. Located about 50 m up the hillside from the roadside from roadside cistern site "C1". Groundwater discharges through highly altered and argillised fractured serpentinite just beneath (0-1 m) the contact with the scree, and feeds the flow in the stream.
Site	3C	3C
BGS Laboratory No.	MPLN829	MPLN830
Original sample label	C3-1	C3-2

XRD CLAY ONLY		
CHEMICAL ANALYSIS	Y	Y
THIN SECTION	Y	Y
XRD SPECIFIC COMPONENT ONLY		
XRD CLAY + BULK	Y	Y
Comments	Altered serpentinite in direct contact with alkaline groundwater through fractures in bedrock in stream bank	Bulk sample of background altered serpentinite. Sample collected in the stream (pH of water at this point was 8.92).
GPS Elevation (m)	1317	1317
X-Y error (m)	9	9
GPS Location	3865635	3865635
	0493058	0493058
	36 UTM S	36 UTM S
Location Description	Chrisovrysi Springs: Stream cutting through steep scree resting on highly fractured and altered serpentinite. Located about 50 m up the hillside from the roadside cistern site "C1". Groundwater discharges through highly altered and argillised fractured serpentinite just beneath (0-1 m) the contact with the scree, and feeds the flow in the stream.	Chrisovrysi Springs: Stream cutting through steep scree resting on highly fractured and altered serpentinite. Located about 50 m up the hillside from the roadside cistern site "C1". Groundwater discharges through highly altered and argillised fractured serpentinite just beneath (0-1 m) the contact with the scree, and feeds the flow in the stream.
Site	3C	3C
BGS Laboratory No.	MPLN831	MPLN832
Original sample label	C3-3	C3-4

XRD CLAY ONLY		
CHEMICAL ANALYSIS		
THIN SECTION	Y	Y
XRD SPECIFIC COMPONENT ONLY		Y
XRD CLAY + BULK		
Comments	Bulk sample of highly altered (argillised) serpentinite which has altered by interaction with high pH groundwater around discharge point	Travertine coated and tufa-cemented rock fragments recovered in situ from stream bed
GPS Elevation (m)	1317	1317
X-Y error (m)	9	9
GPS Location	3865635	3865635
	0493058	0493058
	36 UTM S	36 UTM S
Location Description	Chrisovrysi Springs: Stream cutting through steep scree resting on highly fractured and altered serpentinite. Located about 50 m up the hillside from the roadside cistern site "C1". Groundwater discharges through highly altered and argillised fractured serpentinite just beneath (0-1 m) the contact with the scree, and feeds the flow in the stream.	Chrisovrysi Springs: Stream cutting through steep scree resting on highly fractured and altered serpentinite. Located about 50 m up the hillside from the roadside cistern site "C1". Groundwater discharges through highly altered and argillised fractured serpentinite just beneath (0-1 m) the contact with the scree, and feeds the flow in the stream.
Site	3C	3C
BGS Laboratory No.	MPLN833	MPLN834
Original sample label	C3-5	C3

XRD CLAY ONLY				
CHEMICAL ANALYSIS				
THIN SECTION		Y		
XRD SPECIFIC COMPONENT ONLY				
XRD CLAY + BULK			Y	
Comments	Soil associated with high pH groundwater seeps through scree in stream bank/bed	Altered pillow lava with tufa coatings on fracture surfaces. Stream water was pH7.2 at primary seep, but increased to 7.9 witin 4m (downstream) of this - would seem to be minor seeps coming through the PLVs. Photos D1-1a shows stream in valley and D1-1b sampling in stream. D1-1c is waterfall at bottom and D1-1d is close up of the tufa.	Clay-rich sediment from stream bed associated with tufa deposition. Groundwater sample D2 from here (pH8.21). Photo D2-1a.	Heavily altered PLV shot through with 20-30cm wide dykes. Water pH7.8, photo D3-1a.
GPS Elevation (m)	1363	439	439	439
X-Y error (m)	9	10	10	0
GPS Location	3865643	3853633	3853633	3853633
	0493049	0496585	0496585	0496600
	36 UTM S	36 UTM S	36 UTM S	36 UTM S
Location Description	Chrisovrysi Springs: Stream cutting through steep scree resting on highly fractured and altered serpentinite. Located about 40 m upstream from "C3". Groundwater discharges through soil on scree.	Waterfall site: stream water from above high waterfall in west side of valley. Extensive travertine/tufa deposits. Gabbros and pillow lavas (PLV).	Waterfall site: stream water from above high waterfall in west side of valley. Extensive travertine/tufa deposits. Gabbros and pillow lavas	Area of dykes across stream.
Site	4C	1D	2D	3D
BGS Laboratory No.	MPLN835	MPLN836	MPLN837	
Original sample label	C4	D1-1	D2	

XRD CLAY ONLY		
CHEMICAL ANALYSIS		Y
THIN SECTION	Y	Y
XRD SPECIFIC COMPONENT ONLY		
XRD CLAY + BULK		Y
Comments	A profile of samples collected running from the PLV and up into the marly clay/silt. Photos T1-1a to 1e show details of the sediments (with tufa veins) and T1-1f and g show the altered PLV. 0 cm: Altered pillow lava with tufa veins	12 cm: Pillow lava and carbonate veining at contact with sediments
GPS Elevation (m)		
X-Y error (m)		
GPS Location		
Location Description	Road cutting on the F812 between Trimiklini and Agios Mamas. Vertical profile through exposure of parallel-laminated marly clay and silt resting on altered pillow lavas and autobrecciated pillow lava. The pillows are highly altered with steep irregular tufa veins or carbonate veins penetrating the overlying sediments.	Road cutting on the F812 between Trimiklini and Agios Mamas. Vertical profile through exposure of parallel-laminated marly clay and silt resting on altered pillow lavas and autobrecciated pillow lava. The pillows are highly altered with steep irregular tufa veins or carbonate veins penetrating the overlying sediments.
Site	T	T
BGS Laboratory No.	MPLN838	MPLN839
Original sample label	T1	T2

XRD CLAY ONLY		
CHEMICAL ANALYSIS	Y	Y
THIN SECTION	Y	Y
XRD SPECIFIC COMPONENT ONLY		
XRD CLAY + BULK	Y	Y
Comments	25 cm: clay silt with carbonate veining	40 cm: clay silt with carbonate veining
GPS Elevation (m)		
X-Y error (m)		
GPS Location		
Location Description	Road cutting on the F812 between Trimiklini and Agios Mamas. Vertical profile through exposure of parallel-laminated marly clay and silt resting on altered pillow lavas and autobrecciated pillow lava. The pillows are highly altered with steep irregular tufa veins or carbonate veins penetrating the overlying sediments.	Road cutting on the F812 between Trimiklini and Agios Mamas. Vertical profile through exposure of parallel-laminated marly clay and silt resting on altered pillow lavas and autobrecciated pillow lava. The pillows are highly altered with steep irregular tufa veins or carbonate veins penetrating the overlying sediments.
Site	T	T
BGS Laboratory No.	MPLN840	MPLN841
Original sample label	T3	T4

XRD CLAY ONLY		
CHEMICAL ANALYSIS	Y	Y
THIN SECTION	Y	Y
XRD SPECIFIC COMPONENT ONLY		
XRD CLAY + BULK	Y	Y
Comments	60 cm: clay silt with carbonate veining	100 cm clay with tufa vein and detrital chalk clasts
GPS Elevation (m)		
X-Y error (m)		
GPS Location		
Location Description	Road cutting on the F812 between Trimiklini and Agios Mamas. Vertical profile through exposure of parallel-laminated marly clay and silt resting on altered pillow lavas and autobrecciated pillow lava. The pillows are highly altered with steep irregular tufa veins or carbonate veins penetrating the overlying sediments.	Road cutting on the F812 between Trimiklini and Agios Mamas. Vertical profile through exposure of parallel-laminated marly clay and silt resting on altered pillow lavas and autobrecciated pillow lava. The pillows are highly altered with steep irregular tufa veins or carbonate veins penetrating the overlying sediments.
Site	T	T
BGS Laboratory No.	MPLN842	MPLN843
Original sample label	T5	T6

XRD CLAY ONLY		
CHEMICAL ANALYSIS	Y	
THIN SECTION	Y	
XRD SPECIFIC COMPONENT ONLY		
XRD CLAY + BULK	Y	
Comments	200 cm above contact: Background clay silt sediment.	Too dangerous to sample. Photo P1a
GPS Elevation (m)	631	168
X-Y error (m)	5	3
GPS Location	3857311	3850617
	0492989	0525539
	36 UTM S	36 UTM S
Location Description	Road cutting on the F812 between Trimiklini and Agios Mamas. Vertical profile through exposure of parallel-laminated marly clay and silt resting on altered pillow lavas and autobrecciated pillow lava. The pillows are highly altered with steep irregular tufa veins or carbonate veins penetrating the overlying sediments.	Parsata area: Kalavasos to Parsata road, rock face on ledge above road with Pillow Lava sequence fractured with tufa. Cliff exposure, PLV on top with autobreccia below. Sediments throughout autobreccia and tufa through everything.
Site	T	1P
BGS Laboratory No.	MPLN844	
Original sample label	T7	

XRD CLAY ONLY		
CHEMICAL ANALYSIS	Y	Y
THIN SECTION	Y	Y
XRD SPECIFIC COMPONENT ONLY		
XRD CLAY + BULK	Y	Y
Comments	10 cm (+/- 10 cm): Altered autobrecciated pillow lava and interstitial sediment associated with tufa coatings and impregnations. Photo P2-1a shows Tony pointing to contact, photo P2-1b shows sampling profile (ruler is 1.5m long, 0m is at top). Photos P2-1c-f show sampling and PLV/autobreccia relationship. P2-1c PLV below, autobreccia on top. P2-1d is PLV on top with autobreccia below. P-2-1e and f sample P2-1 at 10 (+/-5) cm along line.	40 cm (+/- 10 cm): Autobrecciated pillow lava and interstitial sediment associated with tufa coatings and impregnations. Photo P2-2a.
GPS Elevation (m)	168	168
X-Y error (m)	4	4
GPS Location	3850613	3850613
	0525561	0525561
	36 UTM S	36 UTM S
Location Description	Parsata area: Kalavasos to Parsata road, rock face on ledge above road with Pillow Lava sequence fractured with tufa. Sampled along a profile from lower pillow lava to overlying autobreccia coatings and fills indicating palaeo water-rock interaction with potential high pH groundwater (no longer active at this site but recorded from nearby Parsata Spring)	Parsata area: Kalavasos to Parsata road, rock face on ledge above road with Pillow Lava sequence fractured with tufa. Sampled along a profile from lower pillow lava to overlying autobreccia coatings and fills indicating palaeo water-rock interaction with potential high pH groundwater (no longer active at this site but recorded from nearby Parsat Spring)
Site	2P	2P
BGS Laboratory No.	MPLN845	MPLN846
Original sample label	P2-1	P2-2

XRD CLAY ONLY		
CHEMICAL ANALYSIS	Y	Y
THIN SECTION	Y	Y
XRD SPECIFIC COMPONENT ONLY		
XRD CLAY + BULK	Y	Y
Comments	Tufa fill in fractures within altered autobreccia (at ~70cm).	Sediments at contact with pillow lava surface. Photo P3-1a overview of site, P3-1b tufa in autobreccia, P3-1c and d contact of autobreccia and sediment, P3-1e and f general lineation of clasts (lst, bentonite, PLV, chert) in (smectite-rich?) sediments - fluvial or sub-sea flow? P3-1g shows cross-cutting by another channel (above knife).
GPS Elevation (m)	168	173
X-Y error (m)	4	4
GPS Location	3850613	3850748
	0525561	0525485
	36 UTM S	36 UTM S
Location Description	Parsata area: Kalavasos to Parsata road, rock face on ledge above road with Pillow Lava sequence fractured with tufa. Sampled along a profile from lower pillow lava to overlying autobreccia coatings and fills indicating palaeo water-rock interaction with potential high pH groundwater (no longer active at this site but recorded from nearby Parsata Spring)	Parsata area: Kalavasos to Parsata road, rock face road cutting with fluvial or channel deposit of chalky conglomeratic silt and sand resting on Pillow Lava sequence,fractured with tufa. Tufa penettrates overlying sediments close to contact indicating discharge of palaeogroundwater from pillow lavas into the overlying sediments. Sampled along a profile from pillow lava to overlying sediments (groundwater no longer active at this site but recorded from nearby Parsata Spring)
Site	2P	3P
BGS Laboratory No.	MPLN848	MPLN849
Original sample label	P2-4	P3-1

XRD CLAY ONLY		
CHEMICAL ANALYSIS	Y	Y
THIN SECTION	Y	Y
XRD SPECIFIC COMPONENT ONLY		
XRD CLAY + BULK	Y	Y
Comments	Tufa vein filling	Sediment 0-5 cm from contact with pillow lavas
GPS Elevation (m)	173	173
X-Y error (m)	4	4
GPS Location	3850748	3850748
	0525485	0525485
	36 UTM S	36 UTM S
Location Description	Parsata area: Kalavasos to Parsata road, rock face road cutting with fluvial or channel deposit of chalky conglomeratic silt and sand resting on Pillow Lava sequence,fractured with tufa. Tufa penettrates overlying sediments close to contact indicating discharge of palaeogroundwater from pillow lavas into the overlying sediments. Sampled along a profile from pillow lava to overlying sediments (groundwater no longer active at this site but recorded from nearby Parsata Spring)	Parsata area: Kalavasos to Parsata road, rock face road cutting with fluvial or channel deposit of chalky conglomeratic silt and sand resting on Pillow Lava sequence,fractured with tufa. Tufa penettrates overlying sediments close to contact indicating discharge of palaeogroundwater from pillow lavas into the overlying sediments. Sampled along a profile from pillow lava to overlying sediments (groundwater no longer active at this site but recorded from nearby Parsata Spring)
Site	3P	3P
BGS Laboratory No.	MPLN850	MPLN851
Original sample label	P3-2	P3-3

XRD CLAY ONLY			
CHEMICAL ANALYSIS	Y		
THIN SECTION	Y		
XRD SPECIFIC COMPONENT ONLY			
XRD CLAY + BULK	Y		
Comments	Background (unaltered) sediment from >135 cm above contact with pillow lavas. Sample from about 1m horizontally from P3-3.	Contact between the (tufa-rich) PLV/autobreccias and the sediments is below the road - could be a good site to trench for contact.	At this point, too high for the hyperalkaline waters (see photo E1-1a and b). Need to drop down into the valley.
GPS Elevation (m)	173	256	1407
X-Y error (m)	4	2	2
GPS Location	3850748	3853829	3866954
	0525485	0523935	0492098
	36 UTM S	36 UTM S	36 UTM S
Location Description	Parsata area: Kalavasos to Parsata road, rock face road cutting with fluvial or channel deposit of chalky conglomeratic silt and sand resting on Pillow Lava sequence,fractured with tufa. Tufa penettrates overlying sediments close to contact indicating discharge of palaeogroundwater from pillow lavas into the overlying sediments. Sampled along a profile from pillow lava to overlying sediments (groundwater no longer active at this site but recorded from nearby Parsata Spring)	Below Parsata village, on track to line of boreholes which drop down to the valley bottom.	Valley system immediately southeast of the main Alles Spring valley
Site	3P	4P	Valley E
BGS Laboratory No.	MPLN852		
Original sample label	P3-4		

XRD CLAY ONLY			
CHEMICAL ANALYSIS			
THIN SECTION			
XRD SPECIFIC COMPONENT ONLY			
XRD CLAY + BULK			
Comments	Clay-rich alteration associated with high pH spring (currently dry). Photo E1-1c showing alteration rims on fractures in harzburgite.	Some evidence of minor seeps, now dry. Photo E2-1a shows heavily altered herzburgite rubble and E2-1b shows typical scree-covered slopes in vally. Most seeps occur at the foot of the scree slopes.	Minor reaction around a boulder, stream pH9.9, 10m downstream, 9.7 (uncorrected). Photos E3-1a and b.
GPS Elevation (m)	1283	1272	1263
X-Y error (m)	n/a	6	2
GPS Location	3867107	3867115	3867120
	0492262	492294	492273
	36 UTM S	36 UTM S	36 UTM S
Location Description	Valley floor, some evidence of minor seeps (tufa) in the streams and coming through the extensive scree.	Valley bottom, weathered and altered (tufa-rich) rubble	Valley bottom, in stream bed, trending N50°E.
Site	1-1E	2E	3E
BGS Laboratory No.			
Original sample label	GPS12	GPS14	GPS16

XRD CLAY ONLY		
CHEMICAL ANALYSIS		
THIN SECTION		
XRD SPECIFIC COMPONENT ONLY		
XRD CLAY + BULK		
Comments	This is groundwater sample E1-. No obvious alteration, sampled immediately below the tree, but water can be heard under the scree above the tree on the slope. Photos E4-1a and b.	Combined stream pH of 9.5 (uncorrected). Photos E5-1a and b.
GPS Elevation (m)	1285	1255
X-Y error (m)	6	6
GPS Location	3867116	3867168
	492258	0492285
	36 UTM S	36 UTM S
Location Description	Spring on west side of valley, 30-40m above stream bed.	Stream from E4 joins another on valley floor.
Site	4E	5E
BGS Laboratory No.		
Original sample label	GPS17	GPS18

Original sample label	BGS Lab No.	Site	Location Description	Comments	XRD analysis		
					Bulk	Specific	Clay
A1-1-2	MPLN 805	A1-1	Allas Springs: artesian discharge through fracture in harzburgite, with tufa deposit. Source of high pH groundwater for A1 site located on the western side of valley about 20-30 m above forest track	Sample of tufa (travertine) forming stalactites and flowstone coating the fracture surface of the harzburgite. Contains fragments of harzburgite within the tufa.		Y	
A1-2	MPLN 807	A1-2	Allas Springs: Flowing water within pit dug in calcified soil profile/tufa deposit (calcified litter of pine needles, leaves, partially decomposed wood, branches and other plant debris). 0.5 m depth. Located ~midway between A1-1 and A1-2	Highly altered (argillised) soil which has altered by interaction with high pH groundwater around discharge point	Y		Y
A2-1	MPLN 808	A2	Allas Springs: Spring discharge in stream bank, through soil and scree resting on fractured harzburgite. About 16 m south (upstream) of A1-2	Soil and altered scree from north side of discharge point	Y		Y
A2-2	MPLN 809	A2	Allas Springs: Spring discharge in stream bank, through soil and scree resting on fractured harzburgite. About 16 m south (upstream) of A1-2	Soil from around seepage point	Y		Y
A3-1	MPLN 810	A3	Allas Springs: Spring discharge in stream bank, through fractured harzburgite and along interface between soil/scree and underlying fractured bedrock. About 10-15 m south (upstream) of A2	Soil with organics developed on scree and associated with high pH seepage	Y		Y
A3-2	MPLN 811	A3	Allas Springs: Spring discharge in stream bank, through fractured harzburgite and along interface between soil/scree and underlying fractured bedrock. About 10-15 m south (upstream) of A2	Altered scree/ultrabasic rock associated with high pH seepage	Y		Y
A3-3	MPLN 812	A3	Allas Springs: Spring discharge in stream bank, through fractured harzburgite and along interface between soil/scree and underlying fractured bedrock. About 10-15 m south (upstream) of A2	Altered and fractured ultrabasic rock associated with high pH seepage	Y		Y
A4-1	MPLN 813	A4	Allas Springs: Main high pH groundwater discharge, near upper source high up Allas Springs valley, with scree and bedrock coated with thick travertine	Clay-rich alteration associated with high pH spring	Y		Y

A4	MPLN 814	A4	Allas Springs: Main high pH groundwater discharge, near upper source high up Allas Springs valley, with scree and bedrock coated with thick travertine	Laminated travertine encrusting stream bed sediments. Contains entrained harzburgite and other ultrabasic rock fragments		Y	
A4-2-1	MPLN 815	A4	Main stream from A4-1, just before joins stream from spring to the west of A4-1	Clay in stream	Y		Y
A4-2-2	MPLN 816	A4	Main stream from A4-1, just before joins stream from spring to the west of A4-1	Sediments around burn	Y		Y
A4-4-1	MPLN 821	A4	Highest spring (A4-1), emits from horizontal joint between harzburgite and overlying altered gabbro. Massive, almost coliform tufa. Sample collected ~7m vertically below spring.	Green tufa and clasts	Y		Y
A4-4-2	MPLN 822	A4	Highest spring, emits from horizontal joint between harzburgite and overlying altered gabbro. Massive, almost coliform tufa. Sample collected ~7m vertically below spring	Clay next to the tufa	Y		Y
A5-1	MPLN 824	A5	Allas Springs: Stream bank 10 m upstream of A3. High pH groundwater spring discharges through soil-covered scree and boulders at interface with altered and fractured bedrock at the base of tree roots	Soil associated with alkaline spring	Y		Y
A5-2	MPLN 825	A5	Allas Springs: Stream bank 10 m upstream of A3. High pH groundwater spring discharges through soil-covered scree and boulders at interface with altered and fractured bedrock at the base of tree roots	Altered bedrock	Y		Y
A6	MPLN 826	A6	Tufa cemented scree, 50 m down valley, north of forest path and A1-1. Alkaline groundwater and stream discharges through the base of the scree at bedrock surface exposed in the stream bed. Discharges from fractured serpentinite with tufa coatings	Tufa/travertine-cemented scree of ultrabasic clasts from stream bed at contact with serpentinite bedrock		Y	
C2-1	MPLN 827	C2	Chrisovrysi Springs: hillside cisterns collecting alkaline groundwater. Located on high hillside above the decorative roadside cistern. Exposure of soil profile through which springs originally discharged	Soil/regolith directly above spring seepages	Y		Y
C2-2	MPLN 828	C2	Chrisovrysi Springs: hillside cisterns collecting alkaline groundwater. Located on high hillside above the decorative roadside cistern. Exposure of soil profile through which springs originally discharged	Soil and regolith clasts reacted with or coated by tufa.	Y		Y
C3-1	MPLN	C3	Chrisovrysi Springs: Stream cutting	Argillised or	Y		Y

	829		through steep scree resting on highly fractured and altered serpentinite. Located about 50 m up the hillside from the roadside from roadside cistern site "C1". Groundwater discharges through highly altered and argillised fractured serpentinite just beneath (0-1 m) the contact with the scree, and feeds the flow in the stream.	altered serpentinite (?clay + organic containing) from altered bedrock directly below the travertine coating and directly in contact with alkaline groundwater seep along scree-bedrock interface.			
C3-2	MPLN 830	C3	Chrisovrysi Springs: Stream cutting through steep scree resting on highly fractured and altered serpentinite. Located about 50 m up the hillside from the roadside from roadside cistern site "C1". Groundwater discharges through highly altered and argillised fractured serpentinite just beneath (0-1 m) the contact with the scree, and feeds the flow in the stream.	Altered serpentinite in direct contact with alkaline groundwater through fractures in bedrock within the stream	Y		Y
C3-3	MPLN 831	C3	Chrisovrysi Springs: Stream cutting through steep scree resting on highly fractured and altered serpentinite. Located about 50 m up the hillside from the roadside from roadside cistern site "C1". Groundwater discharges through highly altered and argillised fractured serpentinite just beneath (0-1 m) the contact with the scree, and feeds the flow in the stream.	Altered serpentinite in direct contact with alkaline groundwater through fractures in bedrock in stream bank	Y		Y
C3-4	MPLN 832	C3	Chrisovrysi Springs: Stream cutting through steep scree resting on highly fractured and altered serpentinite. Located about 50 m up the hillside from the roadside from roadside cistern site "C1". Groundwater discharges through highly altered and argillised fractured serpentinite just beneath (0-1 m) the contact with the scree, and feeds the flow in the stream.	Bulk sample of background altered serpentinite	Y		Y
C3	MPLN 834	C3	Chrisovrysi Springs: Stream cutting through steep scree resting on highly fractured and altered serpentinite. Located about 50 m up the hillside from the roadside from roadside cistern site "C1". Groundwater discharges through highly altered and argillised fractured serpentinite just beneath (0-1 m) the contact with the scree, and feeds the flow in the stream.	Travertine coated and tufa-cemented rock fragments recovered in situ from stream bed		Y	

Sample Site:	A1-1	**Site Sample No.:**	A1-1-2
BGS Sample ID:	MPLN805	**Preparation:**	2xfresh fractured fragments
Site Descn:	Allas Springs: artesian discharge through fracture in harzburgite, with tufa deposit.		
Sample Descn:	Sample of tufa (travertine) forming stalactites and flowstone coating the fracture surface of the harzburgite.		

A: Sample Photo

Sample Description

The sample is a pale orange colour with a variably defined layered structure (A). Sample portions were taken from poorly layered (B, C, D) and moderately layered (E) areas. The bulk of the deposit comprises tightly interlocking prismatic calcium carbonate (E). Halite is present scattered throughout, typically with rounded partially dissolved forms (B, C). The layering, where present, is in part defined by linear variations in porosity, but is also defined by textural variations. The latter typically take the form of planes where one set of prismatic calcium carbonate crystals terminate (E). In the poorly layered portions textural variations are randomly distributed. Some pores contain infiltrated silicate debris.

Pores throughout the structure of the deposit are lined by a thin amorphous film (C, D, E), commonly ridged, also in ribbons that locally bridge pores. This film is most likely biogenic (biofilm).

Calcium carbonate crystal surfaces in pores commonly have rough-looking surfaces. These are formed of multiple aligned overgrowth-like microcrystals, typically partially merged (D). This morphology suggests that although the crystals themselves can have rounded appearances, the most recent episode is of calcium carbonate formation.

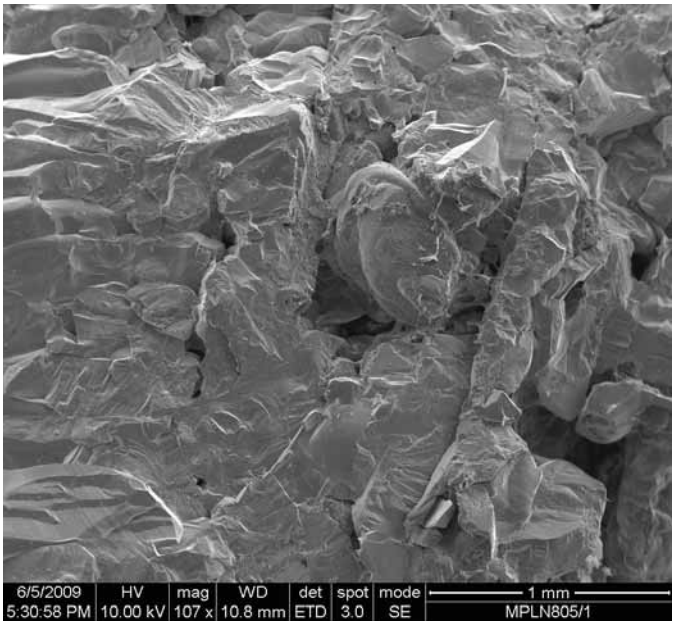

B: A general view from the portion with poorly defined layering. The deposit predominantly comprises interlocking calcium carbonate with lesser halite. There is a high porosity in some parts, other parts comprise tightly interlocking crystal structures (left). Crystal forms are also varied. The rounded form at centre is of halite.

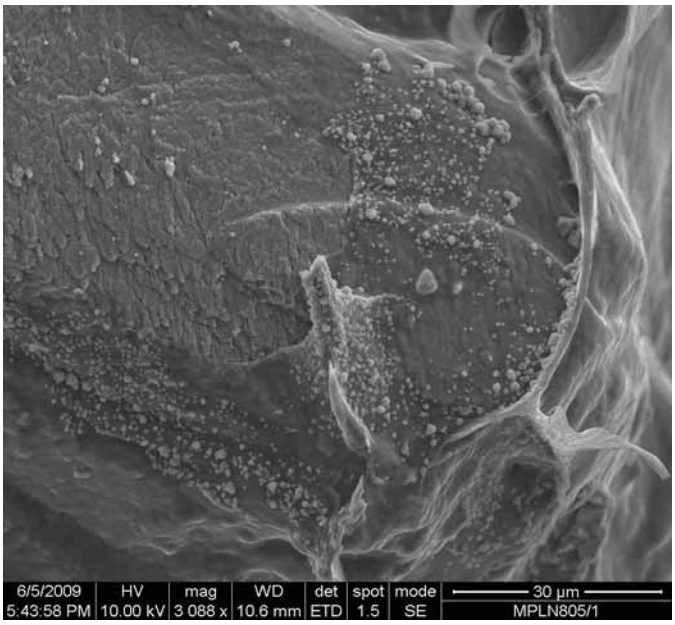

C: Detail of the pore-lining film present in the pore adjacent to the halite in the preceding image. The halite itself shows evidence of minor dissolution. EDXA detects high C and O levels from the thin amorphous fil, this is consistent with it being a biofilm, which would be expected to be composed of polysaccharides. It is in turn coated by fine halite. EDXA of the biofilm typically shows the additional presence of traces of Si, Al, Mg and Ca.

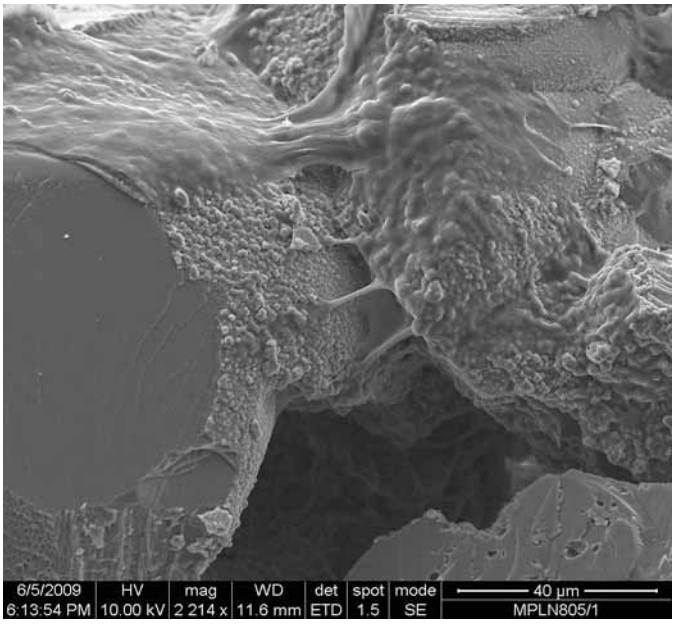

D: Another macropore lined by probable biofilm. The pare walls are here all of calcium carbonate. Their rough-looking surfaces are formed of multiple aligned overgrowth-like microcrystals, typically partially merged. This suggests that although the crystals themselves have a rounded appearance, the most recent episode is of calcium carbonate formation.

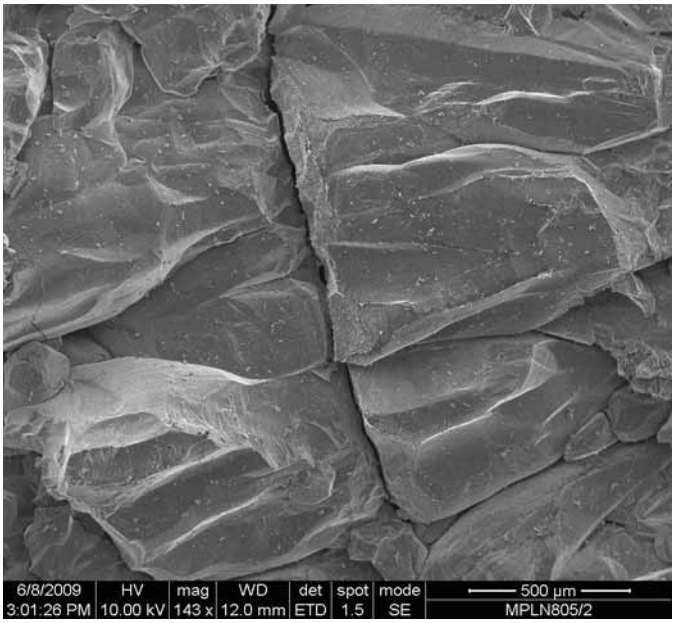

E: This sample portion is from the area with a moderately defined layered texture. Layering is in part defined by linear variations in porosity, but there are also textural variations. Here the lamination is marked by a plane marking the termination of one set of prismatic calcium carbonate crystals and the start of another set.

Pore surfaces are again partially lined by probable biofilm. The calcium carbonate crystal surfaces also again comprise multiple aligned overgrowth-like microcrystals, typically partially merged.

Sample Site:	A1-1	**Site Sample No.:**	A1-1-1
BGS Sample ID:	MPLN806	**Preparation:**	Freshly fractured fragment
Site Descn:	Allas Springs: artesian discharge through fracture in harzburgite, with tufa deposit.		
Sample Descn:	Forest litter and plant debris reacted with and cemented by travertine from discharging high pH groundwater.		

A: Sample Photo

Sample Description

Plant debris in the form of woody stalks and some leaves, partially cemented by a calcium carbonate deposit (A). In the main, the plant debris appears intact, with the cellular structures retained (B, C, G). Locally the calcium carbonate has formed within the cell structure of the plant debris, although the organic matter of the cell walls typically remains enclosed by the carbonate. Strands and ribbons of amorphous organic matter present on some surfaces are most likely fungal (D, E, F). Other biogenic forms are also present enclosed within the cement (I), including probable bacterial chains (I).

The cement comprises a mosaic of interlocking crystals with a locally discernible finely layered internal structure (D, I). Exposed cement surfaces are typically smooth on a coarse scale (D), but in detail are finely pitted (E), often with raised rims at crystal boundaries. In finer detail, the apparent pitting is defined by the surfaces comprising multiple microcrystalline overgrowth-like developments (F). These are typically parallel oriented where developed on a single crystal domain. The microcrystals typically partially and variably merge and this is what creates the pitting. The thicker growth at crystal margins may be due to enhanced growth dynamics at crystal edges, or reflect on growth under conditions of partial saturation during periods of drying where fluids remain longest in hollows and where capillary effects are active.

Calcium-based fibrous deposits have possibly developed within the constituents of the plant debris (H).

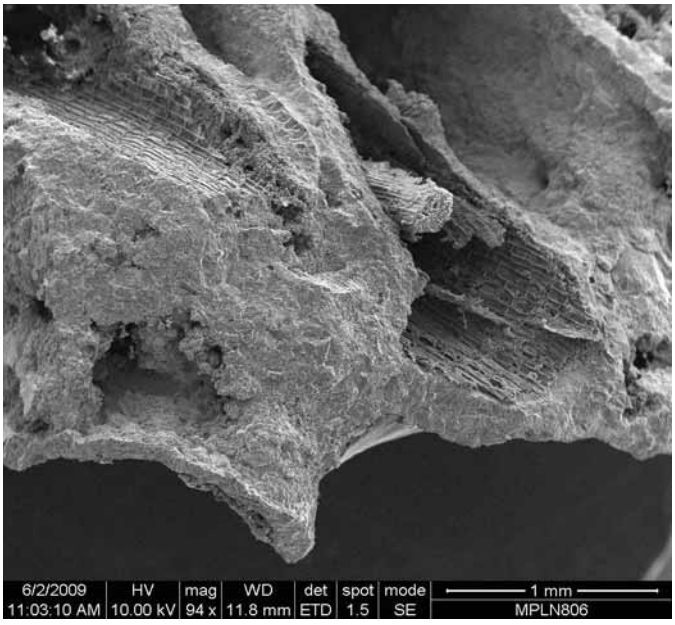

B: A general view showing stems of plant debris cemented by a matrix of interlocking calcium carbonate.

EDXA of the plant matter records C and O with traces of Na and Cl.

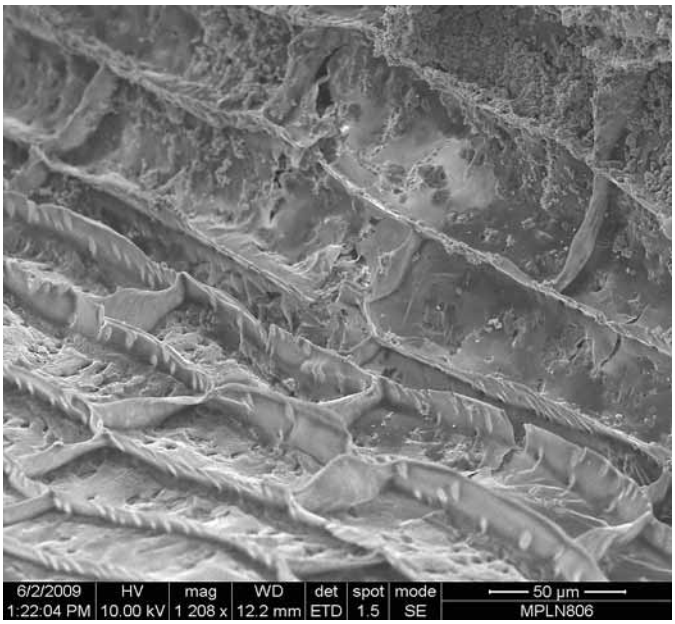

C: Detail of the interior of a fragment of plant debris. Ribbed wall structures are well defined and still comprise organic matter. The lining debris at top right is of calcium carbonate. From EDXA, ribs contain traces of Na (no Cl). Walls also contain Na, although the thinness of the walls means significant Ca from the carbonate is also detected.

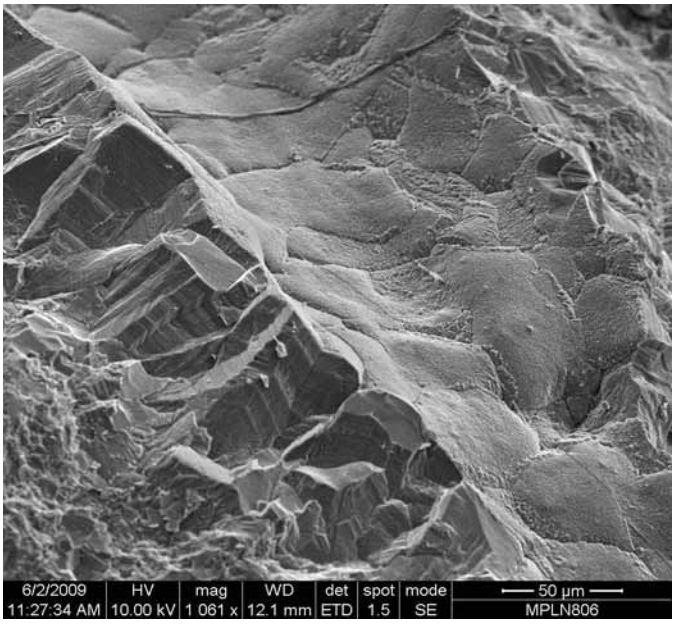

D: Shows the relatively smooth exposed surface of the calcium carbonate cement (centre) and its finely layered cross-section (lower left portion). Note also the probable fungal filament (top).

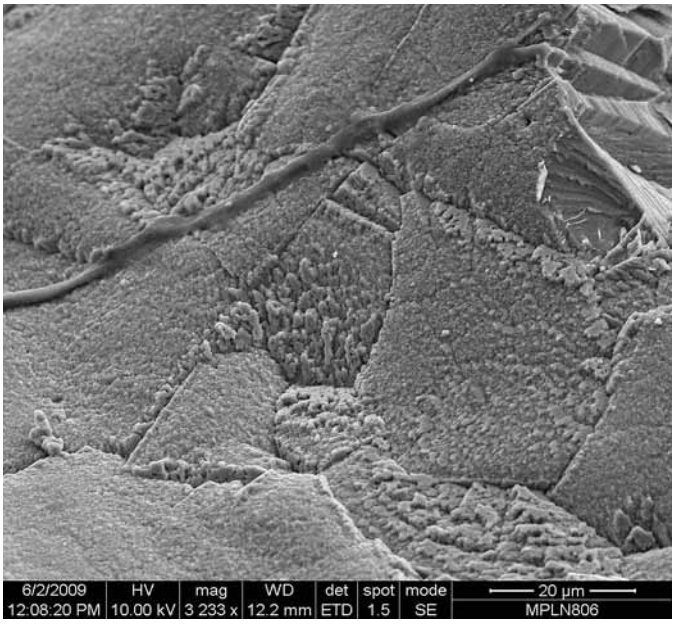

E: This shows a portion of the exposed surface of the calcium carbonate cement, from the upper part of central areas of the preceding image. The interlocking mosaic structure of the cement is reflected by surface textures. Crystal boundaries are well defined by a mix of surface textures. Exposed crystal surfaces are finely pitted with subtly different orientations reflecting crystallographic orientations. Crystal boundary areas appear topographically prominent due to the thicker and coarser overgrowth-like developments.

Strand across the upper left portion of the image is most likely fungal.

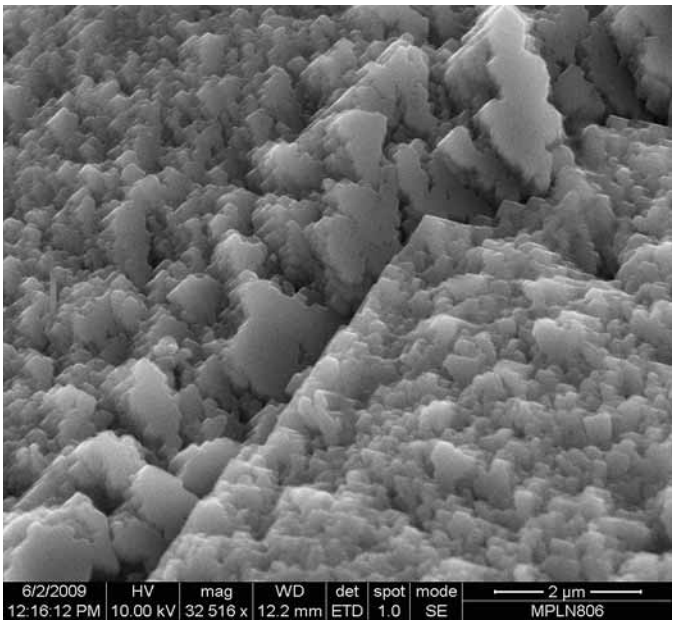

F: Detail of the intersection of two crystals as shown lower left of centre in the preceding image. Euhedral aspects to the crystal faces that define the thicker rims to the intersection suggest the texture is at least in part created by crystal growth. The pitted surfaces are also resolved as comprising parallel-oriented multiple euhedral forms, again suggesting growth origins.

The thicker growth at margins may be due to enhanced growth dynamics at crystal edges, or reflect on growth under conditions of partial saturation during periods of drying where fluids remain longest in hollows and where capillary effects are active.

Note the fine filament inside left of Mg-silicate, and possible biofilm top right.

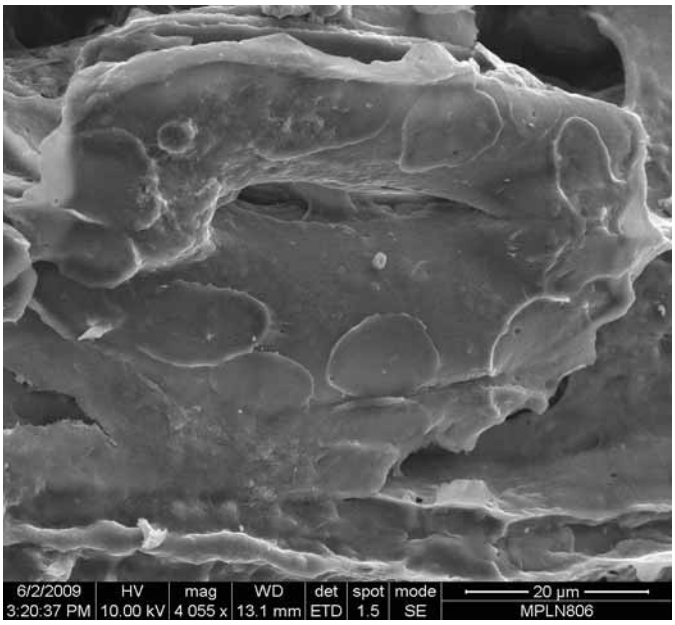

G: Detail of a stomata in a cemented leaf. This is coated by a thin layer of amorphous organic matter that locally displays a matted fibrous texture (below centre). This material is most likely some form of waxy deposit. Disc-like forms are from contact sites where the amorphous phase is thin or absent.

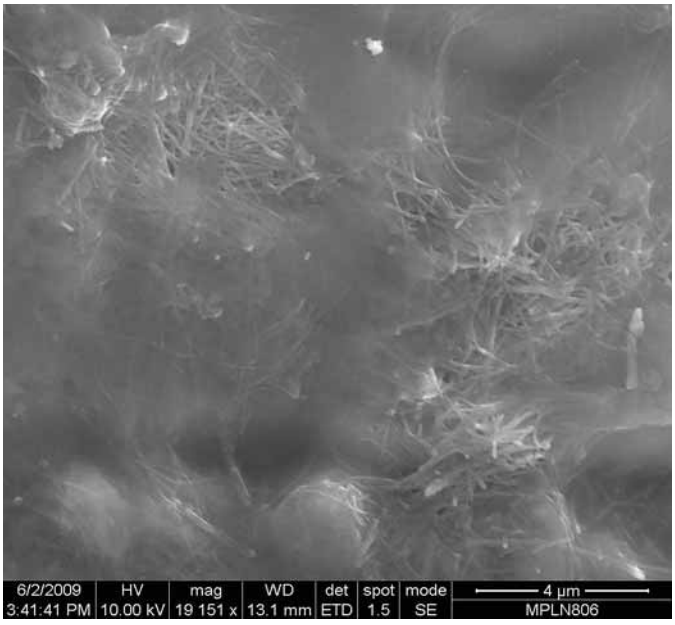

H: From near the bottom of the preceding image, showing a finely fibrous phase that is present within the amorphous coating on the leaf. Minor calcium is detected by EDXA. The fibrous deposit may be a carbonate or oxalate.

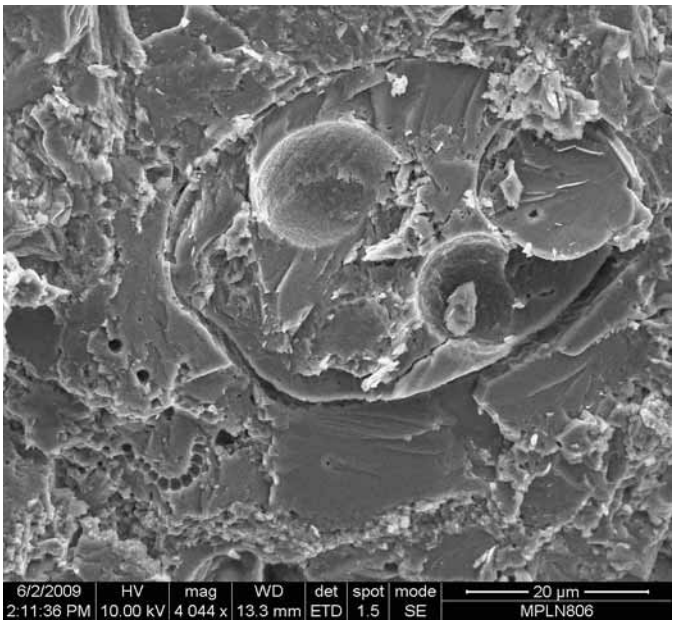

I: Detail from calcium carbonate cement. The nested rounded forms (centre) are unidentified but biogenic. The internal calcium carbonate locally appears etched. Note also the strings of open rounded pores (lower left); these may be bacterial.

A granular 'surface' above bottom is part of the layered structure locally displayed in the cement. This probably represents a hiatus in development. Traces of Na and Cl are associated with it.

Sample Site:	A5	**Site Sample No.:**	A5-2
BGS Sample ID:	MPLN825	**Preparation:**	Freshly fractured fragment
Site Descn:	Allas Springs: Stream bank 10 m upstream of A3. High pH groundwater spring discharges through soil-covered scree and boulders at interface with altered and fractured bedrock.		
Sample Descn:	Altered bedrock.		

A: Sample Photo

Sample Description

The altered rock fragments are pale green in colour (A) and dominantly comprise tightly packed fibrous magnesium silicate (B), most likely serpentine. The fibres have bladed to ribbon-like forms (C). Within the rock fragments there are open macropores, mostly fractures, many of which are lined by a euhedral hexagonal platy phase (D, E, F) that EDXA shows is dominated by Mg but contains some Fe, and is most likely to represent pyroaurite identified by XRD. These plates commonly have perforations and / or secondary growths. These textures suggest that there have been multiple episodes of formation and possibly of dissolution.

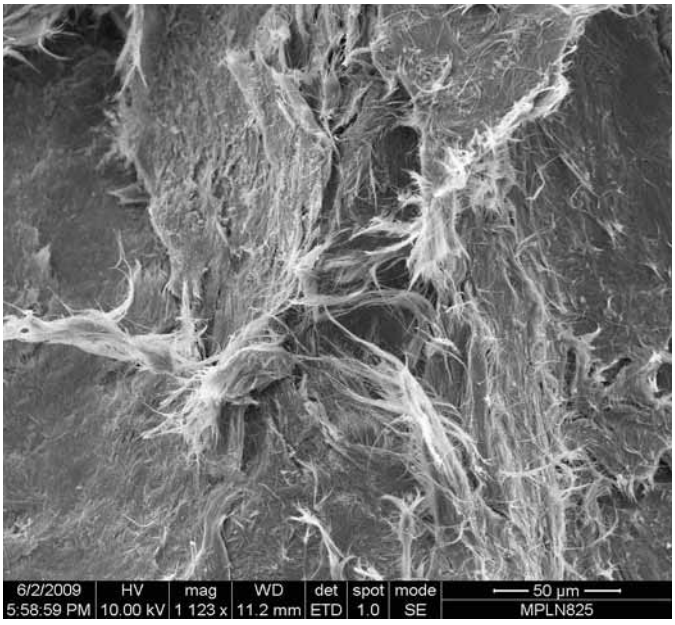

B: A general view showing the dominant constituent of the sample; Mg silicate as dominantly matted fibres (identified by XRD as lizardite), locally bridging pores within the rock structure, mostly fractures.

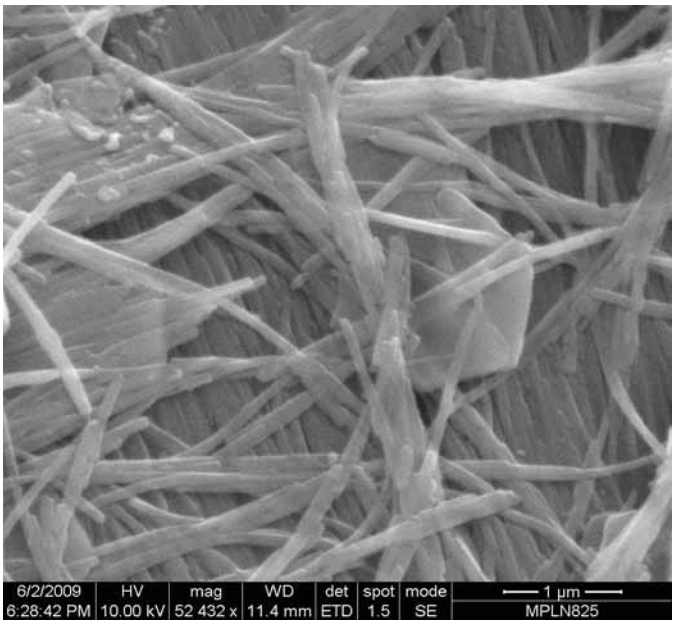

C: Detail of the matted fibres of Mg silicate. This shows that the fibres have a flat, bladed / ribbon form. Also discernible are scattered hexagonal platy crystals within the matted structure. These appear to be forming from the fibrous serpentine mineral (identified as lizardite by XRD) are too thin in this instance to determine elemental constituents by EDXA independently of the fibres but appear to be Mg-rich with some Fe, and on the basis of the morphology, and by analogy with coarser plates observed elsewhere in the sample, probably corresponds to pyroaurite identified by XRD .

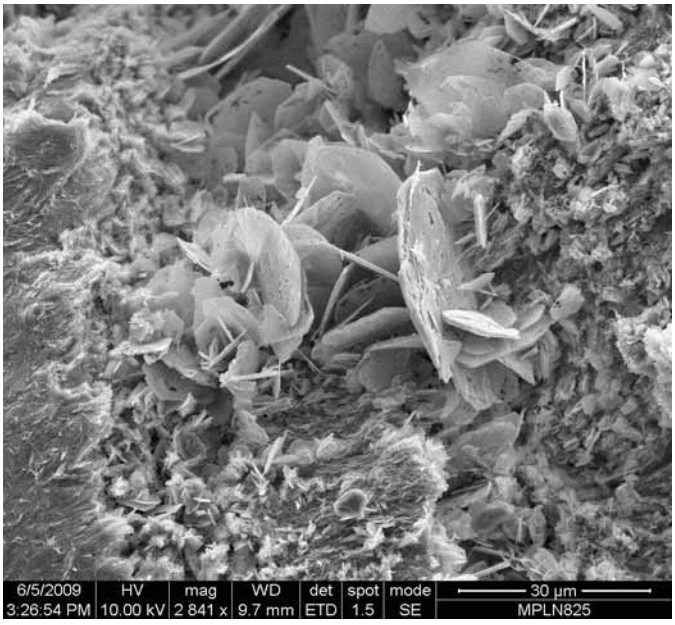

D: An open coarse pore within the dominant fibrous matrix contains a cluster of psuedo-hexagonal plates. These have rounded edges and common perforations, suggesting minor dissolution. EDXA records a Mg+O composition with lesser associated Fe. These are probably of pyroaurite ($Mg_6Fe_2(SO_4, CO_3)(OH)_{16}.4H_2O$)

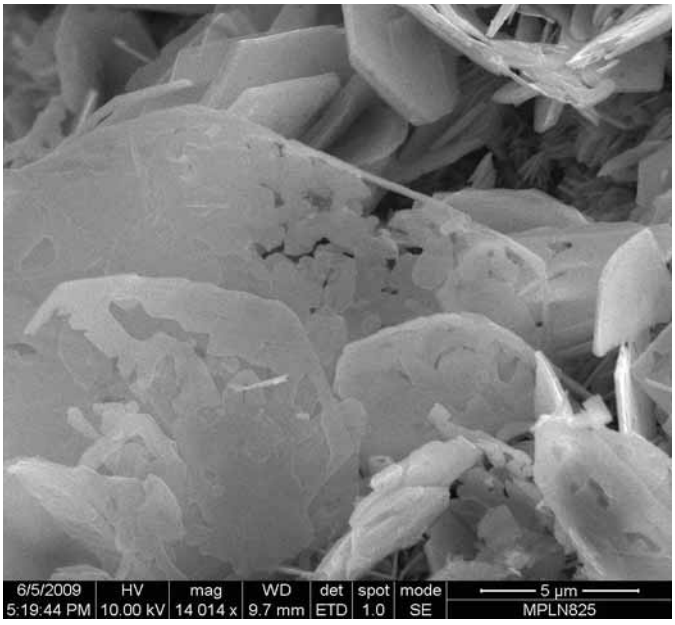

E: Detail from above and right of centre in the preceding image, showing the fine structure of the pyroaurite plates. Strand-like edges and rounded edges to perforations are suggestive of partial dissolution. Euhedral plates and elements to some of the perforations suggest that the larger plates may have accreted by coalescence and coarsening up ("Ostwald ripening" of finer platy crystallites.

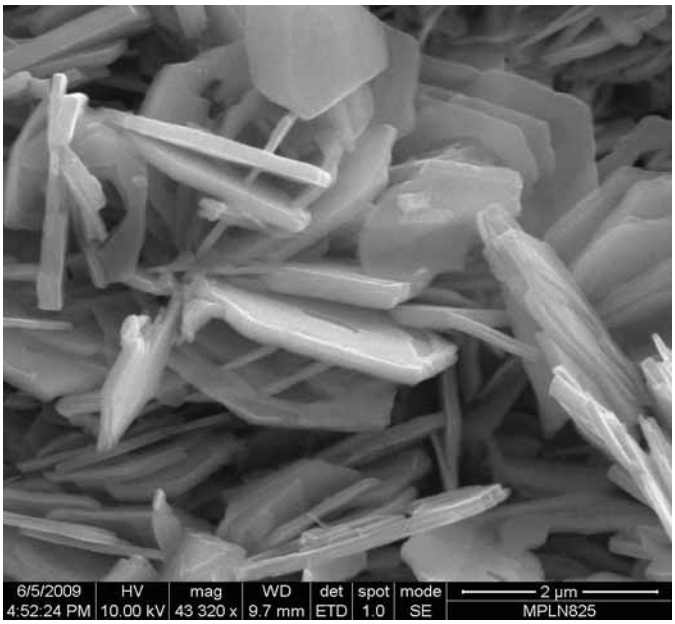

F: Detail of coarser hexagonal plates of probable pyroaurite lining to another open pore. The dominant texture is of euhedral plates, some perforated, others with thicker rims. This last texture appears to have developed through the formation of partial 'overgrowths' on plate surfaces. Again, multiple periods of formation, and possibly of dissolution, are suggested.

Sample Site:	A4	**Site Sample No.:**	A4
BGS Sample ID:	MPLN814	**Preparation:**	4xfresh fractured fragments
Site Descn:	Allas Springs: Main high pH groundwater discharge, near upper source high up Allas Springs valley, with scree and bedrock coated with thick travertine.		
Sample Descn:	Laminated travertine encrusting stream bed sediments. Contains entrained harzburgite and other ultrabasic rock fragments.		

A: Sample Photo

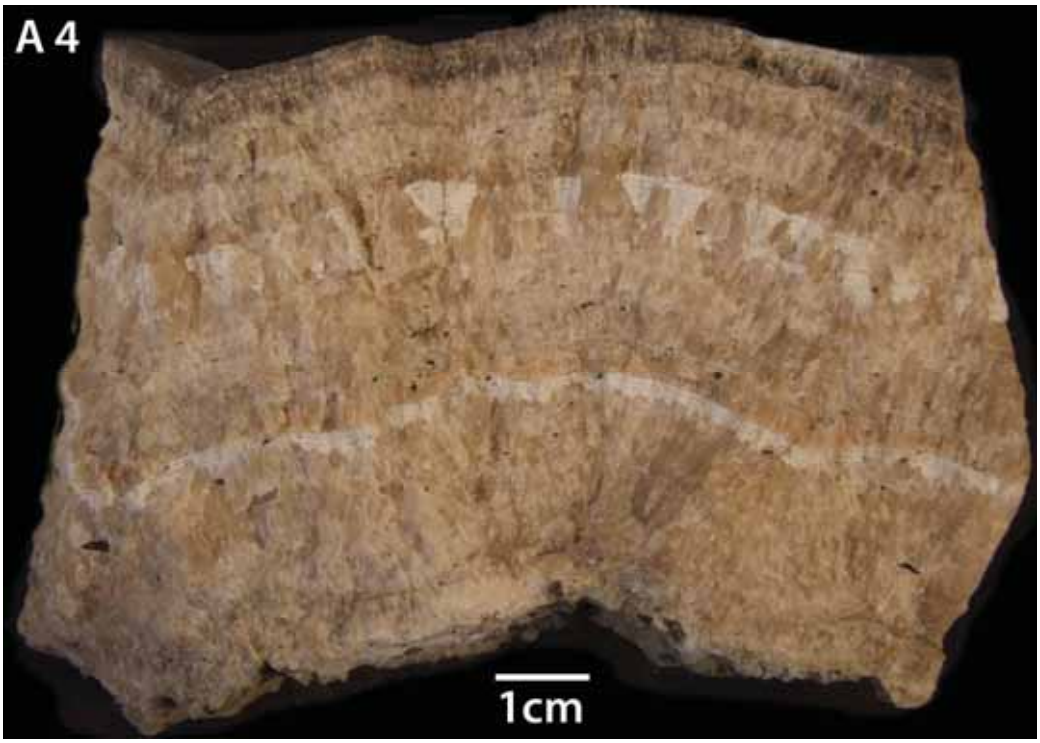

Sample Description

The sample is predominantly a pale orange colour with a fine layered structure (A). Layers have undulating forms and are primarily defined by variations in colour. The top surface has a grey colour. Some laminations have high contents of a white deposit, locally present with fan-like forms. Sample portions were taken through the thickness of the deposit.

The deposit dominantly comprises tightly interlocking prismatic / columnar calcium carbonate (B) crystals. The layers are defined by a range of features. Most are textural, including lines of rounded pores (D; probably after dissolution of a phase such as halite), lines of crystal termination and variations in crystal sizes (D). There are some layers that comprise equant crystal forms (C), possibly representing a period of formation from groundwaters of different salinity. There are also enclosed particles of silicate that are typically aligned (D) and enriched with the layering; these are most likely trapped sediment.

The white deposit is of aragonite, present in fans of acicular crystals (E) with locally discernible chisel-like terminations (F). The dominant prismatic to equant calcium carbonate (calcite) appears to have formed enclosing the aragonite (G). Finely fibrous magnesium silicate enclosed by and coating the carbonates (G) includes trapped detrital sediment, but some may be diagenetic in origin.

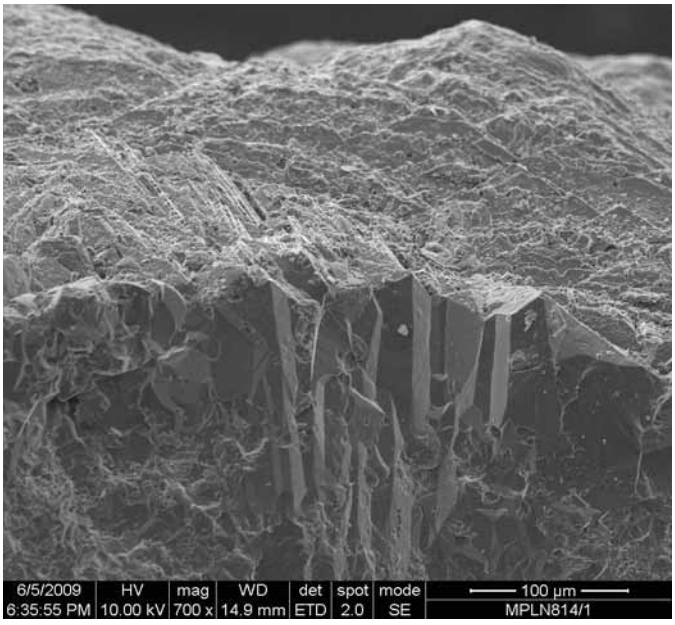

B: An oblique view of the top of the deposit. The internal structure of the deposit is of tightly interlocking prismatic crystals of calcium carbonate. These have euhedral crystal terminations at the deposit surface, typically thinly coated by fine sediment, mostly carbonate but also including clay silicates.

Multiple linear features expressed at the surface are probably carbonate twinning / cleavage planes.

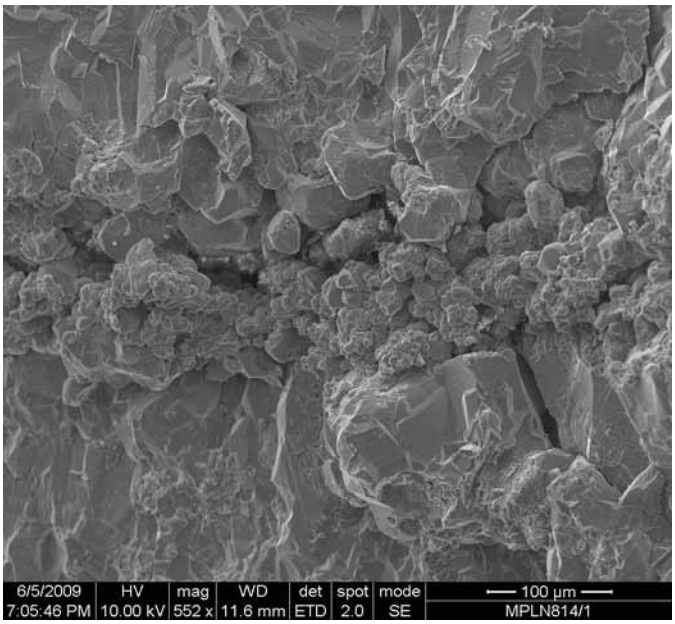

C: Showing a texture that defines the layering in this upper portion of the deposit. This is a discrete layer of finer more equant calcium carbonate, in contrast to the prismatic forms above and below. This layer may represent a period of formation from groundwaters of different salinity. The layer also has a higher porosity.

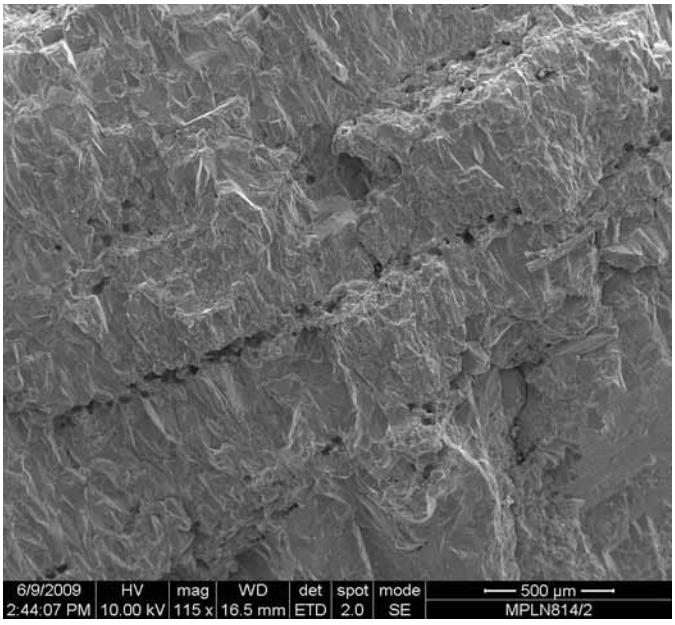

D: From a second sample portion approximately 1cm below the deposit top surface. Layers are defined by a mix of textural features, including truncation surfaces and lines of rounded open pores. There is also some variation in the size of the calcite crystals. Scattered trapped silicate particles also commonly lie parallel to the layers. The flakes are mostly of fibrous Mg silicates (probably serpentine).

The rounded pores may be after dissolution of another phase.

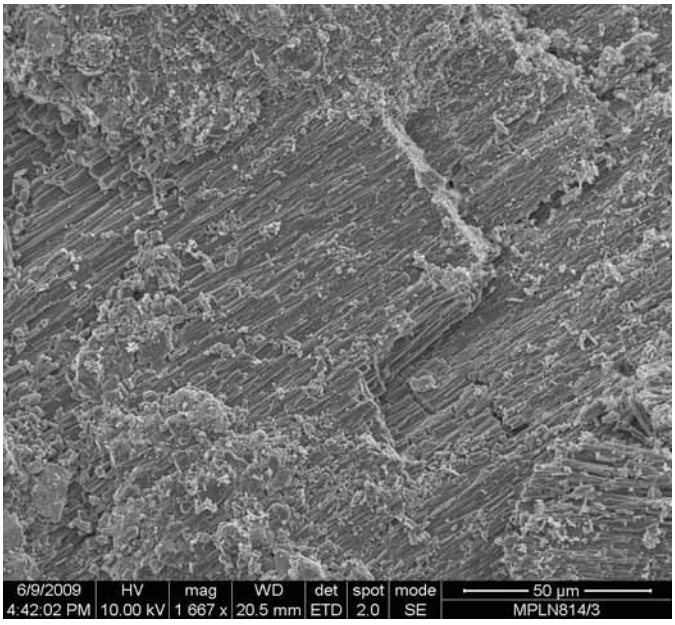

E: This sample portion is from an area of the white-coloured deposit. The white colour coincides with this tightly packed and aligned acicular texture. EDXA shows that this is a calcium carbonate.

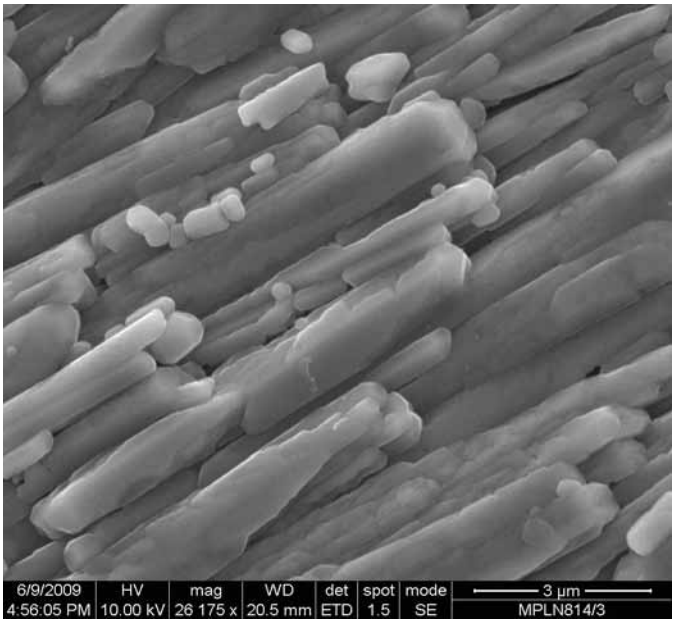

F: Detail of the acicular calcium carbonate. Locally chisel-like crystal terminations are discernible, consistent with this phase being **aragonite.**

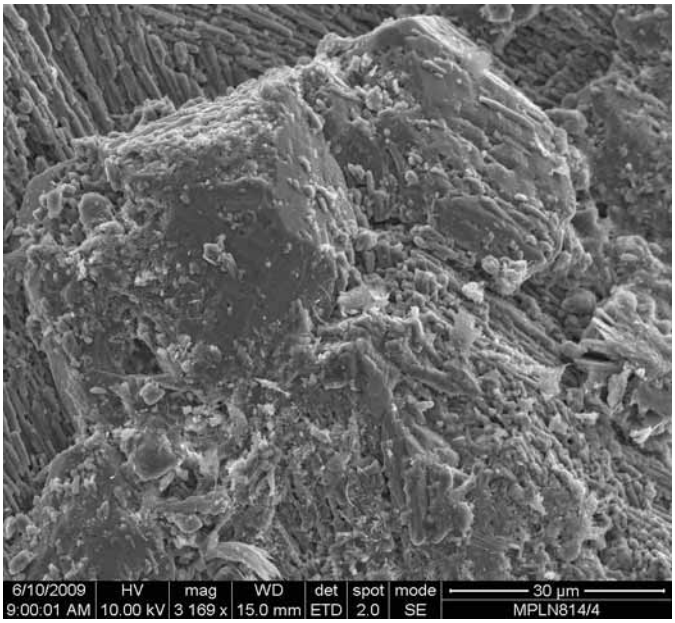

G: From a sample portion taken approximately 2cm below the sample surface. This shows an area of intergrowth of a patch of the acicular carbonate (aragonite) with equant blocky calcium carbonate (most likely calcite). The latter appears to be forming enclosing the former.

There are also common fine fibres of Mg silicate that are both enclosed by and draped over the carbonates.

Sample Site:	A6	**Site Sample No.:**	A6
BGS Sample ID:	MPLN826	**Preparation:**	Freshly fractured fragment
Site Descn:	Alkaline groundwater and stream discharges through the base of the scree at bedrock surface exposed in stream bed. Discharges from fractured serpentinite with tufa coatings		
Sample Descn:	Tufa / travertine-cemented scree of ultrabasic clasts from stream bed at contact with serpentinite bedrock.		

A: Sample Photo

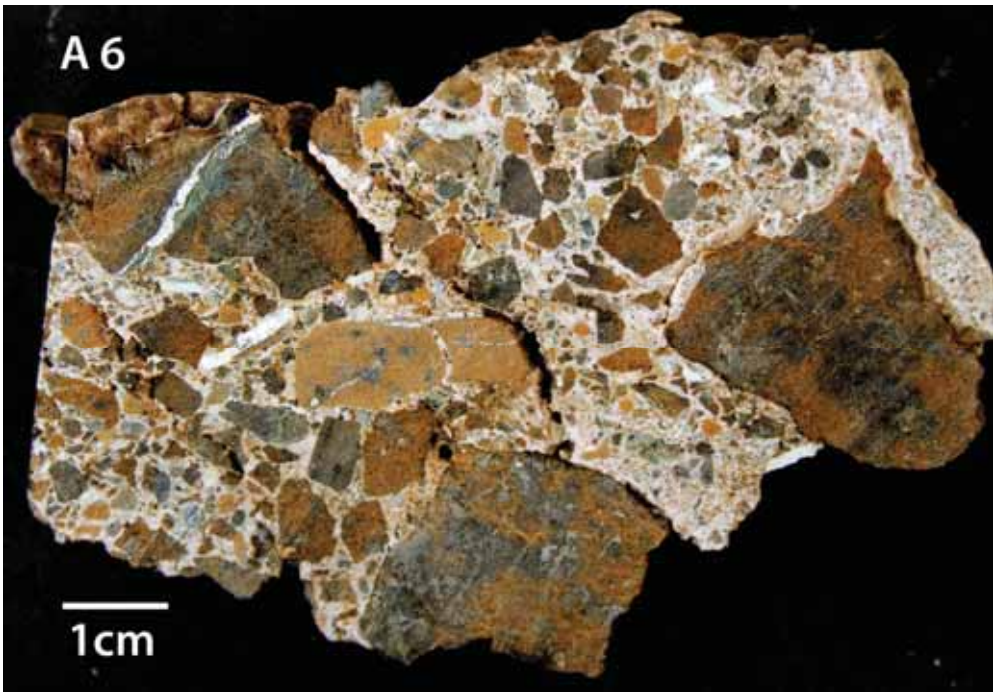

Sample Description

The sample comprises a poorly sorted sediment of altered rock fragments cemented by calcium carbonate. The rock fragments are highly varied in shape and colour, with inherited white veining (A). Most are orange-brown and pale green to grey in colour (A). Scattered white flakes comprise tightly packed fibrous magnesium silicate (most likely serpentine), probably separated fragments of the veining.

The calcium carbonate cement typically only partially occludes intergranular pores, present as a lining with a meniscus-like distribution suggesting formation during periods dominated by partial saturation. Prismatic calcite crystals extend in to some pore centres (B), showing some formation has occurred during full saturation. Some of these crystals have surface textures that show overgrowth-like developments (C) that have formed only on surfaces nearest to the pore walls, forming a ‘tide-mark’ along with fibrous magnesium silicates, again suggesting periods of partial saturation have followed their formation. Primary subhedral dolomite (D) has formed in these ‘tide-mark’ deposits, partially enclosed by the overgrowth calcite.

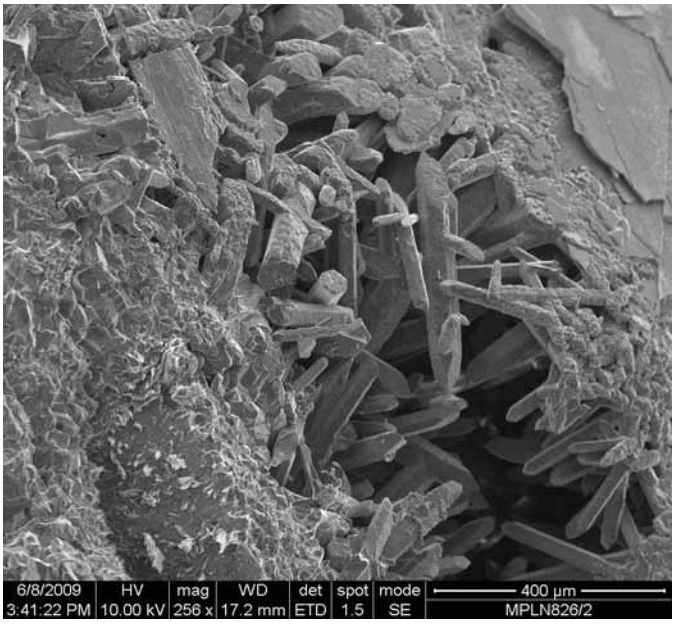

B: Prismatic calcium carbonate crystals with typical calcite terminations here are partially cementing intergranular pores. Platy (upper right, upper left) and fibrous clasts (lower left) comprise Mg silicates (most likely serpentine). Typically crystal tips near the pore centre are clean whilst the bases of crystals near the pore walls appear rough.

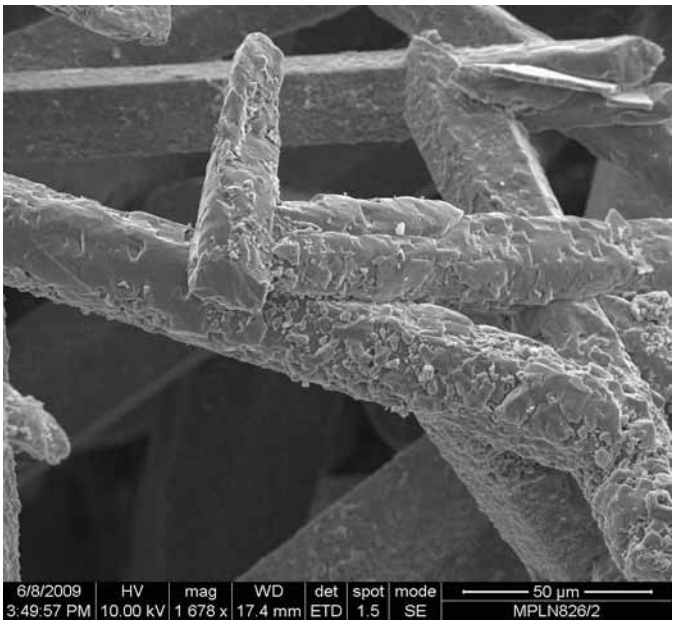

C: Detail from the preceding image, showing the rough crystal surfaces. These result from the presence of multiple partial overgrowth-like developments. Clay-grade matter and other deposits are present on some surfaces, locally partially enclosed by the layered growths.

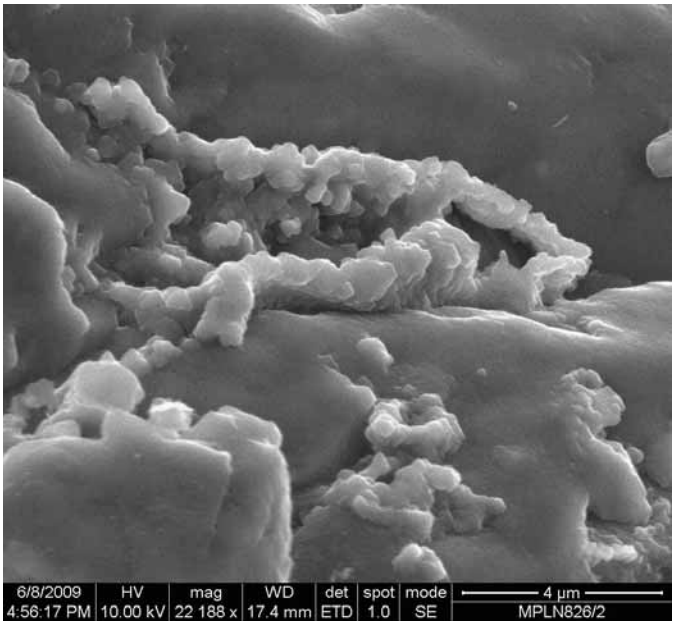

D: Detail from the preceding image. The V-like deposit is of dolomite. The subhedral calcite layer has formed around the dolomite. The tip of the dolomite feature looks like something has been removed from its centre. All the other microcrystal clusters in the field of view are also dolomite, some are clearly enclosed in the subhedral calcite overgrowth layer.

Sample Site:	T	**Site Sample No.:**	T5
BGS Sample ID:	MPLN842	**Preparation:**	Freshly fractured fragments
Site Descn:	Vertical profile through exposure of parallel-laminated marly clay and silt resting on altered pillow lavas and autobrecciated pillow lava.		
Sample Descn:	60 cm: clay silt with carbonate veining.		

A: Sample Photo

Sample Description

The sample comprises a loose mix of clay, silt, sand and gravel sized particles (A). Some of the coarser particles were freshly fractured and mounted for analysis. The sample fragments dominantly comprise subhedral to anhedral micritic calcite (B, C) with scattered elongate forms (B), also of calcium carbonate. Clay minerals are identifiable as scattered matter intermixed and bridging between the carbonate particles (B, C). Euhedral forms to some of the calcite particles suggest some aggrading neomorphism has occurred.
The clay minerals are magnesium-rich aluminosilicates. Magnesium content is variable.

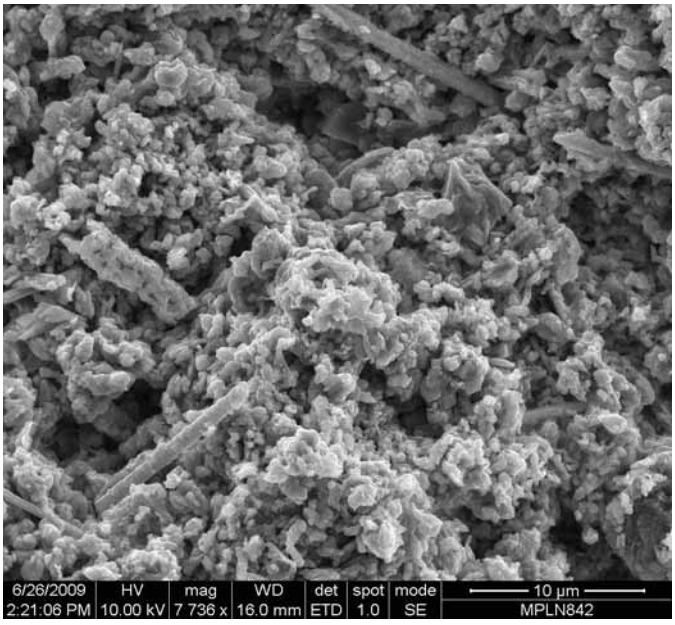

B: The sample fragments dominantly comprise subhedral to anhedral micritic calcite with scattered elongate forms, also of calcium carbonate. Clay minerals are identifiable as scattered matter intermixed and bridging between the carbonate particles. Euhedral forms to some of the calcite particles suggest some aggrading neomorphism.

EDXA indicates that the clay minerals are Mg-rich aluminosilicates. Mg content is variable.

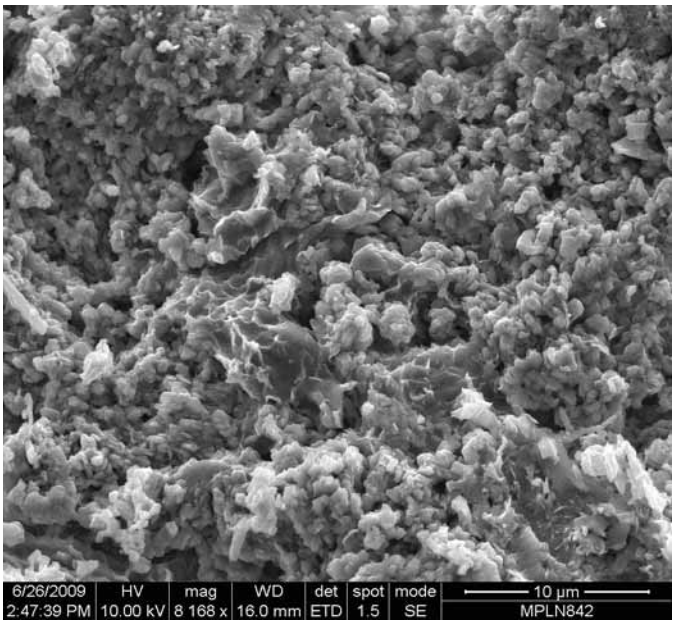

C: This shows an area with a higher clay content than the preceding image, concentrated in a patch. It has the typical ragged webbed appearance of smectitic clays. Again, EDXA analysis indicates that the clay minerals are Mg-rich aluminosilicates.

Sample Site:	P2	**Site Sample No.:**	P2-3
BGS Sample ID:	MPLN847	**Preparation:**	3xfresh fractured fragments
Site Descn:	Parsata area: Kalavasos to Parsata road, rock face on ledge above road with Pillow Lava sequence fractured with tufa.		
Sample Descn:	0 cm: Contact between autobreccia and altered pillow lava with tufa veins.		

A: Sample Photo

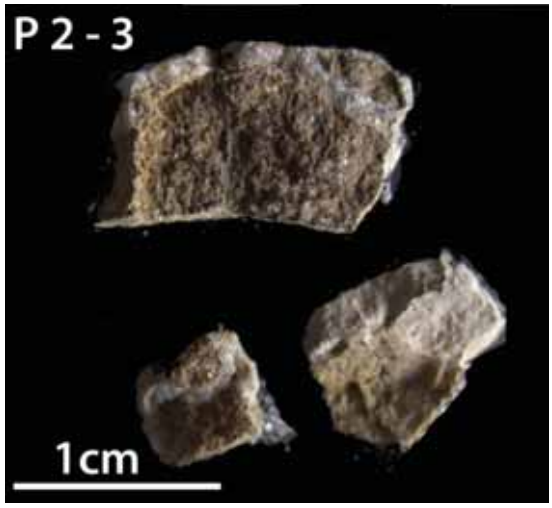

Sample Description

The sample comprises an autobrecciated pillow lava with calcium carbonate veins / fracture fills (A). The matrix of the lava contains partially dissolved feldspars, mostly Ca-rich plagioclase (F), with altered and partially dissolved remnants of matrix (B). Smectitic clays line and fill many of the pores (B, C, D). There are also minor deposits of probable zeolite (F; probably K-rich clinoptilolite).

The smectitic clays have bridging webbed morphologies (C). EDXA shows that they are a magnesium-rich type with traces of potassium, calcium and iron. The morphologies of these clays display a systematic variation with respect to their location relative to the carbonate vein / fracture fills. Smectitic clay pockets within 500 microns of the carbonate typically display a lower relief webbed texture compared to clays further away (C, D). In addition the clays closer to the carbonate typically do not bridge the entire pore and webbed forms commonly look truncated (D, E). These textural variations are interpreted as evidence of minor collapse and alteration / dissolution. Rarely, secondary deposits have formed on the clay surfaces within this alteration zone (E). At one site a Mn-bearing aluminosilicate deposit that is associated with a patch of altered clay may be a product of the alteration (F).

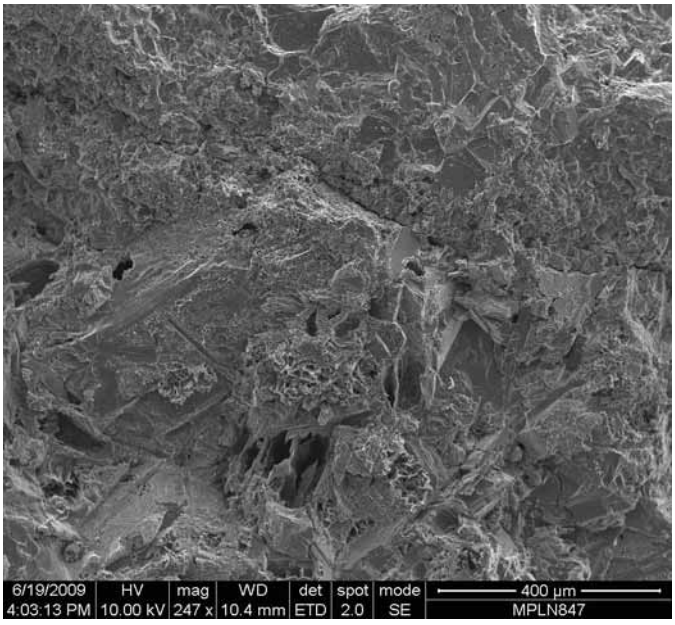

B: View of the region on the coarsest of the three fragments where a vein is in contact with the altered lava. The carbonate cemented vein / fracture is in the top right corner, altered lava is centre and lower left showing evidence for dissolution, with patches of smectitic clay minerals lining and filling the secondary pores throughout.

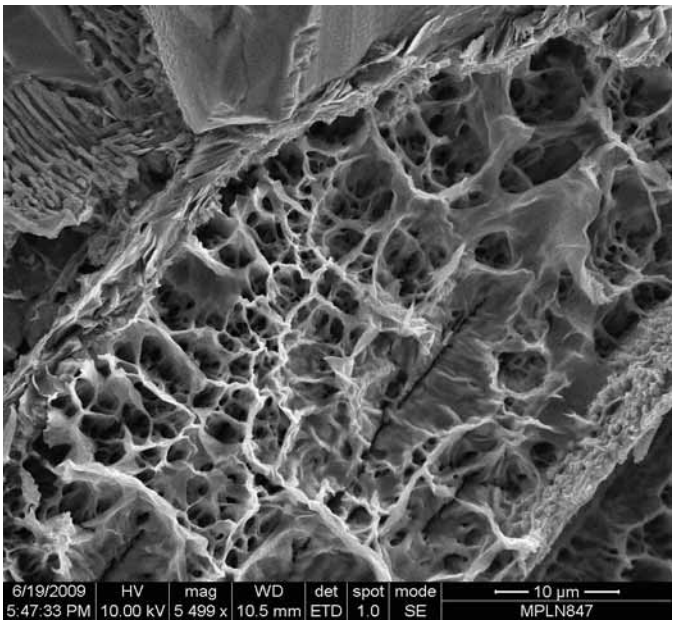

C: This shows smectitic clays filling a pore in the altered lava. EDXA shows that the clay is a Mg-rich type with traces of K, Ca and Fe. This morphology of bridging webbed forms is typical of clays from the portions of the altered lava that are well away from the contacts with the carbonate cement.

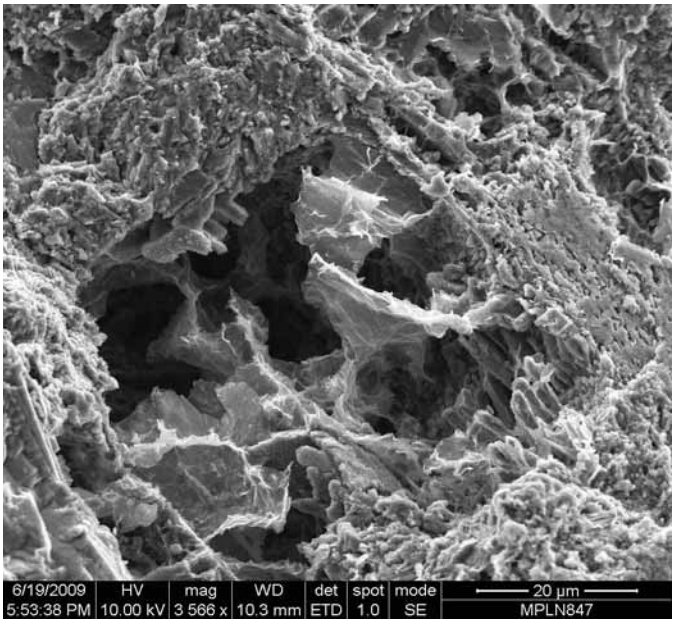

D: The truncated and collapsed texture of the smectitic clays shown here is typical of the textures seen in the lava close to the contact with the vein / fracture fill.

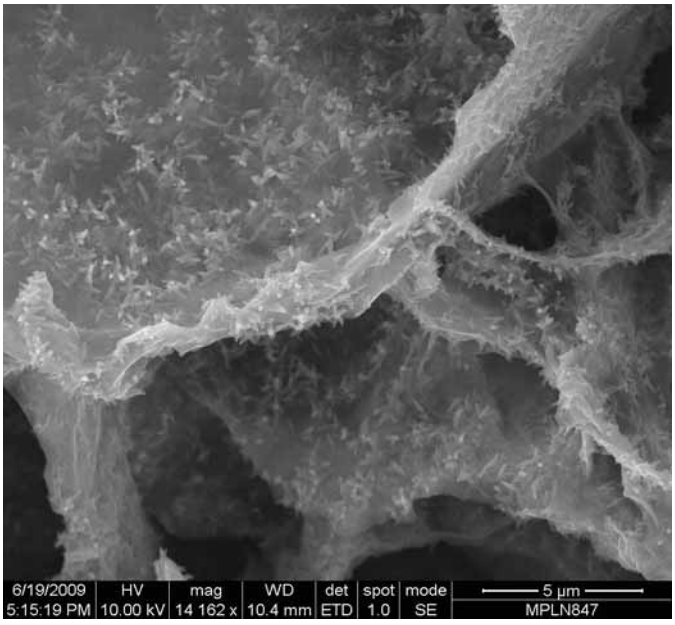

E: This detailed image of a patch of collapsed and truncated smectitic clay shows the presence of an unidentified bladed deposit on the clay surface.

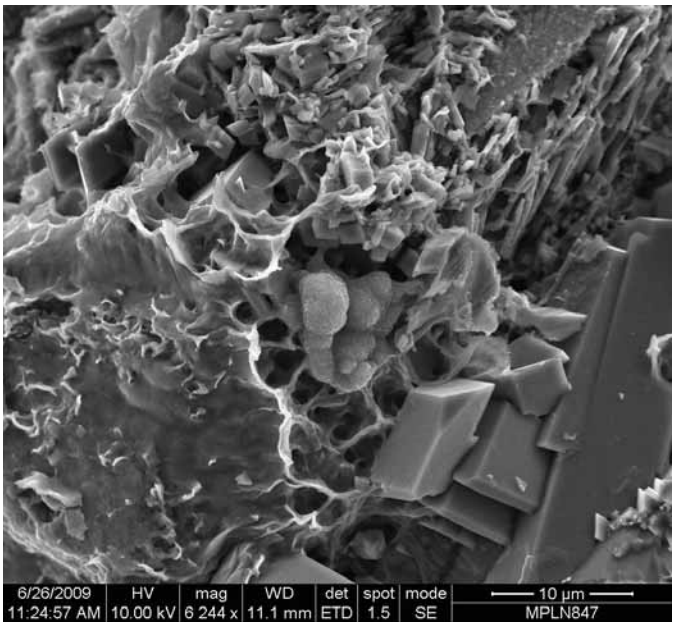

F: This field of view is form within 150 microns of the calcite vein / fracture fill. Here the smectitic clays are associated with a globular aluminosilicate deposit that also contains Ca, Mn and Fe (from EDXA). Euhedral crystals (below right of centre) are of a K-aluminosilicate (probable zeolite, such as clinoptilolite). Etched crystal remnant above centre is of Na-rich plagioclase (possibly albite), whilst that next to the globular cluster is of Ca-rich plagioclase. Again the smectitic clays have a slightly collapsed / truncated appearance.

Sample Site:	P3	**Site Sample No.:**	P3-1
BGS Sample ID:	MPLN849	**Preparation:**	2xfresh fractured fragments
Site Descn:	Parsata area: Kalavasos to Parsata road, rock face road cutting with fluvial or channel deposit of chalky conglomeratic silt and sand resting on Pillow Lava sequence,fractured with tufa.		
Sample Descn:	Sediments at contact with pillow lava surface.		

A: Sample Photo

Sample Description

The sample comprises loose fragments of marly clays and altered lava. The matrix of the lava contains partially dissolved feldspars, mostly Ca-rich plagioclase, with altered and partially dissolved remnants of matrix. Smectitic clays line and fill many of the pores. There are also minor deposits of probable zeolite (most likely K-rich clinoptilolite). The smectitic clays display evidence of some alteration. The alteration is in the form of minor collapse and curling of the webbed edges.

The marly sediment locally has a fibrous calcium-based deposit associated with apparently biogenic matter. The fibres are on a coarse and very fine scale.

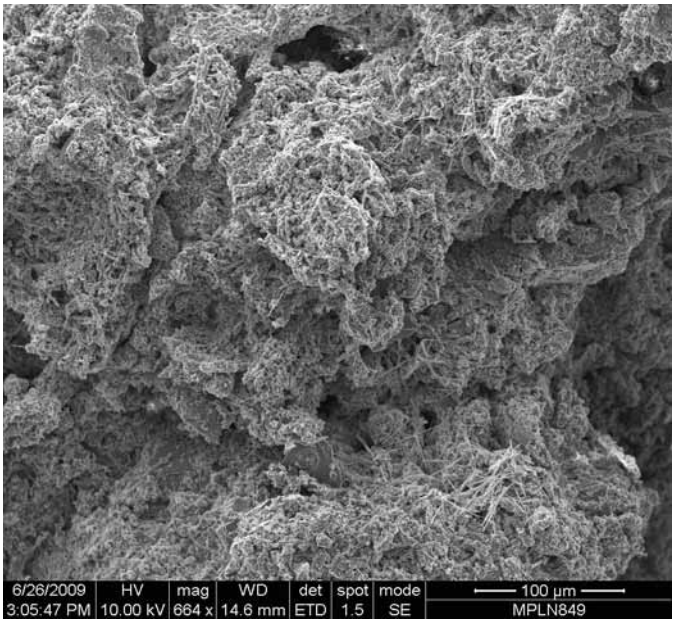

B: A portion of the marly sediment. The irregular surface is patchily coated by elongate fibres of a Ca-based phase. The sample matrix is of carbonate with intermixed silicates.

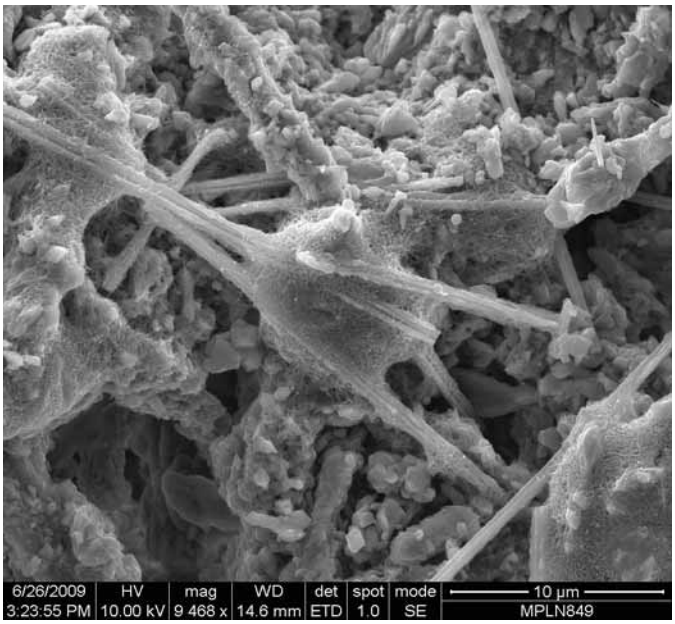

C: Detail from preceding showing fibrous crystals of the Ca-based deposit. These are associated with amorphous globules which appear biofilm-like, but which in detail comprise fibrous forms. These record similar compositions to the coarser fibres. The latter have multi-strand forms. The matrix has a mix of angular, subhedral and euhedral forms of Ca carbonate.

D: From a fragment of altered lava. Macropores are sites of dissolution and alteration and are here lined by a finely webbed and crenulated boxwork of smectitic clays. At centre a spherulitic form is shown. The smectite is Mg-rich but does contain trace Ca. Euhedral crystals (below right of centre, left of bottom) are of a K-silicate (probable zeolite).

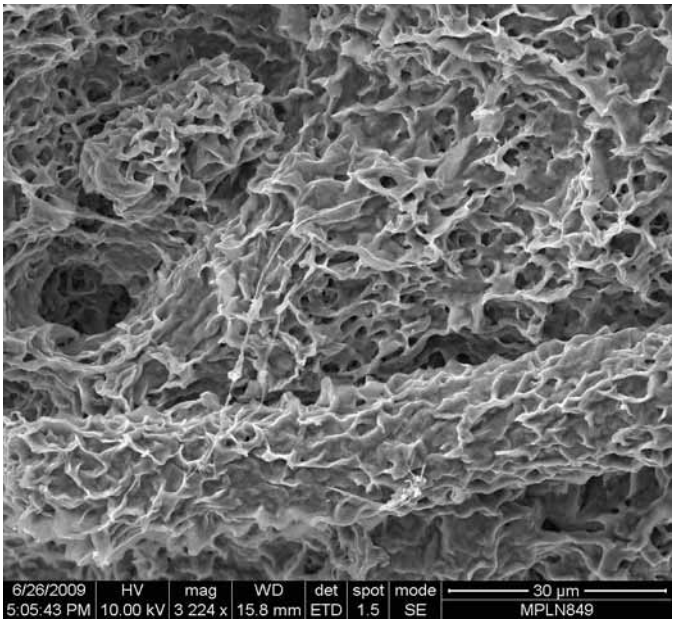

E: From another fragment of altered lava. Here the smectite lines a very large pore surface, probably exposed at the outside of the fragment. This shows a relatively subdued relief, suggesting collapse. Fibres on surface are most likely biofilm or biogenic filaments.

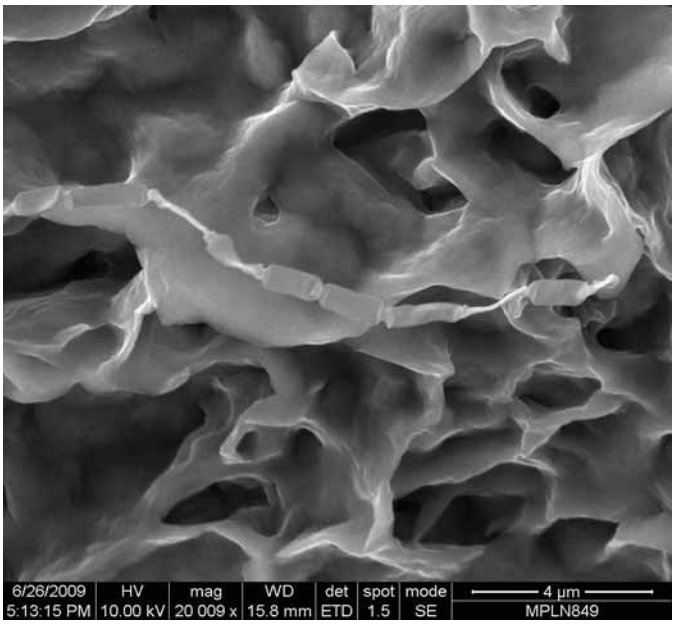

F: Detail from the preceding image showing a linked bacterial chain. This shows the detail of the partially collapsed clay, with curled edges shown. Clays analysed in an adjacent area record similar compositional ranges to the higher relief clays - traces of Ca and K in a Mg-dominant smectite.

BGS Laboratory (LIMS) Code	Original sample number	Corrected sample Code	Field Temp	Field Conductivity	Field pH (temperature-corrected)	Field DO2	Conductivity	pH	Ca2+	Mg2+	Na+	K+	OH-
			°C	µS cm-1		mg L-1	µS cm-1		mg L-1	mg L-1	mg L-1	mg L-1	mg L-1
12081-0008	A4-4	A4-1	n.d.	n.d.	n.d.	n.d.	4160	9.767	3.2006	58.6996	747.17	31.3879	
12081-0007	A4-3	A4-2	n.d.	n.d.	n.d.	n.d.	4990	9.897	3.434	58.4357	892.84	40.5034	
12081-0006	A4-2	A4-3	n.d.	n.d.	n.d.	n.d.	4970	9.706	3.3657	58.7675	921.25	40.6573	
12081-0009	A5-1	A5	9.5	1430	9.8	3	1449	9.22	1.3359	64.1828	224.13	9.75676	
12081-0015	AL-3-1	A3	10.9	1445	9.84	4	1489	9.291	1.3214	63.9431	238.39	10.225	
12081-0014	AL-2-1	A2	10.1	1260	9.69	5	1207	9.04	1.6051	65.5302	171.59	7.32626	
12081-0001	A1-1	A1-1	8.5	6820	11.9	4	n.d.	11.35	37.186	0.101247	1435.3	63.0576	
12081-0003	A1-3	A1-3	8.2	5690	10.01	3	6500	9.314	12.231	0.554354	1336.8	60.1307	
12081-0002	A1-2	A1-2	10.2	295	9.26	3	2970	8.819	4.8726	48.2589	501.54	23.7228	
12081-0004	A1-4	A1-4	9	5150	9.78	3.5	6010	9.27	11.164	5.72502	1213.8	53.9563	
12081-0010	A6	A6	9	4360	9.67	4	5010	9.597	2.2224	50.6642	920.76	42.9002	
12081-0005	E1-1	E1-1	n.d.	n.d.	9.5	n.d.	n.d.	9.48	1.0662	56.3629	75.298	2.62172	
12081-0012	C2	C2	10	n.d.	9.58	5.5	425	8.895	1.6929	67.8841	4.7893	<0.5	
12081-0011	C1	C1	11.8	421	9.41	4	426	8.845	1.7953	68.2555	4.6781	<0.5	
12081-0013	C3	C3	10	n.d.	9.69	5.5	538	9.106	1.6676	92.7236	5.1411	0.92562	
12081-0017	P1	P1	22.9	779	11.42	3	644	10.31	36.501	0.021281	115.57	<0.5	
12081-0016	D2	D2	14.8	1394	8.25	6	1334	8.206	154.69	69.2827	82.767	1.01471	
12081-0018	Distilled water	Distilled water	n/a	n/a	n/a	n/a	n/a	n/a	<0.1	<0.01	<0.35	<0.5	
12081-0001 dup1	A1-1	A1-1	8.5	6820	11.9	4	n.d.	11.33	35.854	0.10098	1462.2	64.9162	
12081-0001 dup2	A1-1	A1-1	8.5	6820	11.9	4	n.d.	11.36	37.412	0.103995	1456	65.6094	
12081-0004 dup1	A1-4	A1-4	9	5150	9.78	3.5	6040	9.325	11.342	5.91455	1154.8	52.872	
12081-0004 dup2	A1-4	A1-4	9	5150	9.78	3.5	6040	9.312	11.535	5.88585	1107.9	50.6353	
12081-0005 dup1	E1-1	E1-1	n.d.	n.d.	n.d.	n.d.	n.d.	9.45	1.0985	57.8871	76.877	2.82407	
12081-0005 dup2	E1-1	E1-1	n.d.	n.d.	n.d.	n.d.	n.d.	9.42	1.0931	57.6365	76.093	2.81406	
12081-0012 dup1	C2	C2	10	n.d.	9.58	5.5	n.d.	8.837	1.6977	68.8709	4.8042	<0.5	
12081-0012 dup2	C2	C2	10	n.d.	9.58	5.5	n.d.	8.873	1.705	68.9219	4.6733	<0.5	

BGS Laboratory (LIMS) Code	CO32-	HCO3-	Cl-	SO42-	NO3-	Cation Total	Anion Total	Balance	Br-	F-	NPOC	Total P	Total S
	mg L-1	mg L-1	mg L-1	mg L-1	mg L-1	meq L-1	meq L-1	%	mg L-1	mg L-1	mg L-1	mg L-1	mg L-1
12081-0008	126.919775	151.932579	1092.995	87.2018	0.343	38.8616616	39.4060865	-0.69559282	2.492	<0.01	0.9	<0.01	28.444
12081-0007	161.125105	120.630807	1341.989	106.002	1.815	45.8188728	47.479841	-1.78026915	3.086	<0.01	1.112	<0.01	34.958
12081-0006	139.701767	153.702075	1320.682	105.966	2.398	47.1276236	46.7160198	0.438605935	3.137	<0.01	0.96	<0.01	35.234
12081-0009	n/a	306.97703	346.024	27.7037	1.976	15.4928014	15.4119709	0.261547111	0.848	<0.01	0.533	<0.01	9.8308
12081-0015	50.4858662	203.150333	368.6957	30.5416	2.22	16.1152949	16.0967549	0.057556293	0.945	<0.01	<0.5	<0.01	10.696
12081-0014	38.4599924	231.755149	253.7375	22.7685	1.662	13.2263831	12.7460744	1.84930037	0.51	0.011	0.542	<0.01	8.1748
12081-0001	n/a	272.441352	2176.993	100.745	<1.5	67.4720629	68.0542835	-0.42959957	6.27	<0.5	0.599	<0.01	42.54
12081-0003	54.0684244	96.407018	1925.67	114.456	10.31	61.2169479	60.3105376	0.745847961	4.471	<0.01	6.879	0.02191	38.298
12081-0002	25.8160224	288.281391	698.592	50.742	3.895	27.0050679	26.433093	1.070349	1.69	<0.01	1.034	<0.01	16.887
12081-0004	61.209537	124.291833	1747.71	78.4558	8.325	55.961965	55.1970839	0.688096139	3.93	<0.5	4.269	0.010188	35.428
12081-0010	101.59583	150.346134	1382.539	97.0248	7.315	46.0115833	47.030017	-1.09460032	3.21	<0.01	0.865	<0.01	32.179
12081-0005	52.2381392	189.519113	92.7169	7.1275	1.027	8.06796005	7.63059153	2.786043784	0.221	<0.01	<1	<0.01	2.7959
12081-0012	23.7336979	255.417581	8.3614	3.2069	0.58	5.88235447	5.28977446	5.304092141	0.036	<0.01	<1	<0.01	1.352
12081-0011	n/a	308.807543	8.4856	3.2719	0.64	5.9131776	5.3791834	4.728809147	<0.03	<0.01	0.512	<0.01	1.3645
12081-0013	44.5269377	310.821107	18.2486	2.4839	1.86	7.9646152	7.17564077	5.211103663	0.055	<0.01	0.526	<0.01	1.0542
12081-0017	27.5772968	<10	80.8823	149.186	<0.03	6.85152677	6.31605021	4.066629419	0.273	0.109	0.846	<0.01	52.242
12081-0016	n/a	413.268818	204.3232	151.318	<0.03	17.0670006	15.7060689	4.152591764	0.383	0.254	5.814	<0.01	51.679
12081-0018	n/a	n/a	<0.05	<0.05	<0.03	0	0	n/a	<0.03	<0.01	<0.5	<0.01	<0.25
12081-0001 dup1	n/a	282.326122	2193.041	102.712	<1.5	68.6296297	68.7094779	-0.05813946	6.23	<0.5	0.559	<0.01	43.839
12081-0001 dup2	n/a	279.946455	2180.212	100.886	<1.5	68.4479261	68.2609304	0.136783915	5.462	<0.5	0.561	<0.01	44.172
12081-0004 dup1	64.5100513	113.247738	1750.486	81.5259	9.347	53.3668762	55.2895713	-1.76951773	4.312	<0.5	4.217	<0.01	36.393
12081-0004 dup2	57.7229938	131.015917	1754.875	82.204	8.762	51.2420972	55.4797812	-3.97077346	4.047	<0.5	4.332	<0.01	36.119
12081-0005 dup1	48.2115118	192.277086	90.6237	6.9305	0.963	8.2700866	7.47741921	5.033605932	0.223	<0.01	<1	<0.01	2.8499
12081-0005 dup2	49.303682	188.286567	90.8894	6.8007	0.969	8.21423745	7.45329081	4.856839136	0.222	<0.01	<1	<0.01	2.8619
12081-0012 dup1	23.4336512	258.224367	8.2636	3.151	0.548	5.96435313	5.32089696	5.701744859	<0.03	<0.01	<1	<0.01	1.3537
12081-0012 dup2	21.8974118	258.419622	8.2037	3.0872	0.547	5.96333385	5.26986656	6.173372396	<0.03	<0.01	<1	<0.01	1.3649

BGS Laboratory (LIMS) Code	Reduced S	S Diff	NH4+	Si	SiO2	Ba	Sr	Mn	Total Fe	Reduced Fe	Oxidised Fe	Al	Co
	mg L-1	%	mg L-1	mg L-1	mg L-1	mg L-1	mg L-1	mg L-1	mg L-1	mg L-1	mg L-1	mg L-1	mg L-1
12081-0008	0.02	<2.3197	2.4	0.339065	0.72536175	0.0035286	<0.005	<0.002	0.054114	<0.05	0.0541142	<0.01	<0.002
12081-0007	0.02	<1.2054	7.3	0.311093	0.66552125	0.0033404	<0.005	<0.002	0.056102	<0.05	0.0561022	<0.01	<0.002
12081-0006	<0.01	<0.3766	8.1	0.297018	0.63541061	0.0034984	<0.005	<0.002	0.056721	<0.05	0.0567206	<0.01	<0.002
12081-0009	0.02	5.94619972	<0.3	0.105465	0.22562127	<0.002	<0.005	<0.002	0.063072	<0.05	0.0630716	<0.01	<0.002
12081-0015	0.02	4.69674984	<0.3	0.090287	0.19315077	<0.002	<0.005	<0.002	0.058503	<0.05	0.0585029	<0.01	<0.002
12081-0014	0.02	7.0414929	<0.3	0.344595	0.73719208	<0.002	<0.005	<0.002	0.060579	<0.05	0.0605789	<0.01	<0.002
12081-0001	0.02	20.9588143	10.7	<0.075	<0.1604475	0.0190229	0.018545	<0.002	<0.01	<0.05	<0.05	<0.01	<0.002
12081-0003	<0.01	0.25548616	0.5	0.152559	0.32636947	0.0099493	0.014669	<0.002	0.014554	<0.05	0.0145537	0.017532	<0.002
12081-0002	<0.01	<0.2898	1.7	2.00623	4.29192784	0.0047383	0.008034	<0.002	0.051277	<0.05	0.0512774	<0.01	<0.002
12081-0004	0.01	26.0882051	<0.3	0.919849	1.96783297	0.0075965	0.011954	<0.002	0.021503	<0.05	0.0215025	<0.01	<0.002
12081-0010	0.02	<0.6327	<0.3	0.131955	0.28229133	0.0024552	<0.005	<0.002	0.051323	<0.05	0.0513225	<0.01	<0.002
12081-0005	0.1	14.916	<0.3	<0.075	<0.1604475	<0.002	<0.005	<0.002	0.054252	<0.05	0.0542516	<0.01	<0.002
12081-0012	0.02	20.8323847	<0.3	0.704645	1.50744705	<0.002	<0.005	<0.002	0.062587	<0.05	0.0625872	<0.01	<0.002
12081-0011	0.02	19.9665393	<0.3	0.848375	1.81492864	0.0022044	<0.005	<0.002	0.061802	<0.05	0.0618024	<0.01	<0.002
12081-0013	0.02	21.3590891	<0.3	<0.075	<0.1604475	0.0057964	<0.005	<0.002	0.070285	<0.05	0.0702851	<0.01	<0.002
12081-0017	0.46	4.68984412	<0.3	3.48486	7.455161	<0.002	0.054143	<0.002	<0.01	<0.05	<0.05	<0.01	<0.002
12081-0016	0.02	2.27411165	<0.3	25.8249	55.2472086	0.0301653	0.720676	0.0070764	0.064155	<0.05	0.0641547	<0.01	<0.002
12081-0018	0.02	93.3248782	<0.3	<0.075	<0.1604475	<0.002	<0.005	<0.002	<0.01	n/a	n/a	<0.01	<0.002
12081-0001 dup1	n/a	21.8025008	n/a	<0.075	<0.1604475	0.0193745	0.021123	<0.002	<0.01	<0.05	<0.05	<0.01	<0.002
12081-0001 dup2	n/a	23.7717859	n/a	<0.075	<0.1604475	0.0195312	0.019933	<0.002	<0.01	<0.05	<0.05	<0.01	<0.002
12081-0004 dup1	n/a	25.2335183	n/a	0.956933	2.04716677	0.0077074	0.012004	<0.002	0.023196	<0.05	0.0231961	<0.01	<0.002
12081-0004 dup2	n/a	24.0391107	n/a	0.965169	2.06478604	0.0077568	0.011462	<0.002	0.023589	<0.05	0.0235891	<0.01	<0.002
12081-0005 dup1	n/a	18.8367227	n/a	<0.075	<0.1604475	<0.002	<0.005	<0.002	0.05646	<0.05	0.0564599	<0.01	<0.002
12081-0005 dup2	n/a	20.6902017	n/a	<0.075	<0.1604475	<0.002	<0.005	<0.002	0.055483	<0.05	0.0554829	<0.01	<0.002
12081-0012 dup1	n/a	22.3112055	n/a	0.721748	1.5440355	<0.002	<0.005	<0.002	0.060804	<0.05	0.0608043	<0.01	<0.002
12081-0012 dup2	n/a	24.511568	n/a	0.72369	1.54819002	0.0020764	<0.005	<0.002	0.06246	<0.05	0.0624599	<0.01	<0.002

BGS Laboratory (LIMS) Code	Ni	Cu	Zn	Cr	Mo
	mg L-1	mg L-1	mg L-1	mg L-1	mg L-1
12081-0008	<0.005	<0.005	<0.005	0.0025508	<0.015
12081-0007	<0.005	<0.005	<0.005	0.0024436	<0.015
12081-0006	<0.005	<0.005	<0.005	0.0023786	<0.015
12081-0009	<0.005	<0.005	<0.005	0.0028714	<0.015
12081-0015	<0.005	<0.005	<0.005	0.0034592	<0.015
12081-0014	<0.005	<0.005	<0.005	0.0053687	<0.015
12081-0001	<0.005	<0.005	<0.005	<0.002	<0.015
12081-0003	<0.005	<0.005	<0.005	<0.002	<0.015
12081-0002	<0.005	<0.005	<0.005	0.0059974	<0.015
12081-0004	<0.005	<0.005	<0.005	0.0020067	<0.015
12081-0010	<0.005	<0.005	<0.005	0.0053867	<0.015
12081-0005	<0.005	<0.005	<0.005	<0.002	<0.015
12081-0012	<0.005	<0.005	<0.005	0.0252944	<0.015
12081-0011	<0.005	<0.005	<0.005	0.0244437	<0.015
12081-0013	<0.005	<0.005	<0.005	<0.002	<0.015
12081-0017	<0.005	<0.005	<0.005	<0.002	<0.015
12081-0016	<0.005	<0.005	<0.005	0.0125333	<0.015
12081-0018	<0.005	<0.005	0.0073376	<0.002	<0.015
12081-0001 dup1	<0.005	<0.005	<0.005	<0.002	<0.015
12081-0001 dup2	<0.005	<0.005	0.0107016	<0.002	<0.015
12081-0004 dup1	<0.005	<0.005	<0.005	<0.002	<0.015
12081-0004 dup2	<0.005	<0.005	<0.005	0.0021769	<0.015
12081-0005 dup1	<0.005	<0.005	<0.005	<0.002	<0.015
12081-0005 dup2	<0.005	<0.005	<0.005	<0.002	<0.015
12081-0012 dup1	<0.005	<0.005	<0.005	0.0240077	<0.015
12081-0012 dup2	<0.005	<0.005	<0.005	0.0246601	<0.015

Fig. 1 A2-1a

Fig. 2 A3-1a

Fig. 3 A4-1a

Fig. 4 A4-1b

Fig. 5 A4-1d

Fig. 6 A4-2a

Fig. 7 C2-1a

Fig. 8 C2-1b

Fig. 9 C2-1c

Fig. 10 C2-1d

Fig. 11 C2-1e

Fig. 12 C2-1f

Fig. 13 C3-1a

Fig. 14 C3-1b

Fig. 15 C3-2a

Fig. 16 C3-2b

Fig. 17 C3-2c

Fig. 18 C3-2d

Fig. 19 C3-2e

Fig. 20 C3-2f

Fig. 21 C3-2g

Fig. 22 C3-2h

Fig. 23 C3-2i

Fig. 24 C3-2j

Fig. 25 D1-1a

Fig. 26 D1-1b

Fig. 27 D1-1c

Fig. 28 D1-1d

Fig. 29 D2-1a

Fig. 30 D3-1a

Fig. 31 E1-1a

Fig. 32 E1-1b

Fig. 33 E1-1c

Fig. 34 E2-1a

Fig. 35 E2-1b

Fig. 36 E3-1a

Fig. 37 E3-1b

Fig. 38 E4-1a

Fig. 39 E4-1b

Fig. 40 E5-1a

Fig. 41 E5-1b

Fig. 42 P2-1a

Fig. 43 P2-1b

Fig. 44 P2-1c

Fig. 45 P2-1d

Fig. 46 P2-1e

Fig. 47 P2-1f

Fig. 48 P2-2a

Fig. 49 P3-1a

Fig. 50 P3-1b

Fig. 51 P3-1c

Fig. 52 P3-1d

Fig. 53 P3-1e

Fig. 54 P3-1f

Fig. 55 P3-1g

Fig. 56 T1-1a

Fig. 57 T1-1b

Fig. 58 T1-1c

Fig. 59 T1-1d

Fig. 60 T1-1e

Fig. 61 T1-1f

Fig. 62 T1-1g